DENDRIMER BASED NANOTHERAPEUTICS FOR OCULAR DRUG DELIVERY

by

SIVA PRAMODH KAMBHAMPATI

DISSERTATION

Submitted to the Graduate School

of Wayne State University,

Detroit, Michigan

In partial fulfillment of the requirements

for the degree of

DOCTOR OF PHILOSOPHY

2015

MAJOR: BIOMEDICAL ENGINEERING

Approved by:

_____

Advisor Date

_____

Advisor Date

_____

_____

_____

ProQuest LLC.
789 East Eisenhower Parkway
P.O. Box 1346
Ann Arbor, MI 48106 - 1346

DEDICATION

I dedicate my work to

My advisor and well-wisher Dr. Kannan Rangaramanujam

My parents Aluri Chenchulakshmi and Kambhampati Krishna Vinayak

and to the Almighty

ACKNOWLEDGEMENTS

I would like to express sincere gratitude to my advisor Dr. R. M. Kannan for giving me this opportunity and for his enormous support in all aspects throughout my stay at the department and in his lab. I would also thank my co-advisor Dr. Howard matthew for all his help and support regarding his insightful advice and all the formalities at wayne state. I sincerely thank mu committee members Dr. Mahendra Kavdia, Dr. Harini Sundararaghavan and Dr. Sujatha Kannan, their suggestions and invaluable time to review my dissertation report. I am thankful to Dr. Gerard Lutty for his in-valuable help, support, guidance and liberty to work in his lab for *in-vivo* evaluation. I would like to extend a special thanks to Dr. Charles Manke for his continuous advice, support and help regarding my funding and paperwork formalities between Johns Hopkins and Wayne State. I owe and sincerely thank Dr. Manoj Mishra for his guidance, training and support throughout my thesis. I also thank Dr. Imran Bhutto for his excellent training and guidance for *in-vivo* and imaging experiments. I also thank Dr. Justin Hanes for his encouragement, Dr. Uri Soibermen, Dr. Elizabeth Nance, Dr. Zhi Zhang, Dr. Laura Ensign and Dr. Malia Edwards for all their help with experiments. Many thanks to my friends Fan, Fenguyang, Panos, Kunal, Clark, Jane, Raj and many more in center for nanomedicine for all their motivation and support. Finally I thank my parents A.C. Lakshmi and K.K.Vinayak for their moral support and guidance. Finally I thank my little brother Rohith Pranav for all the playful troubles, encouragement and affection.

TABLE OF CONTENTS

LIST OF TABLES

LIST OF FIGURES

CHAPTER 1 "DENDRIMERS FOR OCULAR DRUG DELIVERY"

1.1. Ocular drug delivery- Importance and challenges

Blindness is a leading health care issue (after cancer) worldwide, with important socio-economic consequences. According to World Health Organization (WHO) more than 314 million people age 40 or older visually impaired due to age related eye diseases such as Age Related Macular Degeneration (AMD), Choroidal neovascularization (CNV), Diabetic retinopathy, Retinitis pigmentosa (RP), Glaucoma, Central vein occlusion and Intra ocular tumors, uveits and cataracts [1]. It is expected to dramatically increase from 28 million today to 43 million by the year 2020 in US population [2]. Blindness and irreversible sight impairment cost $50 billion in the United States. The commercial ophthalmic market is estimated to be $14 billion in 2009 and it is expected to reach $19 billion by end of 2014 [3]. Drugs are being used for treating these ocular diseases by conventional routes such as topical and systemic. Topical applications are mostly used for treating anterior segment related diseases. Mostly Anti-inflammatory (corticosteroids), Steroids, Anti-fungal (imidizoles, polyenes), Antibiotics, Miotics etc are being used in the form of liquid formulations via topical route for treating various diseases associated with anterior chamber [4, 5]. These drugs have delayed permeability through intact corneal epithelium [6, 7] and due to this reason they do not remain for prolonged time and are susceptible to be washed out by tear (30 s) or occurrence of drug – protein binding in tear fluid. 90% of these drugs are diluted and washed by lachrymal gland secretion and its nasolachrimal drainage. Some percentage of drugs is lost by tear dilution and tear turnover and typically less than 5% of the total administered drug reaches the aqueous humor by crossing the pre-corneal and corneal barriers (epithelium, stroma and endothelial tight junctions) [8, 9]. In order to maintain and deliver therapeutic concentration to the target site, repeated dosage is

adopted which results in poor patient compliance. Due to low ocular bioavailability invasive methods like peribulbar, Sub-tendon, Sub-conjunctival injections are used. Drug delivery to posterior segments was previously by systemic dosage but major drawback is that only 2% of the injected drug reaches the vitreous cavity due to the blood retinal barrier selective permeability and drug metabolization in systemic route. Hence frequent administration of high amounts of drugs results in systemic side effects [10]. Intraocular injections such as Intravitreal, suprachoridal and retrobulbar methods are used [11]. Since intravitreal injections offers high concentrations of drugs in vitreous cavity and retina leads to accumulation and side effects which results in retinal detachment, endophthalmitis and intravitreal hemorrhages. Implantable devices can be used for sustained delivery of drugs. There are different types of implantable devices based on their location such as reservoir free floating implants - Medidur (Alimera Sciences, USA and pSivida Inc.,USA) and Posurdex (Allergan Inc., USA) , Intrascleral - Surodex (Allergan Inc., USA) , intravitreal paras-planar mediated implants - Retisert (Bausch & Lomb, Rochester, USA) and Vitrasert (Bausch & Lomb, Rochester, USA), Scleral plugs - Surmodics Inc. (Eden Prairie, MN) and PLGA (Biodegradable scleral plugs). Some of these implants needs minor surgery for implantation and requires another surgery for surgery to harvest the device once is depleted of the drug; these surgeries are associated with ocular complications such infections at implant site, inflammations and tissue rejections. In case of biodegradable Implants final uncontrolled burst drug release profile which results in side effects.

Since the above ocular drug delivery systems have disadvantages, optimum ocular drug delivery systems should be developed such that they satisfy the following parameters

- Control over drug release kinetics (sustained release is preferred).

- Should enhance drug permeation in to the cells (crossing of blood retinal barriers).
- Targeting drug to the required specific areas of ocular tissue.
- Patient compliance, low irritation, bioavailability and compatible. Ocular diseases such cataracts, The critical need to fight blindness is also aided by the large commercial ophthalmic market, which together can be a powerful driving force for clinical translation of novel nanotechnology-based drug delivery approaches.

Biocompatible Particulates (microparticles and nanoparticles) are being investigated in all systems such as Central nervous systems, Respiratory, Cardiovascular, digestive, etc. Recent years there is an unprecedented growth of investigating various nanoparticles in field of drug delivery because of their controllable surface chemistry, easy formulations, small size, increased surface stability and increased surface area which helps in drug targeting, reduced toxicity, increases drug stability and provide more efficient drug distribution.

1.2. Anatomy of the eye – A special reference to ocular barriers:

"Eye is deemed to be a unique organ of extreme perfection and complication" – as a whole it appears to be simple, small and transparent with three tunics the fibrous corneo-sclera, vascular choroid and sensory retina. The eye ball is divided in to two segments (i) anterior segment containing cornea, crystalline lens, iris, ciliary body and fluid filled aqueous humor. (ii) Posterior segment includes sclera, choroid vessels, retina, macula, optic nerve and fluid filled vitreous humor [12]. The actual complexity arises when probed in to micro anatomy, physiology and biochemical perspective. The tunics are highly complex structures arranged with descending degree of light transparency that transverses light to retina where the photo signals are converted

to electrical signals and transmitted to higher centers of the brain. This organ is well protected

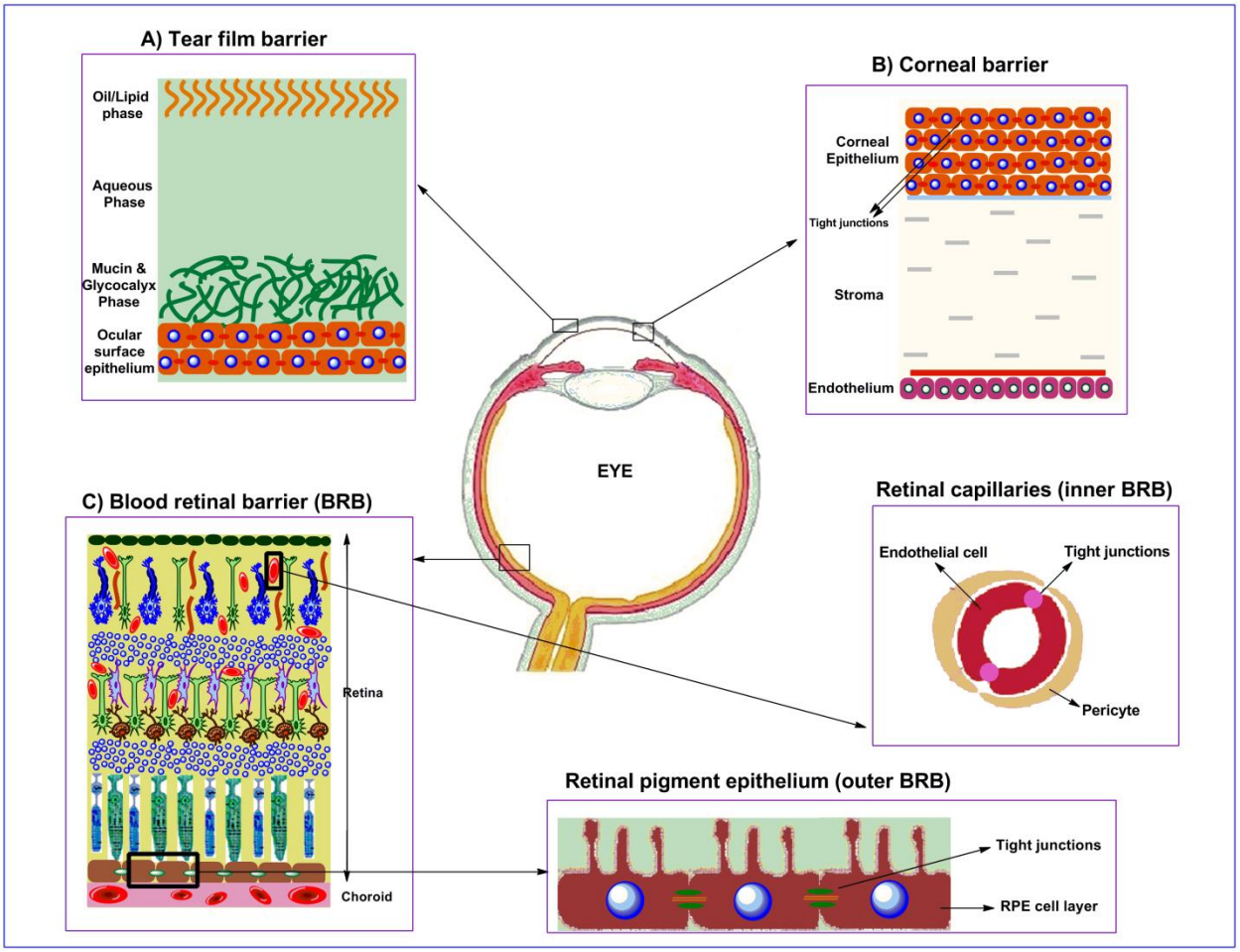

Figure 1: A schematic representation of critical ocular barriers that offers challenge to ocular drug delivery. **A)** Tear film barrier: A protective barrier of tear film contains mucins that prevent foreign materials coming in contact with corneal epithelium. They are frequently washed away via lachrymal drainage to remove entrapped materials **B)** Corneal barrier: consisting of 4-5 epithelial layers fused together by tight junctions preventing entry of particles followed by thick stroma and endothelial cells. **C)** Blood-Retinal barrier (BRB) consisting of Inner BRB formed by retinal capillaries. The endothelial cells fused together by tight junctions impeding outward passage of foreign materials, toxins and proteins. Outer BRB formed by the tight junctions between RPE, making retina impervious but allowing oxygen and other nutrients diffuse through them.

with various specialized cellular modifications that maintain its normal physiology and structure [13]. Moreover these modified cellular structures gives rise to various barriers that partially isolates the eye from rest of the body [14]. These special processes consists of the (i) inner and outer Blood Retinal Barriers (BRB) in retinal blood vessels and tight junctions of retinal pigment epithelium (RPE) respectively separates the retina from systemic circulation and avoids entry of

unnecessary components into retina, (ii) Barrier formed by fusion of Müller cells in the Inner limiting membrane (ILM) controls the exchange and entry of particles from vitreous to retina, (iii) Blood-aqueous barrier formed by cilia epithelial cells limits the passage of molecules from blood to inner part of eye, (iv) blood vessels of iris lack fenestrations, (v) intact corneal epithelium with desmosomes as an outer barrier and corneal endothelium abundant with tight junctions as inner corneal barrier, (vi) Muco-aqueous barrier formed by the tear film prevents and continuously washes away the particles at anterior surface of eye [14, 15]. A schematic diagram of structure of eye with all the ocular barriers are illustrated in **Figure 1**.

1.3. PAMAM dendrimers – physiochemical characteristics and biomedical applications

Dendrimers are globular, nanostructured polymers (~ 3-20 nm) with a well-defined shape, narrow polydispersity. Polyamido amine (PAMAM) (Figure 2) were first synthesized by tomalia [16] and it was the first commercialized dendrimers in dendrimer family and are promising drug delivery vehicles because of their multivalency, well-defined and globular structure, low polydispersity, and amenability to post-synthetic manipulation that are extensively investigated for various biomedical applications [17]. PAMAM dendrimers have ethylene diamine (EDA) core and an amidoamine repeat branching structure. They are synthesized via Michael addition of amino groups of EDA with methyl acrylate, followed by amidation of the resulting esters with EDA, and generation 0 is formed (**Figure 2**). A repetition of these two synthetic steps adds another layer of branching units and produces next generation. The size of dendrimer grows linearly in diameter as a function of added generations, approximately 1 nm per generation. Each new generation also doubles the number of terminal groups and approximately doubles the molecular weight of the previous generation. Figure 4 shows the synthesis of amine (NH_2)

terminated PAMAM dendrimers that are cationic; however there is also neutral hydroxyl (OH) and anionic carboxyl (COOH) terminated PAMAM dendrimers.

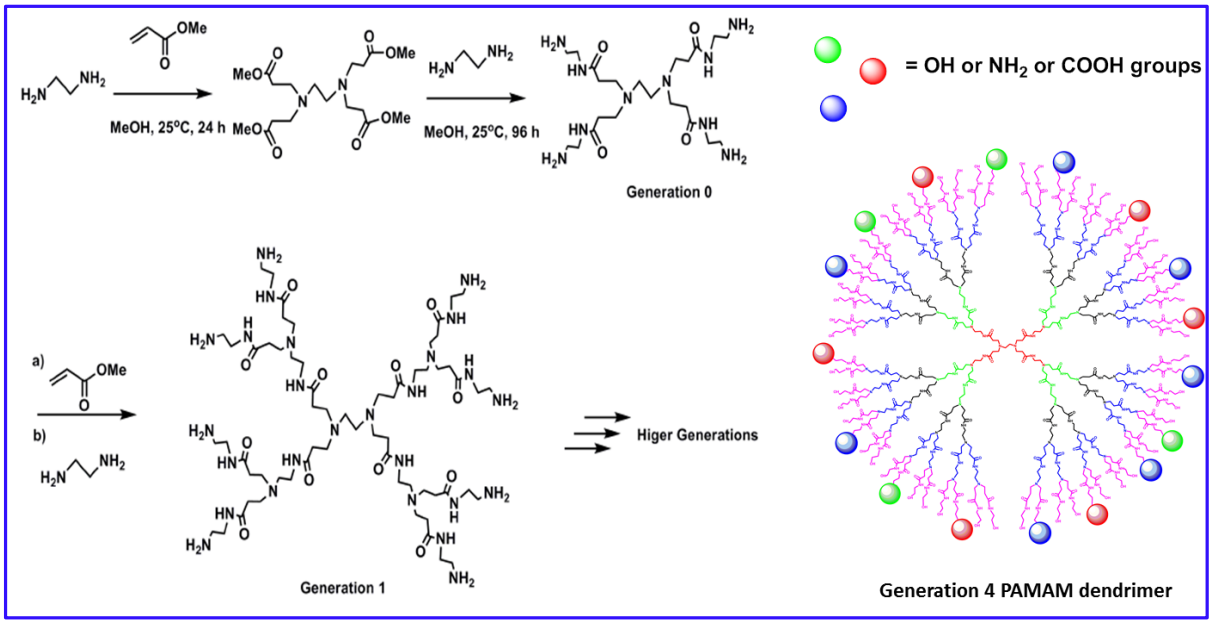

Figure 2: Synthesis of PAMAM dendrimers by Tomalia [17], and a schematic structure of fully synthesized generation 4 (G4) dendrimer with hydroxyl (OH), amine (NH2) or carboxyl (COOH) end groups.

Properties those are beneficial for drug delivery:

1) **Appropriate size:** The size of these nanoparticles is a major positive property that makes dendrimers idle to work with in terms of conjugation chemistry, ease for characterization and in biological aspect they can give desired cellular internalization, biodistribution and effective clearance. Dendrimers have different size based on different generations from G2-G10. For example in the case of Generation 4 dendrimer the size ranges from 4-5nm makes it idle for crossing biological barriers.
2) **Branching structure:** They have exceptional structural properties such as branching, multiple surface functional groups that make them highly amenable for various chemistries such as conjugation of multiple copies of single or multiple drugs, targeting

ligands thereby providing high pay load. Their multivalency also makes them suitable for complex with therapeutic genes for their safe delivery to the targeted cells. The multiple surface groups also provide an additional feature and opportunity for high crosslinking densities with short polymers and are suitable designing tissue engineering scaffolds with desirable mechanical strengths, sealants and hydrogels for wound healing and depot release drug delivery.

3) **Composition:** The composition of dendrimer makeup is also an important criterion as it determines the biocompatibility nature of these nanostructures. PAMAM dendrimers are made up of subunits that have chemical structure similar to amino acid β-Alanine. Moreover dendrimers behave as protein molecules by exhibiting active conformational changes at different pH environments. Generation 4 PAMAM dendrimer has size comparable to cytochrome-C (4 nm), generation 5 PAMAM dendrimer has size comparable to hemoglobin (5 nm), and so on [18]. Conformation of dendrimers strictly depends on pH. At low pH (~3), all primary amine groups of PAMAM dendrimers are protonated leading to an extended conformation due to electrostatic repulsion between the positively charged NH3 + groups. At neutral pH back folding occurs which is due to the hydrogen bonding between the uncharged tertiary amines in the interior and the positively charged surface amines. At basic pH the dendrimer is completely neutralized and repulsive interactions between the wedges and end-groups reach a minimum leading to a conformation with a higher degree of back folding so dendrimer acquires a more spherical (globular) structure. The conformation of dendrimers is also affected by the polarity of the solvent as well as the ionic strength (high concentration of salts) [18].

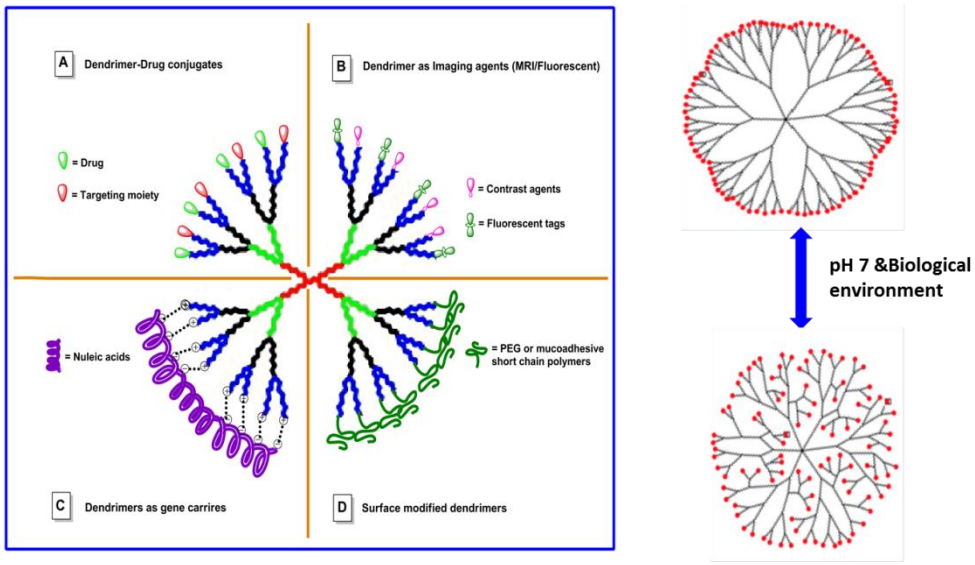

Figure 3: A diagrammatic representation of the versatility of the dendrimer structure that enables tailorability. **A)** Dendrimers as drug delivery vehicles where drug molecules and targeting moieties can be covalently linked to surface groups. **B)** Dendrimers as carriers of contrast agents for MRI and fluorescent imaging. **C)** Dendrimers as gene delivery vehicles where genes such as mRNA, siRNA, or DNA can be complexed. **D)** Surface modification of dendrimer surface with short mucoadhesive and bioactive polymers to enhance their activity or to increase their circulation time.

4) **Surface charge:** The surface charge (zeta potential) of dendrimers is also an important factor as it determines the cellular entry and various biological interactions with the extra cellular matrix (ECM), proteins and enzymes. For example, hydroxyl dendrimers (G4-OH) have a surface charge of ~ +4.0mV due to the internal amines and there is a perfect balance between the amine and hydroxyl groups in terms of charge and it is suitable for cellular entry. The amine terminated dendrimer (G4-NH2) has a surface charge of +16.0 mV and have susceptible for plasma proteins, and cell membrane interactions. On other hand Carboxyl terminated dendrimers (G3.5-COOH) has negative surface charge that can help avoid un-necessary interactions that can delay or inhibit targeted delivery of therapeutic agents. All the above characteristics make dendrimers versatile and suitable for biomedical applications. Figure 3 illustrates the versatility of PAMAM dendrimers

and a schematic representation of conformational changes due to their external environment [19].

1.4. Dendrimers for Ocular drug delivery: Advantages

1) **Corneal Permeation enhancers & improved drug delivery:** Polyamidoamine (PAMAM) dendrimers can have different cell entry pathways, depending on the surface functionality. Anionic PAMAM dendrimers are endocytosed primarily through a caveolin-mediated process, whereas neutral and cationic dendrimers were reported to follow clathrin-mediated internalization in cells [20, 28]. These cellular internalization processes can be highly beneficial in the case of crossing the epithelial and retinal barriers in cornea and retina. PAMAM dendrimers showed remarkable interactions with membrane-associated mucin layers. Surface plasmon resonance (SPR) was used to probe the interfacial interactions between dendrimer surfaces and ocular mucins at the molecular levels [21]. For example dendrimer formulation in the form of eye drops showed improved drug delivery through the corneal layers can be attributed to multivalent interactions with glycocalyx and ocular mucins. Pharmacokinetic studies of concentrations of topically instilled puerarin in the form of PAMAM-puerarin complexes were carried out using micro-dialysis and mass spectroscopy, which suggested that up to a 3.5- fold increase in drug concentration, could be achieved in groups treated with PAMAM dendrimer-drug complexes, compared to the free drug [22]. Synthetic antiglaucomatic drugs, timolol and brimonidine are hydrophobic and have very limited solubility in aqueous ophthalmic solutions and dramatically influence their cellular uptake, corneal transport and bioavailability. Developed dendrimer hydrogel (DH)

consisting PAMAM (G3-NH2) dendrimers with PEG acrylate chains (cross linkers) conjugated to their surface and brimonidine or timolol maleate encapsulated into their hydrophobic cores forming a viscous formulation are aimed to increase the bioavailability of drugs after topical instillations [23].

2) **Desirable biodistribution and drug targeting in ocular tissues:** Biodistribution, bioavailability and targeting of drugs are the key parameters that are necessary for evaluating and achieving desired efficacy. Nanoparticles and dendrimers can be designed with various surface modifications, decorating with targeting ligands to target specific cells or to cross the retinal barriers [24]. Delivery of drugs to retinal layers is a difficult task as the retina itself is isolated from blood circulation and vitreous fluid similar to the brain by the inner and outer BRB to maintain its homeostasis and clear vision. Dendrimers and nanoparticles showed differential biodistribution based on their size, surface charge and targeting ligands. Based on targeting ligands for example, Rhodamine-conjugated liposomes, loaded with the vasoactive intestinal peptide (VIP-Rh-Lip), injected intravetrially were bio distributed in inner retinal layers and up taken by Müller and resident macrophages at earlier time points (24hrs) and finally retained in retinal pigment epithelium (RPE) upto 4 months, thereby manifesting their prolonged bioavailability [25]. Based on size polystyrene nanoparticles (2 μm, 200 nm, and 50nm) showed differential uptake. Larger particles (200μm) were cleared out from the vitreous chamber and were seen accumulated in trabecular meshwork, whereas smaller particles (50nm) were found crossing the retinal layers and the intermediate particles (100nm) were found both in trabecular meshwork, retinal layers and entangled in vitreous networks [26]. Dendrimers showed differences in biodistribution based on their

composition, size and route of administration. PAMAM dendrimers injected intravetrially showed pathology dependent accumulation in RCS rat models. They were specifically localized and up-taken by activated resident microglial cells in inner nuclear layers, photoreceptor layers where the degeneration & neuroinflammation occurs in many retinal diseases such as macular degeneration, CNV, retinitis pigmentosa, diabetic retinopathy and etc. In diseased retina the dendrimers were retained for more than 1month after single intravitreal injection retinas whereas in normal retina they were completely cleared out within 24hrs [27]. When dendrimers injected via intravenous route were distributed in outer retina and RPE layers. Polylysine dendrimers complexes with anti-vascular endothelial growth factor (anti-VEGF) oligonucleotides (ODN-1) targeted the RPE layers and suppressed neovascularization in CNV rat model for 3 weeks [28]. The above studies give us knowledge for wide opportunities for designing different dendrimer and nanoparticle formulations for desired biodistribution and prolonged availability for different diseases.

3) **Enhanced efficacy at lower drug concentrations:** Achieving enhanced efficacy at very low drug concentrations and decreasing the frequency of dosages is always desirable for avoiding side effects from drug, retinal & ocular toxicity and achieve patient compliance. Delivery a drug via nanoparticle is a challenge in offers researchers an opportunity window to develop novel formulations and ultimately helps in clinical translation. PAMAM dendrimer (G4-OH) conjugated to fluocinolone acetonide (drug-anti-inflammatory) (D-FA) showed sustained in-vitro release for 3months and in-vivo was shown to provide sustained attenuation of neuro-inflammation, long-term neuroprotection, along with maintaining photoreceptor. The attenuation of neuro-

inflammation is done by reverting the proinflammatory activated resident microglia to its resting state and such targeted drug delivery is very beneficial in many neurodegenerative and neovascular retinal diseases [27]. Cytomegalovirus (CMV) retinitis, uveitis or microbial endophthalmitis leading to structural damage in the retina, retinal detachment or inflammation, resulting in a permanent vision loss. PAMAM dendrimer formulations were also investigated for their ability to increase efficacy in the case of intraocular infections and endophthalmitis where antibacterial and antiviral agents are injected in to the eye at very strong doses frequently and such high drug doses cause retinal toxicity. PAMAM dendrimer loaded with ofloxacin and fluconazole showed 4 fold better efficacies in inhibiting retinal infections at 6 fold lower doses than commercial formulations [29]. Carboplatin is an anticancer drug commonly used for intra ocular tumors and retinoblastoma but causes toxicity to optic nerve and corneal lens scarring at therapeutic levels. PAMAM dendrimers with carboxyl end groups (G3.5-COOH) for extended half-life and sustained delivery of carboplatin with lowered therapeutic toxicity [30].

The above studies prove that dendrimer formulations can be beneficial for various applications such as ocular infections, corneal neovasculartion, glaucoma, corneal surgeries and corneal transplantation. **Table 1** provides a summary of different dendrimer formulation studied and their enhanced results for different ocular diseases.

TABLE 1: Summary of pre-clinical studies on dendrimers for ophthalmic applications

Dendrimer Type	Drug	Disease Conditions	Outcomes & Advantages	Reference
PAMAM	Peurarin	Catracta gluca & Ocular Hypertension	Increased drug bioavailability	*Yao et al*
PAMAM (G3.5-COOH)	Glucosamine-6-sulfate Glucosamine	Corneal scarring & neovascularization	No scar formation & Reduced inflammation	*Shaunak et al.*
PAMAM (G1.5-4)	Pilocarpine & Tropicamide	Glaucoma	Increased corneal residence & Prolonged reduction of IOP	*Vandamme et al.*
PAMAM (G4-OH)	Nadifloxacin & Prulifloxacin	Corneal Infections	Enhanced antimicrobial activity & drug solubility	*Cheng et al.*
PAMAM (G3.5-COOH)	Carboplatin	Retinoblastoma	Increased ½ life & drug bioavailability Reduced drug toxicity & tumor mass	*Kang et al*
PAMAM (G4-OH)	Fluocinolone acetonoide	Retinal neuroinflammation & Retinitis Pigmentosa	Reduced inflammation by selective accumulation in inflammatory cells	*Kannan & Iezzi*
PAMAM (G5-NH_2)	siRNA & Antisense Oligonucleotide		Enhanced nuclear transfection	*Kang et al.*
Poly lysine Biodendrimer	AntiVEGF (OND-1)	Choroidal neovascularization	Prolonged suppression of VEGF & abnormal neovascularization	*Marano et al.*
Phosphorous dendrimers	Carterol	Glaucoma	Increased corneal residence, reduced toxicity & IOP	*Spataro et al.*
Dendrimeric polyganidilyated translocators	Gatifloxacin	Conjuntivitis & intraocular infections	Enhanced corneal transport and increased antimicrobial activity	*Durairaj et al.*
Peptide dendrimers	Self	CMV retinitis	Enhanced antiviral activity	*Luganini et al.*
Porphyrin-glycodendrimers	Self with concanavalin A	Intraocular tumors & retinoblastoma (PDT)	Effective & enhanced targeting Reduced toxicity	*Makky et al.*
Porphyrin dendrimers	Self	AMD & CNV	Selective accumulation in CNV lesions & prolonged retention in neovessels	*Nishiyama et al.*
Phthalocyanine dendrimers	DNA		Accumulation in photoirradiated areas & increased trans gene expression	*Nishiyama et al.*
Lys_3Cys_1 dendritic polymers	Self	Cataract incisions	*In situ* gel formation, wound sealing	*Grinstaff et al.*
PLGSA-MA biodendrimers	Self	Corneal wound healing & sealants	Wound sealing, corneal transplant success & no scar formation	*Grinstaff et al.*

1.5. Ocular neuroinflammation and neovascularization- a target of dendrimer therapeutics:

As a part of central nervous system (CNS) retina and choroid are constantly under surveillance for maintaining their proper health and function. Retina is innervated directly from the branches of the optic nerve that relays to the optic center in the cerebral cortex of the brain. The optic nerve enters the retina via the optic disc and radially distributes and synapses with the ganglionic cells forming the nerve fiber layer. There are three major types of glial cells found in retina: Müller cells, astrocytes and microglia. Microglia enters the retina from the circulation and has phagocytic activity. On other hand the vascular supply to retina and choroid is intense and

crucial. Choroid receives 80% of all ocular blood. The choroidal blood vessels are not regulated, leaky and often have fenestrations up to 20nm. In contrast, retina has regulated blood supply with all the blood vessels having tight junctions [inner blood retinal barrier (BRB)]. The ophthalmic artery enters the retina along with the optic nerve and radially branches out to supply the entire retina forming a network of retinal capillaries where the blood flow is highly regulated.

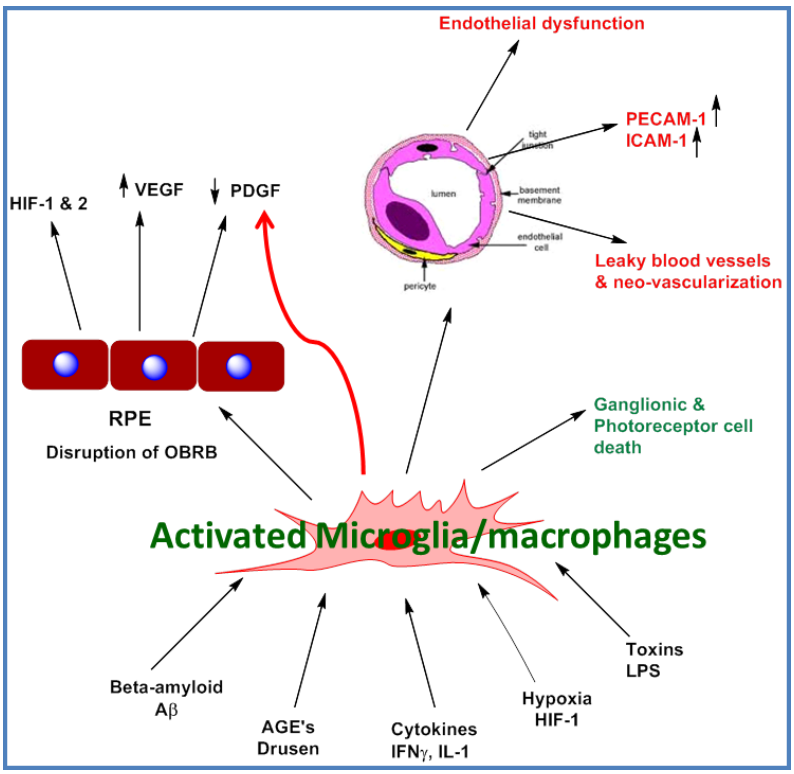

Figure 4: A schematic representation of Activated microglial interactions with retinal cells and their pathological effects.

Microglial cells are responsible for maintaining the tissue metabolism and health by eliminating the invading microbes, clear cellular debris and also the house keeping function such as angiogenesis during early development, releasing growth factors when required and also maintaining the tissue inflammatory response by producing anti-inflammatory cytokines for neuronal survival. On other hand these microglial cells in the case of pathology where the

molecular signals and tissue damage passes beyond a certain limit causes themselves activated to pro-inflammatory cells [31]. Retinal microglia has been implicated in number of retinal degenerative diseases and vascular diseases. Activated microglia cells exhibit pathological changes both morphologically and functionally.

It is widely accepted that microglia contribute the process of neurodegeneration by releasing and maintaining various neurotoxic factors and inflammatory cascades [32]. They perform and maintain numerous cross-talks with other cells in the retina such as neurons, RPE, ganglionic cells and endothelial cells. They produce agents like fibroblast growth factor causing retinal scarring and fibrosis thereby paving a way for neuronal cell death. Microglial cells were reported to cause ganglionic cell atrophy in disease conditions such as diabetic retinopathy and glaucoma and manifested by ganglionic layer thinning [33]. Microglial cells when activated have dynamic cell movement within the retina and tends it to accumulate in the photoreceptor and RPE layer. They also induce photoreceptor dystrophies in conditions such as retinal ischemia and dry AMD [27].

Potential role of microglia in retinal blood vessel neovascularization was also reported as many cross-talk and molecular mechanisms [34]. They interact with perivascular cells that maintain the permeability of the blood vessels causing endothelial dysfunction by oxidative stress pathway [31] Moreover they were found accumulated in the neovascular tufts in mice model of laser induced CNV. Activated microglial cells causes RPE and endothelial cells to produce VEGF thereby causing promotion of pathologic blood vessels. They also decrease the expression of VCAM-1 and increases the ICAM-1 expression in retinal endothelial cells thereby the blood vessels lose their vascular integrity. Increase in ICAM expression causes circulatory and choroidal macrophages to infiltrate in to the retina exacerbating the disease process [35]. A

schematic representation of effects of activated microglia and their cross-talk with various retinal cells is depicted in **Figure 4**.

1.6. Research Objective:

Eye is a complex and delicate organ well supplied with neurons and rich vasculature. They are connected directly to the CNS and share many common properties. Ocular diseases are projecting a major health problem and the cost of treating the ocular diseases increases every year. Neuroinflammation and neovascular are the two major events that occur in many retinal diseases such as age related macular degeneration (AMD), diabetic retinopathy (DR), choroidal neovascularization (CNV), and etc. Neuroinflammation mediated by activated microglia plays a key role in many retinal degenerative diseases as aforementioned. Activated microglial cells display multifaceted changes in all aspects - phenotypically, morphologically and physiological causing damage to neurons and ganglionic cells. Additionally these proinflammatory microglial cells have intense cross-talk with RPE and endothelial cells causing disruption in retinal barriers and leading to infiltration of macrophages thereby making retina viable for disturbed hemostasis and function. Hence, therapeutic strategies that target neuroinflammation will be beneficial.

On other hand delivery of drugs to the eye is a challenge as in free form causes ocular toxicity at therapeutic levels. In many cases the drug molecules are cleared out and requires frequent multiple dosage causing side effects and patient incompliance. Systemic delivery of drugs is not effective in above cases and requires high dosages as only 2% of the injected dose reaches retina but such high dosage may cause systemic toxicity. Dendrimer mediated drug delivery offers many advantages such as high drug pay load, sustained delivery and effective targeting. Dendrimers have been investigated and reported to target and selectively localize in

activated microglia in brain and retina upon systemic and intravitreal injections without any targeting ligands respectively. Hydroxyl terminated (G4-OH) PAMAM dendrimers upon systemic injection are cleared intact from circulation through kidney urine without causing any organ toxicity. Dendrimer – drug conjugates significantly improved therapeutic in animal models of neuroinflammation induced cerebral palsy and retinitis pigmentosa. Based on the literature and preliminary studies from our lab, we are aiming to develop and evaluate PAMAM dendrimer based nanotherapeutics for targeting retinal neuroinflammation via systemic delivery and also investigate their enhanced therapeutic potential of the same both in-vitro and in-vivo. **Four specific goals are persuaded** **1)** Development of G4-OH PAMAM dendrimer-drug conjugates for ocular drug delivery. **2)** Development of G4-OH PAMAM dendrimer based Gene delivery formulation for ocular gene delivery. **3)** Evaluating the ocular biodistribution of dendrimers injected intravenously in ischemia reperfusion (I/R) mice model and **4)** Efficacy of dendrimer-drug conjugates in rat model of CNV. Harnessing the amicable properties of dendrimers having multiple functional groups multiple copies of drug or different kinds of molecules can be conjugated to same dendrimer (multifunctional dendrimer). By choosing appropriate linker (spacer) between the dendrimer and the drug molecule will result in stability of the drug, desired release profile, and high drug payload. Designing and developing the conjugates involves various linking chemistries, modification of surface groups and its proper characterization using various methods.

In this thesis four chapters are discussed. In **Chapter 1** and overview of dendrimer and their role in ocular drug delivery is summarized. The synthesis, characterization and evaluation of *in-vitro* efficacy of dendrimer-triamcinolone acetonide (D-TA) conjugates for sustained treatment of ocular inflammation and neovascularization are described in **Chapter 2**. Designing

and developing a formulation for safe delivery of gene into hard to transfect human retinal pigment epithelial cells (RPE) is described in **Chapter 3**. **Chapter 4** describes the ocular biodistribution and microglial uptake of intravenously and intravitreally injected dendrimer in mice I/R model. **Chapter 5** discusses evaluation of efficacy of the prepared conjugates in rat model of CNV.

CHAPTER 2 "SYNTHESIS, CHARACTERIZATION, AND IN-VITRO EFFICACY OF PAMAM DENDRIMER-TRIAMCINOLONE ACETONIDE CONJUGATES FOR OCULAR DRUG DELIVERY"

2.1 Abstract

Triamcinolone acetonide (TA) is an intermediate acting, potent steroid that has anti-inflammatory and anti-angiogenic activity. It is typically and administered intravitreally for retinal inflammation and neovascularization. Since large concentrations of TA are injected in to the eye due to its insolubility often causes vision blurring, retinal toxicity and damage and elevated IOP. In this study we explore PAMAM dendrimer-TA nanodevice (D-TA) as a potential option to overcome TA's disadvantages. The conjugates have high drug payload (~21%) and were readily soluble in aqueous solutions. D-TA was significantly less toxic than compared to free TA in both microglial and retinal pigment epithelium (RPE) cells which were reported to be involved in pathogenesis of many retinal diseases. Interestingly, the conjugates showed significant suppression of cytokines and VEGF production in activated microglia and hypoxic RPE at ~100 fold lower concentration than compared to free TA. We also demonstrated that D-TA enhanced intracellular transport of TA and also it's enhances intra-nuclear localization via glucocorticoid (GR) receptors.

2.2. Introduction

Synthetic corticosteroids such as Triamcinolone acetonide (TA) have both anti-inflammatory and anti-angiogenic activity and are thereby therefore a popular choice of viable therapeutic options for treating various inflammatory and neovascular ocular pathological conditions [36,37]. Triamcinolone acetonide (TA) on other hand is a FDA- approved gluco-corticosteroid used intravitreally for diabetic macular edema [38], post-operative retinal surgery related inflammation, and other diseases with aforementioned conditions such as choroidal neovascularization (CNV) [39-41], age related macular degeneration (AMD) [42-47], diabetic retinopathy (DR) [45], scleritis and uveitis [46,47].

Several independent in-vitro and clinical investigative studies have been reported the multimodal therapeutic effects of TA [48]. For instance, TA exerts anti-inflammatory effect inhibiting microglial activation by suppressing the release of inflammatory cytokines and nitric oxide (NO) [49, 50]. TA reduces VEGF expression in RPE cultures that were subjected to oxidative stress, which is more similar to the state of pathologic in AMD and similar results were manifested with significant reduction neovascularization in many clinically relevant animal models [51-54]. Intracellular and vascular cell adhesion molecule (ICAM-1 and VCAM-1) and major histocompatibility complexes (MHC-I &II) are the critical components involved in leukocyte and monocyte infiltration, extravasation leading to blood retinal barrier (BRB) disruption and vessel leakage respectively [55]. TA improves BRB health by enhancing the expression of adhesion molecules in endothelial cells [56], and significantly suppressing the blood vessel formation in choroidal endothelial cells [57].

One advantage of possible explanation for the prolonged activity of intravitreal TA has prolonged duration of action possiblyis that it may form epi-retinal crystals in the vitreous due to its lack of solubility, acting as drug depot, due it its insolubility and hydrophobic nature making them to form crystals in vitreous and act as depot injection [58], though this characteristic has also been attributed to toxicity problems. When injected intravitreally, precipitation of TA in vitreous. This precipitation can cause visual obscurity with unequal distribution, and as time progress they tend to settle forming epi-retinal crystals causing mechanical damage and local toxicity to the retinal tissue [58, 59]. To address insolubility and sedimentation issues, TA formulations with benzyl alcohol or benzalkonium chlorides as vehicle preservatives were commercialized but resulted in vehicle- mediated toxicity and sterile-endophthalmitis [60, 61]. Other side effects associated with TA are evaluation of intraocular pressure (IOP), cataractogenesis and photoreceptor cell death [62].

PAMAM dendrimers are the class of branched polymeric nanocarriers that are being investigated for ocular drug and gene delivery [63, 64]. Their amicable properties such as small size, multivalency and water solubility allows high pay load for many biologically unstable drugs [65, 66]. Therefore, dendrimer-TA conjugates may be a viable formulation for targeted intracellular delivery of TA. Upon intravitreal administration, Dendrimer dendrimer fluocinolone acetonide (D-FA) conjugates upon intravitreal injection selectively co-localized in activated microglial cells and attenuated retinal inflammation for a period of 30 days at a 30- fold lower concentration than that of free drug [67]. Upon systemic administration, dendrimer N-acetyl cysteine conjugates (D-NAC) accumulates accumulated selectively only in the area of inflammation in the brain and dendrimer N-Acetyl cysteine conjugates (D-NAC) shown to attenuated neuroinflammation and improved the motor function in rabbit model of cerebral palsy

[68, 69]. We have reportedreported dendrimer-TA based gene delivery platform for safe delivery gene and enhanced transfection in human retinal pigment epithelial cells [70]. PAMAM dendrimer formulations increase the solubility of drugs such as pilocarpine, brimonidine and etc. in aqueous solutions by acting as cargos with drugs encapsulated in their cores, thereby enhancing their bioavailability and permeation in ocular tissues [71, 27].

In this chapter we investigate the ability of PAMAM dendrimers to deliver TA into human retinal pigment epithelial cells (hRPE). We synthesize, characterize and evaluate the efficacy of dendrimer-TA conjugates, relating to its anti-inflammatory and anti-VEGF activity. With all the preliminary data described above in the consideration, in this article we describe the synthesis and characterization, cytotoxicity and in vitro efficacy of generation 4 hydroxyl PAMAM dendrimer-TA conjugate (D-TA) with high loading (~21%). The conjugates demonstrate superior solubility in aqueous solutions that free drug, sustained release, significantly enhanced anti-inflammatory and anti-VEGF activity with very low toxicity. We have show that D-TA conjuagtes also demonstrated the D-TA conjugates have result enhancedin enhanced cellular uptake, and with no compromise binding to glucocorticoid receptors and nuclear translocation in human retinal pigment epithelial cells.

2.3. Material and methods

2.3.1 Chemicals and reagents.

Hydroxyl- and amine- functionalized ethylenediamine core generation four PAMAM dendrimers (G4-OH; diagnostic grade; 64 end-groups) were purchased from Dendritech Inc. (Midland, MI, USA). Triamcinolone acetonide (TA), glutaric anhydride, piperidine, N,N'-diisopropylethylamine (DIEA), trifluoroacetic acid (TFA), anhydrous dimethylformamide

(DMF), dimethylacetamide (DMA) and 6-(Fmoc-amino) caproic acid were purchased from Sigma-Aldrich (St. Louis, MO, USA). (Benzotriazol-1-yloxy)tripyrrolidino-phosphonium hexafluorophosphate (PyBOP) was purchased from Bachem Americas Inc. (Torrance, CA, USA). Cy5-mono-NHS ester was purchased from Amersham Biosciences-GE Healthcare (Pittsburgh, PA, USA). ACS grade DMF, dichloromethane (DCM), diethylether, hexane, ethyl acetate, HPLC grade water, acetonitrile, and methanol were obtained from Fisher Scientific and used as received for dialysis, purification and column chromatography. Dialysis membrane (MW cut-off 1000 Da) was obtained from Spectrum Laboratories Inc. (Rancho Dominguez, CA, USA).

The reactions were carried out under nitrogen. Thin-layer chromatography (TLC) was performed on silica gel GF254 plates (Whatman, Piscataway, NJ), and the spots were visualized with UV light. Proton NMR spectra of the final conjugates as well as intermediates were recorded on a Bruker (500 MHz) spectrometer using commercially available DMSO-d6 solvent. Proton chemical shifts were reported in ppm (δ) and tetramethylsilane (TMS) used as internal standard. All data were processed using ACD/NMR processor software (Academic Edition).

2.3.2. Synthesis of Triamcinolone acetonide-21-glutarate (TA-linker, *1*)

TA (300 mg, 0.69 mmol) was dissolved in 10 mL of DMF/DMA mixture (8:2) in a 50 mL round bottom flask under nitrogen atmosphere. Glutaric anhydride (158 mg, 1.38 mmol) dissolved in 5 mL of DMF/DMA mixture (8:2), and 0.35 mL of TEA were added to it and the reaction mixture was stirred for 48 h to complete the reaction. The completion of the reaction was monitored by thin layer chromatography using ethyl acetate/methanol (95:5) as mobile phase. The solvent was evaporated under reduced pressure and the crude product was purified

with column chromatography by passing through silica gel using ethyl acetate:methanol (99:1) as eluent to get TA-*21*-glutarate (348 mg, >90% yield). The obtained purified product was characterized by using ^{1}H NMR spectroscopy. ^{1}H NMR (DMSO-d_6): δ 0.81 (s, 3H, -CH_3), 1.13 (s, 3H, -CH_3), 1.33 (s, 3H, -CH_3), 1.47-1.56 (m, 5H, -CH_2 and -CH_3), 1.68-2.04 (m, -CH_2 of linker and -C*H* proton of TA), 2.20-2.34 (m, -CH_2 of linker and -C*H* protons of TA), 2.43-2.47 (t, -CH_2 protons of linker), 2.57-2.64 (m, 1H, -C*H*), 3.57 (s, 1H, -CH), 4.18 (brs, 1H, -C*H*), 4.72-4.85 (m, 2H, -C*H*), 5.11-5.15 (d, 1H, -C*H*), 5.47-5.48 (d, 1H, -C*H*), 6.00 (s, 1H, aromatic proton), 6.21-6.24 (dd, 1H, aromatic proton), 7.26-7.29 (d, 1H, aromatic proton), 12.10 (bs, 1H, COO*H* proton).

2.3.3. Synthesis of Dendrimer-Triamcinolone acetonide conjugates (D-TA, 2).

TA-21-glutarate (TA-Linker,139.8 mg, 0.255 mmol) was dissolved in anhydrous DMF (5 mL) in a 50 mL round bottomed flask under nitrogen, to which PyBOP (266.2 mg, 0.516 mmol) dissolved in DMF (5 mL) and DIEA (200 μL) was added, and the reaction mixture was allowed to stir for 1 hour in an ice bath. PAMAM G4-OH (238.8 mg, 0.017 mmol) dissolved in anhydrous DMF (10 mL) was added drop wise to the reaction mixture above, and stirred for 48 hours under nitrogen. The mixture of solvents was evaporated at 25°C under vacuum. The crude product was redissolved in DMF (20 mL) and subjected to dialysis in DMF (membrane MW cutoff = 1 kDa) for 24 hours, where the solvent was changed at least 4 times. The obtained solution was evaporated under reduced pressure at room temperature, followed by high vacuum overnight, to produce an off-white semi-solid dendrimer-triamcinolone conjugate (D-TA, 470.9 mg). The resultant semi solid product was dissolved in ice cold DI water and dialyzed against DI water (membrane MWCO = 1 kDa) at 4ºC for 5 hours by changing the water every hour to remove traces of DMF. The resultant water layer was lyophilized to get fluffy white powder of

D-TA (402.3 mg) (Figure S1-B). The D-TA conjugates were characterized by ^{1}H NMR for drug loading and reverse-phase HPLC for purity. 1H NMR (DMSO-d6) δ 0.82 (s, -CH3 protons of TA), 1.14 (s, -CH3 protons of TA), 1.34 (s, -CH3 protons of TA), 1.49 (s, -CH3 protons of TA), 1.53-2.05 (m, -CH protons of TA, -CH2 protons of linker), 2.20 (brs, -CH2 protons of G4-OH), 2.31-2.48 (m, -CH protons of TA, -CH2 protons of linker, -CH2 protons of G4-OH), 2.64 (bs, -CH2 protons of G4-OH), 3.09-3.11 (t, -CH2 protons of G4-OH), 3.28 (m, -CH2 protons of G4-OH), 3.38-3.40 (t, -CH2 protons of G4-OH), 3.58 (s, -CH protons of TA), 4.00-4.02 (m, CH2OC=O protons, G4-OH), 4.20 (brs, -CH protons of TA), 4.73-6.01 (singlets and doublets, -CH protons of TA, OH protons of G4-OH), 6.22-7.31 (two doublets, aromatic protons of TA), 7.79-8.07 (m, amide protons of G4-OH).

2.3.4. Synthesis of bifunctional dendrimer (D-OH-NHFmoc, 3)

Fmoc-caproic acid (62.3 mg, 0.176 mmol) was dissolved in DMF (5 mL) in a 50 mL round bottom flask under nitrogen environment. PyBOP (152.7 mg, 0.2935 mmol) dissolved in DMF (5 mL) and DIEA (150 μL) were added, and the reaction mixture was allowed to stir for 1 h in an ice bath. Finally, PAMAM G4-OH (164.4 mg, 0.022 mmol) dissolved in anhydrous DMF (10 mL) was added to the reaction mixture and stirred for 48 h. The mixture of solvents was evaporated at 25°C under vacuum. The crude product was redissolved in DMF (20 mL) and subjected to dialysis in DMF (membrane MW cutoff = 1 kDa) for 26 h by changing the solvent at least 3 times. The obtained solution was evaporated under reduced pressure at room temperature, and the final product was subjected to high vacuum overnight, to produce an off-white semi-solid Fmoc-functionalized dendrimer (D-OH-NHFmoc, 3, 190 mg). ^{1}H NMR (DMSO-d6) δ 1.24-1.51 (m, CH2 protons of linker), 2.26 (bs, CH2 protons of G4-OH), 2.38-2.47 (m, CH2 protons of G4-OH, and CH2 protons of linker), 2.73 (CH2 protons of G4-OH),

3.12-3.13 (CH2 protons of G4-OH), 3.28 (CH2 protons of linker), 3.39-3.42 (CH2 protons of G4-OH) 4.00 (bs, CH2OC=O protons of G4-OH), 4.20 (bs, CH proton of Fmoc group), 4.29 (bs, OCH2 protons of Fmoc group), 4.73 (bs, OH protons of G4-OH), 7.26-7.68 (m, aromatic protons of Fmoc), 7.88-8.07 (m, aromatic protons of Fmoc, and internal amide protons of G4-OH).

2.3.5. Synthesis of Fmoc-functionalized dendrimer-Triamcinolone acetonide conjugate (4)

TA-linker (107.6 mg, 0.196 mmol) was dissolved in 5 mL of anhydrous DMF under nitrogen atmosphere in a 50 mL round bottomed flask, and PyBOP (255.5 mg, 0.49 mmol) and DIEA (220 μL) were added to it. The reaction mixture was stirred at 0°C in an ice bath for 30 min followed by the addition of D-OH-NHFmoc (227.2 mg, 0.013 mmol) dissolved in DMF (10 mL), and the reaction was allowed to stir for 48 h under nitrogen condition. The reaction mixture was evaporated under reduced pressure and dialyzed in DMF for 24 h, while the solvent was replaced every 6 h (dialysis membrane cutoff = 1 kDa) to remove the unreacted starting materials and byproducts. The resultant DMF was evaporated, and the conjugate was dissolved in water and re-dialyzed against water for 6 h and lyophilized to get Fmoc-functionalized D-TA conjugate (4) as an off-white color solid product (280 mg). The conjugate was characterized by ^{1}H NMR, and the drug loading was assessed using the proton integration method.

2.3.6. Synthesis of bifunctional dendrimer-triamcinolone acetonide conjugates (NH2-D-TA, 5)

The Fmoc-functionalized dendrimer intermediate (4, 180 mg) was dissolved in anhydrous DMF (10 mL) and piperidine/DMF (2:8; 10 mL) was added to it under nitrogen. The reaction mixture was stirred for 30 min. and solvent was evaporated under vacuum at room temperature. The resultant crude product was subjected to dialysis in DMF (membrane MWCO = 1 kDa) for

24 h. The solvent was evaporated and the conjugate was re-dialyzed against water for 3-4 h and lyophilized to get NH2-D-TA, 5 (120 mg) as off-white solid product with free amine groups. ^{1}H NMR (DMSO-d6) δ 0.83 (s, -CH3 protons of TA), 1.15 (s, -CH3 protons of TA), 1.24-1.53 (m, -CH3 protons of TA, and -CH2 protons of linker), 1.71-2.06 (m, -CH protons of TA), 2.21-2.65 (m, -CH2 protons of G4-OH, -CH protons of TA), 3.10-3.12 (t, -CH2 protons of G4-OH), 3.28 (bs, -CH2 protons of G4-OH), 3.39-3.41 (t, -CH2 protons of G4-OH), 4.01 (d, CH2OC=O protons of G4-OH), 4.20-7.31 (singlet and doublet, -CH and aromatic protons of TA), 7.80-8.07 (m, amide protons of G4-OH).

2.2.7. Synthesis of Cy5-labeled dendrimer-triamcinolone acetonide conjugates (Cy5-D-TA, 6).

The NH2-D-TA (5), (25 mg, 0.0013 mmol) was dissolved in 1 mL of borate buffer (pH 9.0) at room temperature. The reaction mixture was cooled to 0°C, and Cy5 mono NHS ester (2.18 mg, 0.0027 mmol) dissolved in 1 ml of DMF was added. N-Hydroxysuccinimide (1.58 mg, 0.013 mmol) dissolved in 500 μL of DMF was added to reaction. The reaction mixture was stirred overnight at room temperature. The crude product was dissolved in water and subjected to dialysis against pure DI water (membrane MWCO = 1 kDa) for 12 hours with successive change of water in every 2 hours at 4ºC. The resultant water layer was lyophilized to get Cy5-D-TA, 5 (12.8 mg). The Cy5-D-TA was characterized by reverse-phase HPLC for purity, and fluorescence spectroscopy. ^{1}H NMR (DMSO-d6) δ 0.82 (s, -CH3 protons of TA), 1.14 (s, -CH3 protons of TA), 1.23-1.26 (m, -CH2 protons of linker), 1.34 (s, -CH3 protons of TA), 1.48-1.52 (s, -CH3 protons of TA, -CH2 protons of linker), 1.69-2.04 (m, -CH protons of TA, -CH2 protons of linker), 2.20 (bs, -CH2 protons of G4-OH), 2.39-2.47 (m, -CH protons of TA, -CH2 protons of linker and -CH2 protons of G4-OH), 2.64 (bs, -CH2 protons of G4-OH), 3.09-3.11 (t,

-CH2 protons of G4-OH), 3.38-3.40 (t, -CH2 protons of G4-OH), 4.00-4.01 (d, CH2OC=O protons of G4-OH), 4.20-7.33 (singlet and doublet, -CH and aromatic protons of TA and Cy5), 7.65 (s, aromatic protons of Cy5), 7.79-8.05 (m, amide protons of G4-OH), 8.38 (m, aromatic protons of Cy5).

2.4. Characterization of the conjugates

2.4.1 High performance liquid Chromatography (HPLC).

The purity of the dendrimer conjugates was analyzed by HPLC (Waters Corporation, Milford, MA) equipped with a 1525 binary pump, a 2998 photodiode array (PDA) detector, a 2475 multi-wavelength fluorescence detector, and a 717 auto sampler (kept at 4°C) interfaced with Empower software. The HPLC chromatograms were monitored at 205 (G4-OH) and 238 nm (TA conjugated dendrimers) using PDA detector. For Cy5-labelled conjugates, fluorescence detector was used for the detection (excitation: 645 nm and emission: 662 nm). The water/acetonitrile (0.1% w/w TFA) was freshly prepared, filtered, degassed, and used as mobile phase. A TSK gel ODS-80 Ts (250 X 4.6 mm, i.d., 5 μm) with TSK gel guard column were used for the study (Tosoh Bioscience LLC, Japan). A gradient flow was used with initial condition of 90:10 (H2O/ACN) was maintained until 20 min and gradually changing the ratios to 10:90 (H2O/ACN) at 40 min and returning to initial conditions 90:10 (H2O/ACN) in 60 min with flow rate of 1 mL/min for all conjugates.

2.4.2 Dynamic light scattering (DLS) and Zeta potential (ζ).

The particle size and ζ-potential of G4-OH, PEG and their respective conjugates were determined by dynamic light scattering (DLS) using a Zetasizer Nano ZS (Malvern Instrument Ltd. Worchester, U.K) equipped with a 50 mW He-Ne laser (633 nm). The conjugates (G4-OH,

D-TA and NH2-D-TA) were dissolved in deionized water (18.2 Ω) to make the solution with the final concentration of 0.1 mg/mL. The solution was filtered through a cellulose acetate membrane (0.45 micron, PALL Life Science) and DLS measurements were performed in triplicate, at 25°C with a scattering angle of 173°.

2.4.3 Drug release study in simulated vitreous humor.

The release of TA from the D-TA conjugate was characterized in simulated vitreous humor [Hanks balanced salt solution with 0.03% sodium hyaluronate (Lifecore biomedical, MN, USA) and 0.1% Tween 80 (DakoCytomation, CA, USA)] as a stabilizer and surfactant to reduce released TA settling. A concentration of 3mg/mL was maintained in water bath at 37ºC equipped with shaker. At appropriate time points, 200µL of solution was withdrawn from the incubation mixture, frozen in liquid nitrogen and lyophilized. To this lyophilized powder, 400µL of 50:50 (DCM:EtOAc) was added and sonicated for 10 min and centrifuged at 10,000 rpm for 5min at 4ºC. The supernatant was collected and the solvent was evaporated by nitrogen flush and reconstituted with 200µL of 50:50 H2O:ACN and subjected to HPLC analysis following the method described in HPLC section. The percent of released TA from D-TA was quantified using the calibration graph.

2.5 In-vitro characterization of the conjugates.

2.5.1 Cell culture.

Murine brain microglial cells (BV-2) passage 18 (P:18) were cultured in Dulbecco's modified Eagle's medium (DMEM, Life technologies, Grand Island, NY) supplemented with 5% heat in activated fetal bovine serum (Hi-FBS, Invitrogen Corp., Carlsbad, CA) and 1% antibiotics (penicillin/streptomycin) (Invitrogen Corp., Carlsbad, CA). Human retinal pigment

epithelial cells (ARPE-19) passage 21 (P: 21) were cultured in DMEM/F12(1:1) (Life technologies, Grand island, NY) supplemented with 10% HI-FBS and 1% antibiotics. The above mentioned cell cultures were in a humidified incubator at 37 °C with 5% CO2.

2.5.2 Cytotoxicity assay.

BV-2 and ARPE-19 cells were plated at a concentration of 1.0x104/well in a 96 well plate (Costar, Cambridge, MA) and incubated at 37ºC for 24 hrs in their respective growth medium. After 24 hrs the cells were treated with medium containing different concentrations (0.1-200µg) of TA and D-TA at increasing concentrations for 24 hrs. The cells treated with fresh medium serves as control. Cell viability was assessed by using MTT cell proliferation assay kit (Molecular probes, Invitrogen, Oregon, USA). Absorbance was read at 540 nm using fluorescence microplate reader (BioTek Instruments, Winooski, Vermont, USA) and cell viability was determined as percent absorbance relative to untreated control cells.

2.5.3 Anti-inflammatory assay in microglial cells.

Microglial (BV-2) cells were plated at a concentration of 1X106 cells per well in a 12 well plate. After 24hrs the microglial cells were activated using Lipopolysaccharides (LPS) (Sigma, St Louis, MO) at a concentration of 100ng/mL for 3hrs. After 3hrs of pre-activation of microglial cells the activated microglial cells confirmed as they assume an amoeboid shape, the cells were treated with 1mL of medium with 100ng of LPS containing various concentrations of free TA (1-100µg) and D-TA containing equivalent concentration conjugated TA that of free TA treated for 12hrs. A stock solution of 10mg/mL of free TA was prepared by dissolving TA in absolute ethanol and subjected to serial dilution immediately to obtain desired concentration thereby avoid settling of TA particles in aqueous medium. Whereas D-TA being water soluble

was dissolved in medium and serially diluted to obtain desired concentrations. After 12 hours the medium containing free TA and D-TA were removed and the cells were washed with warm medium and replenished with new medium containing LPS.

The cell culture medium was sampled at 24 hours and 48 hours, immediately centrifuged at 1500 rpm for 5 min at 4ºC and subjected for TNF-α cytokine levels using a mouse TNF-α ELISA kit (R&D systems, Minneapolis, MN, USA).

2.5.4 Anti-VEGF activity in oxidative stress exposed retinal pigment epithelial cells.

Retinal pigment epithelial cells (ARPE-19) cells were plated at an initial concentration of 1x106 cells per well in a 12 well plate. After 24hrs the medium was changed every day until day 5 to form RPE monolayers. The monolayers were exposed to hypoxia in a low oxygen incubator in a humidified atmosphere for 8hrs and medium is rapidly changed to fresh medium and incubated normal culture conditions (reoxygenation) for 2hrs. After reoxygenation the monolayers were exposed to various concentrations of free TA and D-TA containing equivalent concentrations of TA in conjugated form for 24 hours. The monolayers with no treatment serves as positive control and the monolayers which were not exposed to hypoxia serve a negative control. After 24hrs of treatment the treatment medium was removed and the monolayer was washed with warm medium twice to remove any TA or D-TA particles and replaced with fresh medium and incubated at 37ºC overnight (18 hours). The culture medium was collected in 2 mL vials and centrifuged at 1000 rpm for 5 min at 4ºC to remove debris, the supernatant was immediately assessed for VEGF levels were assessed using human VEGF ELISA kit (R&D systems, Minneapolis, MN, USA). Optical density at the end point was measured at 540nm with wavelength correction at 570nm using fluorescence microplate reader (BioTek Instruments,

Winooski, Vermont, USA). The VEGF levels were calculated using the calibration graph according to the manufacturer's instructions.

The monolayers were subjected to trypsin treatment and the cell pellets were collected via centrifugation. Total RNA was purified with TRIzol reagent (Life Technologies, Grand Island, NY) following the manufacturer's instruction. 3 μg of total RNA were reverse-transcribed to cDNA using High-capacity cDNA Reverse Transcription System (Life Technologies) according to the manufacturer's instructions. qRT-PCR was performed with fastSYBR Green Master Mix (Life Technologies) by a StepOnePlus Real-Time PCR System (Life Technologies). The sequence of primer used for human VEGF forward primer 5′-CAGCGCAGCTACTGCCATCCAATCGAGA-3′, and reverse primer, 5′-GCTTGTCACATCTGCAAGTACGTTCGTTTA-3′ was used for amplification. Human GAPDH forward 5'-AATCCCATCACCATCTTCCA-3', reverse 5'-TGGACTCCACGACGTACTCA-3' was used to normalize the expression levels of target gene and calculated by the comparative cycle threshold Ct method (2-ΔΔCt).

2.6 Cell uptake and intracellular localization of D-TA

2.6.1 Flow cytometry.

The cellular uptake of Cy5-D-TA was measured via flow cytometric analysis. Cells were seeded in 12-well plates at an initial concentration of 1.0 × 105 cells/well and left to attach overnight. Cells were incubated with Cy5-D-TA or D-Cy5 at 2 μg/ml; at different time points (1, 3,6 and 12 hours) the media was removed and cells were washed with 1x PBS as well as Trystan blue prior to being incubated with 1 volume of 0.25% Trypsin with EDTA for 5 min at 37°C. Two volumes of DMEM medium with 10% FBS were added to neutralize trypsin. The cellular

uptake of D-TA was measured using the Accuri C6 flow cytometer (BD Biosciences, San Jose, CA) with an FL4 band-pass filter with emission detection wavelength of 675/25 nm. Data were analyzed using the BD Accuri C6 software. The thresholds were set using untreated samples.

2.6.2 Confocal microscopy.

ARPE-19 cells were seeded at a concentration of 1x105 in a glass 35 mm glass bottom culture dish (MatTek Corporation, Ashland, MA). The cells were incubated with Cy5-D-TA or D-Cy5 at 2 μg/mL and at different time points (1 h, 3 h, 6 h and 12 h) the media was removed and cells were washed with 1x PBS twice and fixed with 4% PFA and blocked with normal goat serum (NGS) for 2hrs at 4ºC. The blocked cells were stained for glucocorticoid receptors (GR) using anti-GR antibody (abcam) (1:200) overnight at 4ºC and then goat α rabbit Cy3 conjugated secondary antibody (life techonologies) (1:100) for 4 hours. The cells were washed and stained with DAPI (1:1000) for 10 min and imaged using confocal Zeiss LSM 710 microscope.

2.7. Results and discussions

2.7.1. Preparation of Triamcinolone acetonide-21-glutarate (TA-linker, 1)

TA was functionalized with a carboxylic acid terminal group using glutaric acid as linker since an acid group is required to conjugate with the dendrimer according to a previously published procedure. In brief, TA was reacted with glutaric anhydride dissolved in DMA/DMF mixture in presence of triethylamine (TEA) as base to get the TA-linker (**Figure 5**). The TA-linker was characterized by ^{1}H NMR. TA has two reactive hydroxyl groups and the most reactive 21-position hydroxyl group has reacted with glutaric acid via ester bond. Apart from the protons signal from TA, an additional multiplet at 1.79 (CH2 protons of linker), and two triplets at 2.32 and 2.47 (CH2 protons of linker) confirmed the formation of the TA-linker. A characteristic

peak at 12.12 ppm belonging to carboxylic acid confirmed that TA-linker has one acid group **(Figure 6).**

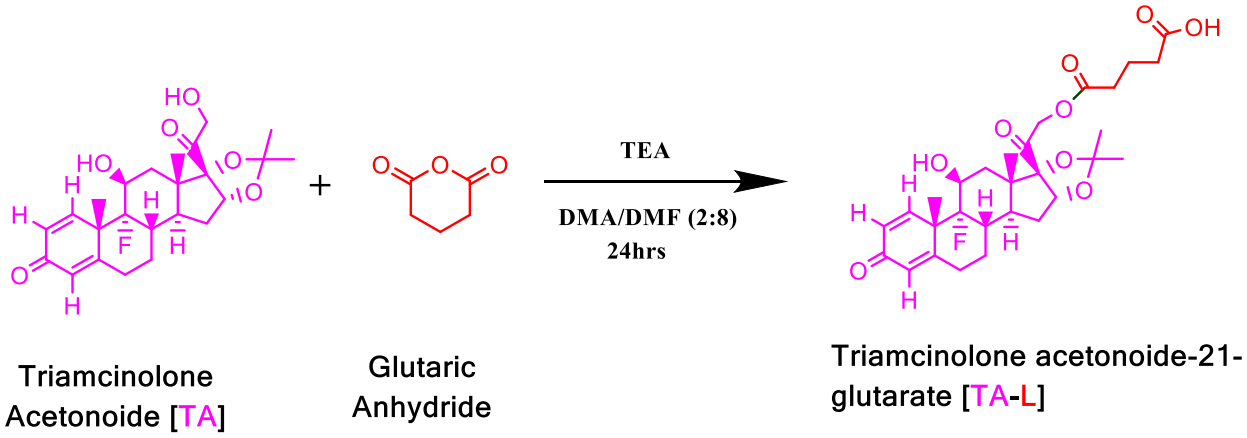

Figure 5: Synthesis of Triamcinolone acetonide linker

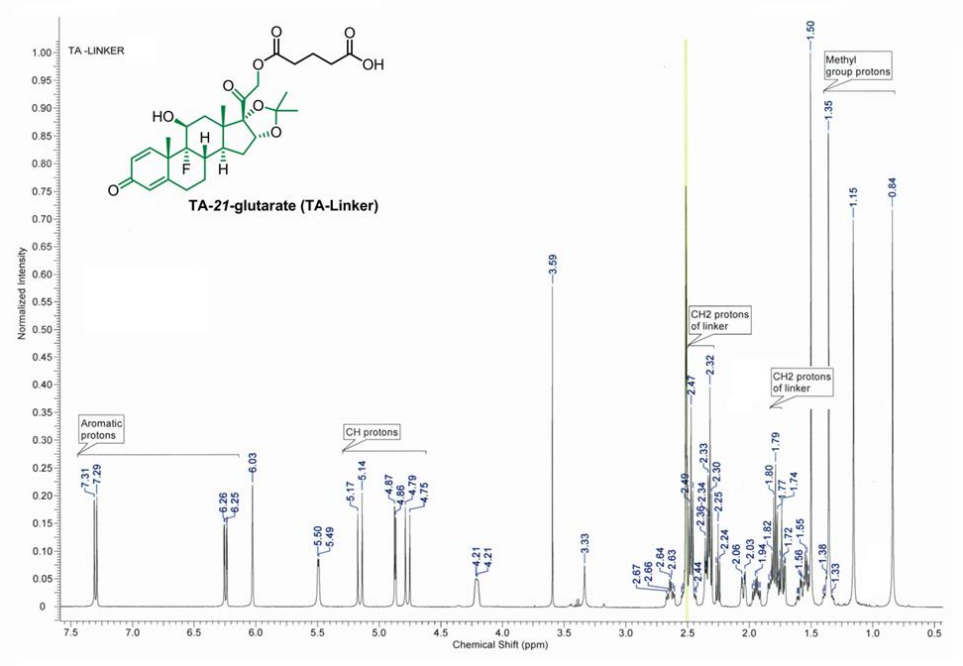

Figure 6: ^{1}H NMR spectrum of triamcinolone acetonide-21-glutarate (TA-linker) in DMSO-d_6.

2.7.2. Preparation of dendrimer-TA conjugate (D-TA, 2)

The ester-linked dendrimer-triamcinolone acetonide (D-TA, 2) was prepared by a two-step process as shown in **Figure 7**, and characterized by ^{1}H NMR and HPLC. TA was functionalized with a carboxylic acid terminal group using glutaric acid as spacer. In brief, TA was reacted with glutaric anhydride dissolved in DMA/DMF mixture in presence of a base to get the TA-linker (1). The most reactive hydroxyl group at 21-position was reacted with anhydride to get an ester linkage. The structure of TA-linker was established by 1H NMR and the purity was determined by HPLC. In 1H NMR, characteristic peaks at 1.79, 2.32 and 2.47 ppm for CH2 protons of the linker, and a peak at 12.12 ppm corresponding to carboxylic acid confirmed the formation of the TA-linker. The TA-linker was further conjugated with PAMAM dendrimer (G4-OH) using PyBOP as coupling reagent to get therapeutic conjugate, D-TA (2). In 1H NMR spectrum, four peaks in between 0.82-1.49 ppm represent methyl protons of the TA. Additionally, as shown in **Figure 8A**, apart from dendrimer and TA peaks in between 2.0-8.1 ppm, a characteristic peak at 4.01 ppm was observed which corresponds to methylene protons of the dendrimer reacted with TA. Using NMR proton integration technique, we estimated that approximately 10 molecules of TA were conjugated to one dendrimer molecule (~21%). The conjugate is readily soluble in DI water, PBS buffer and saline, in contrast to free TA which has poor water solubility (**Figure 16**). The maximum solubility of free TA reported to be 21 μg/mL in PBS [38], whereas achieved-TA is soluble up to 4 mg/mL (on a TA basis), and corresponds to a 200-fold enhancement in solubility.

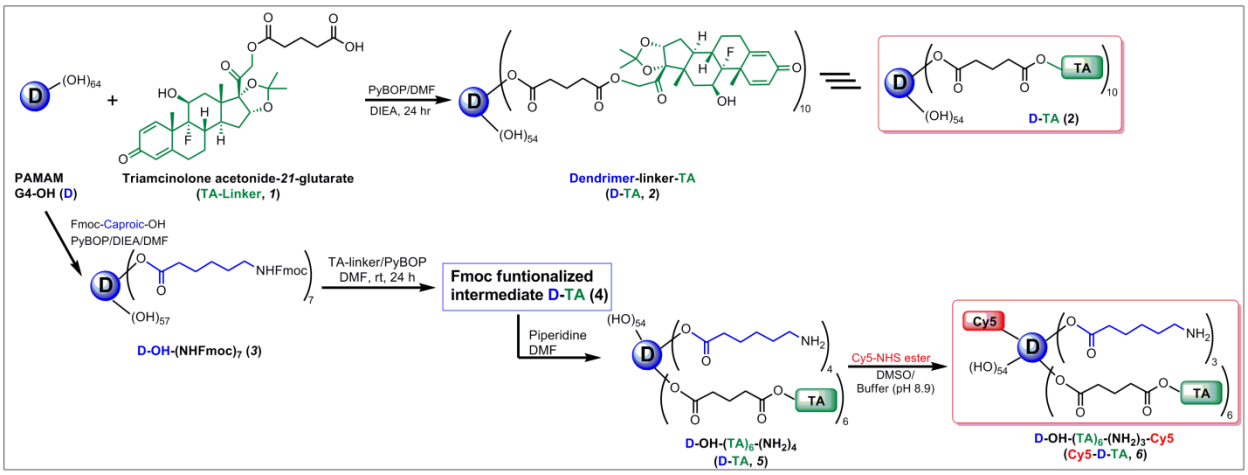

Figure 6: Preparation of the dendrimer conjugates. Preparation of the dendrimer-triamcinolone acetonide conjugate (D-TA, **2**); and Cy5-labeled dendrimer-TA conjugate (Cy5-D-TA, **6**).

The purity of the conjugate and the TA-linker were determined using reverse phase HPLC. The hydrophobic free TA eluted at 37.1 min, whereas the TA-linker eluted at 39.0 min (with no trace at 37.1 min) At similar HPLC conditions, a broad peak at 36.0 min was observed for D-TA conjugate (monitored at 238 nm) which is different from that for the starting dendrimer (retention time 15 min). The conjugate is largely pure since we did not observe any 'characteristic' peaks related to free TA and TA-linker. The broad peak of D-TA conjugate can be attributed to the high loading of TA (~10 molecules per dendrimer) resulting in some non-polar character (**Figure 9A**).

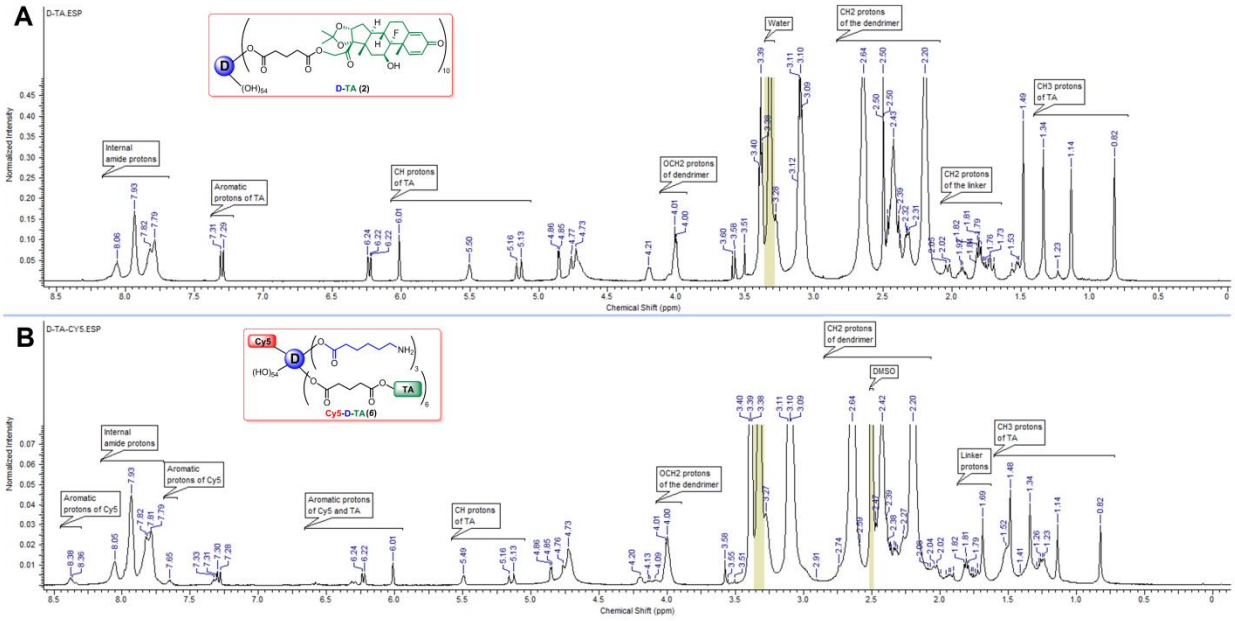

Figure 7: Proton NMR spectra of dendrimer-triamcinolone acetonide conjugate (D-TA, **2**) and Cy5-labelled dendrimer-TA conjugates (Cy5-D-TA, **6**) in DMSO-d_6.

2.7.3. Preparation of Cy5 labelled dendrimer-triamcinolone acetonide conjugate (Cy5-D-TA, 6)

The Cy5-D-TA conjugate was prepared using a four-step process following a modified synthetic procedure published recently [64], **(Figure 7**). In the publication mentioned above, we have reported the preparation of Cy5-D-TA conjugate with more than 20 surface amine groups for the gene delivery study. For the present study, we designed Cy5-D-TA (6) with fewer amine groups on the surface of the conjugate, so that we could reacts approximately one molecule of Cy5. In brief, Fmoc-caproic acid was reacted with the dendrimer using PyBOP as coupling agent, to get Fmoc-functionalized dendrimer (D-OH-NHFmoc, 3). Three multiplets (1.24-1.51 ppm) for caproic acid CH2 protons, a singlet at 4.00 ppm for internal CH2 protons of G4-OH, and multiplets between 7.26-7.68 ppm for Fmoc aromatic protons in NMR spectra confirmed the formation of the intermediate (**Figure 8**). Using proton integration method, it was estimated that

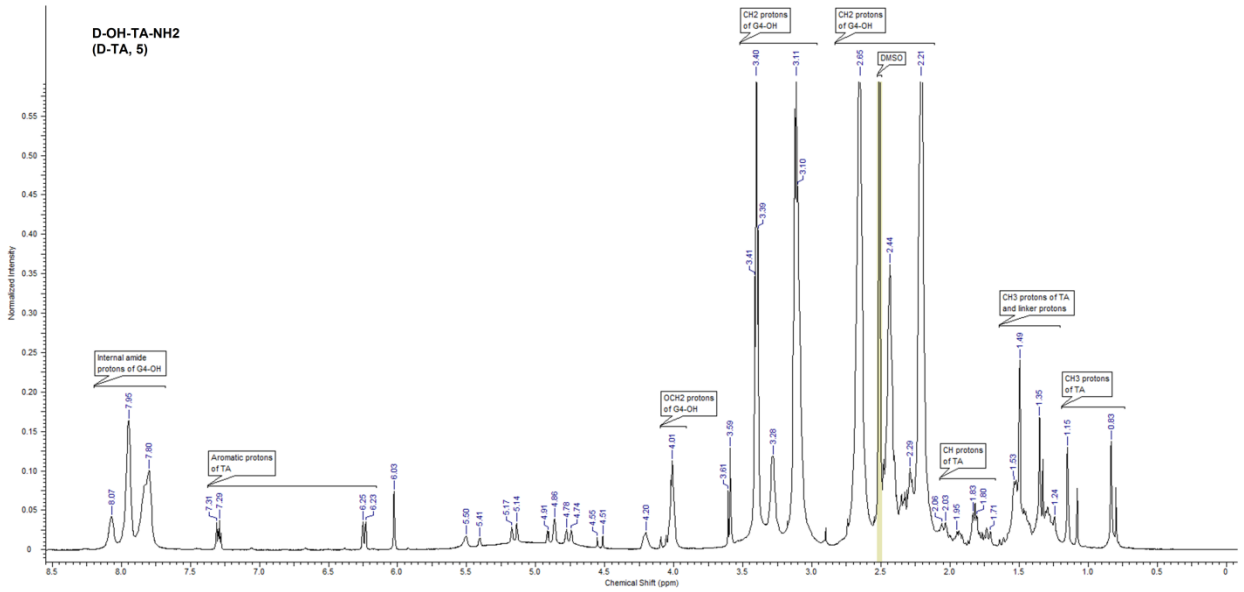

Figure 8: Proton NMR spectrum of dendrimer- triamcinolone acetonide conjugate (NH_2-D-TA, ***5***) in DMSO-d_6

7 linker molecules were reacted with the dendrimer. Further, the Fmoc-functionalized dendrimer (3) was reacted with TA-linker using PyBOP/DIEA to get Fmoc functionalized D-TA (4). In the ^{1}H NMR spectrum, peaks at 0.84-1.50 ppm represent methyl protons of TA, and peaks at 4.75-6.25 ppm represent aromatic protons of TA along with dendrimer peaks confirmed the formation of the conjugate. The Fmoc groups were deprotected with piperidine in DMF to get dendrimer-TA conjugate (NH2-D-TA, 5) and characterized by ^{1}H NMR. The NH2-D-TA conjugate has few free amine groups which would react with Cy5. In the NMR spectrum, absence of aromatic Fmoc protons signal and presence of all signals related to TA confirmed the formation of the product. As per proton integration analysis, 6 molecules of TA and ~3 amine groups were present in NH2-D-TA conjugate. Finally, Cy5-mono-NHS ester was reacted with NH2-D-TA in DMSO/buffer (pH 8.9) mixture to get Cy5-labeled dendrimers-TA conjugate, Cy5-D-TA (6). The final conjugate was purified by dialysis and further by GPC fractionation and characterized by reverse-phase HPLC and NMR spectroscopy. In NMR spectrum, peaks corresponding to TA

and linker molecules were present as mentioned above along with Cy5 peaks (**Figure 7B**). In HPLC analysis free Cy5 eluted at 15.05 min whereas Cy5-D-TA eluted at 33.08 min as a broad peak (monitored at 645 nm excitation) confirming the formation of the conjugate free from unreacted dye (**Figure 9B**). Since one molecule of Cy5 dye was used in the reaction, we could not see intense peak in the NMR spectrum in aromatic region.

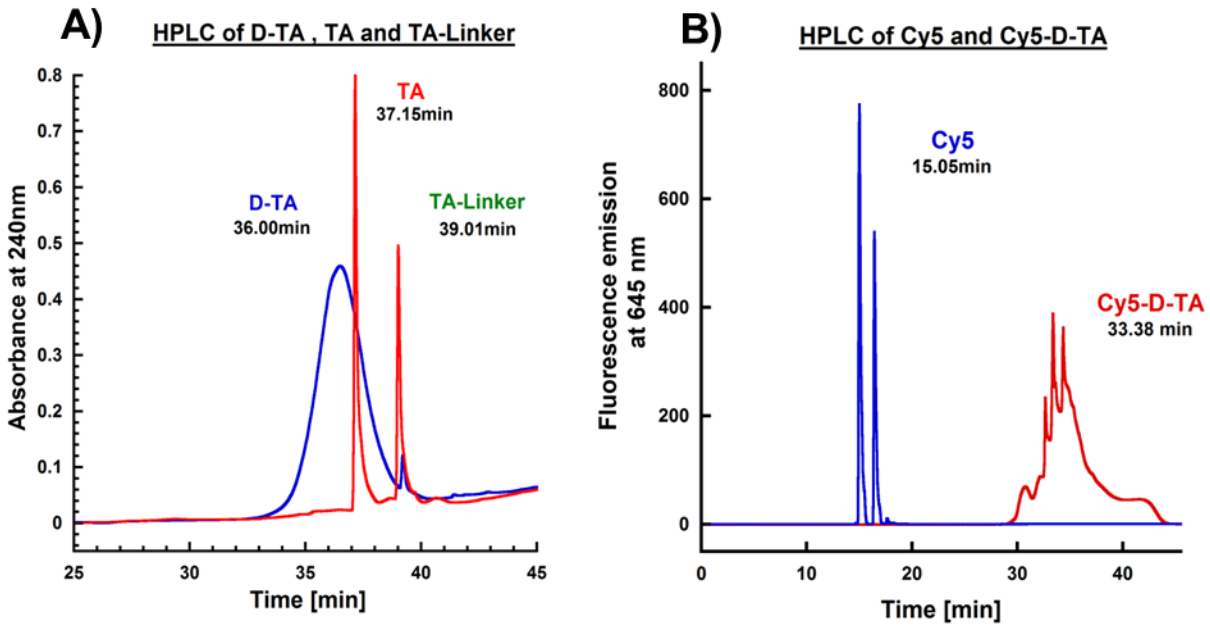

Figure 9: HPLC chromatogram of **A)** D-TA and **B)** Cy5-D-TA conjugates.

2.7.4. Particle size and zeta potential

Size and surface charge of the dendrimer conjugate influences its cellular entry, receptor binding or targeting to specific site of the tissue [57, 74]. We investigated the particle size and zeta potential G-OH (D), D-TA, and NH2-D-TA. The size of G4-OH was 4.4 ± 0.2 nm and zeta potential was slightly positive (4.5 ± 0.2 mV) due to their tertiary amines in its core. Upon conjugating ~10 molecules of TA to the dendrimer there was small increase in size (5.2 ± 0.3 nm), but there was no change in its surface charge (4.2 ± 0.7 mV). In the case of NH2-D-TA

conjugate the size and zeta potential were 5.0 ± 0.5 nm and 5.9 ± 0.2 mV respectively. There is a small increase in the zeta potential due to the presence of 3-4 primary amine groups on the dendrimer surface after deprotection, which was further used for Cy5 conjugation. We couldn't analyze the size and zeta potential of Cy5-D-TA due to the presence of Cy5 molecule and its interference with the laser used in the zetasizer.

2.7.5. Release study:

In vitro release characteristics of D-TA conjugate were investigated in simulated vitreous humor as a physiologically relevant pH 7.0 mimicking the intravitreal injection of D-TA conjugates. A calibration curve for both TA and TA-linker was established over a concentration of 10 ng to 20 μg at 238 nm. We used HPLC method to quantify the release characteristics of the D-TA conjugate. The conjugate has two ester linkages that are susceptible to hydrolysis i) an ester linkage between the –OH group of the dendrimer surface and the -COOH group of the TA-linker, and ii) another ester linkage between the hydroxyl group at 21- position of TA and the carboxyl group (-COOH) of one end of the glutaric acid linker. Our results suggest that the drug was released as free TA and TA-linker, confirmed by the two peaks that appeared in the HPLC chromatogram that coincide with the retention time of TA and TA-linker. Since there was an overlap of the peaks between the released drug forms and the conjugates, we adopted solvent precipitation method for extracting the released TA and TA-linker from the incubation mixture. The conjugates were insoluble in organic phase (DCM/ethyl acetate, 50:50) and precipitated out, while the organic phase containing the drug and drug linker was reconstituted in HPLC mobile phase and analyzed.

D-TA conjugates released the drug more in the form of TA-linker than as TA. This phenomenon was also reported by Macky et al [66] where the ester bond between the TA and the linker was more stable for a period of 7 days. The conjugates exhibited initial burst release of ~18% of its payload within 24 hrs. From day 3 to day 20, there was a sustained release, with a further ~ 40% release, followed by a nearly zero order release over the period from day 20 to day 45, resulting in ~95% of the payload released (**Figure 10**). The hydroxyl group in TA used in the conjugation is not required for any therapeutic activity or receptor binding [75, 76] and thus the dendrimer-TA may be able to maintain the same therapeutic activity as that of free TA.

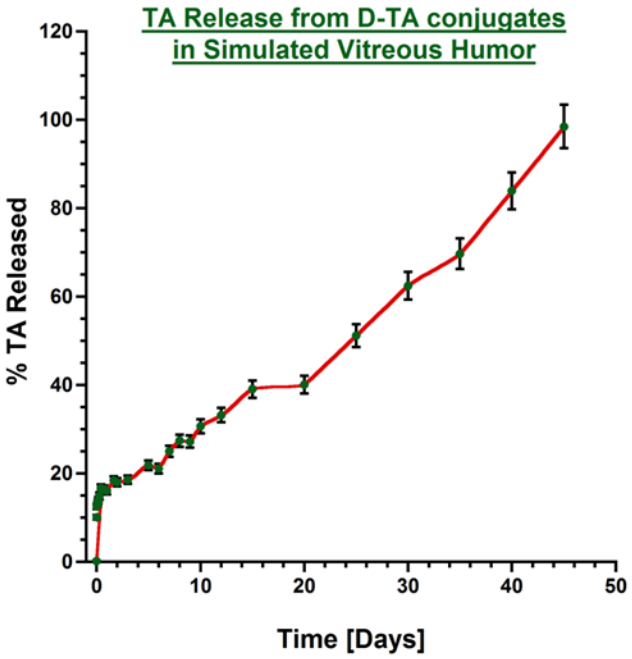

Figure 10: Drug release profile from D-TA conjugates in simulated vitreous humor

2.8. *in-vitro* efficacy of D-TA conjugates in microglial and RPE cells.

2.8.1. D-TA conjugates cytotoxicity assay in cells.

The D-TA conjugates should be non-cytotoxic at the concentrations used in cell studies. We performed a cell viability assay to establish the range of concentrations where both free TA and D-TA are non-toxic, to establish the therapeutic window for efficacy studies in cells. Previous studies showed that 400 μg/mL TA was toxic to retinal cells [51], hence we treated the cells with preservative free TA within the concentration range from 0.1 to 200 μg/mL of TA and D-TA which contains equivalent concentrations of TA. We also tested the toxicity of free dendrimer based on the amount of dendrimer present in D-TA. Since we used ethanol to dissolve free TA and serially diluted with cell medium we also used the same amount of ethanol for D-TA and controls. The ethanol treatment did not illicit any toxicity in both BV-2 and ARPE-19 cells. At 200 μg/mL, free TA showed significant decrease in % cell viability in BV-2 and ARPE-19 cells (58.3% ± 5.9% and 54.2% ± 6.8% respectively), but interestingly D-TA conjugates did not induce any cell death resulting (90.7% ± 8.5% and 91.6% ± 2.6%) respectively at this concentration (**Figure 11A & 11B**). We noticed that at the highest concentrations (200 μg/mL) free TA precipitated and formed crystals to some extent, and deposited over the cells (Figure 17), whereas D-TA is highly soluble and did not precipitate. Cytotoxicity of free TA can be attributed to the direct cellular contact with the epicellular crystals as noticed by Szurman et al in ARPE-19 cells [77]. Similar effect was also noticed at 100 μg/mL of free TA but not with D-TA. At concentrations below 100 μg/mL, both free TA and D-TA did not show significant decrease in cell viability upon 24 hours of incubation. Free dendrimer did not show any cytotoxic effects in both cell types in any concentrations thereby negating the effect of delivery vehicle on cytotoxicity.

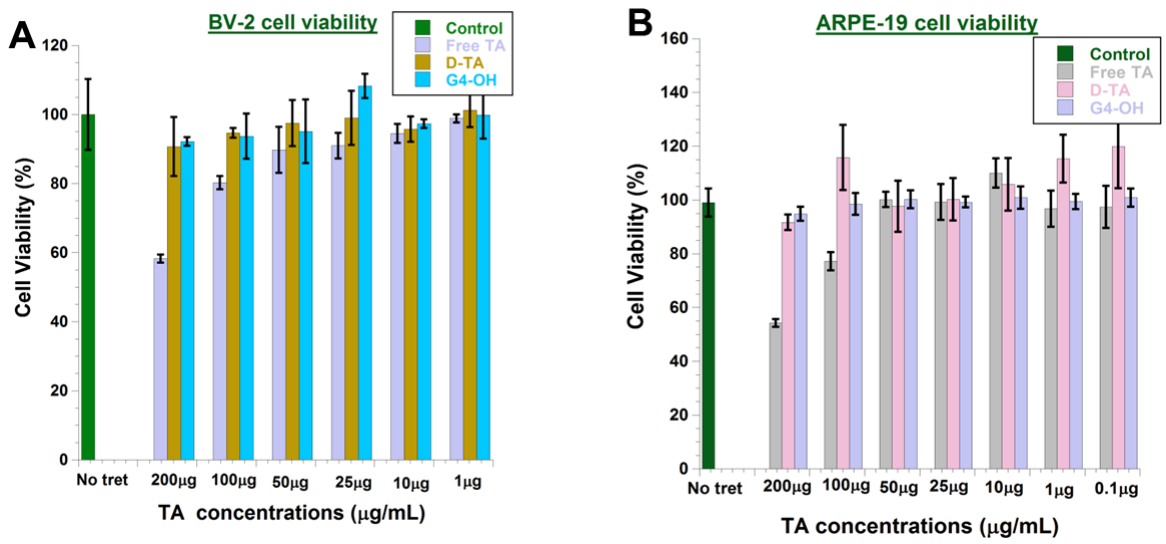

Figure 11: Cytotoxicity of free TA and D-TA in **A)** BV-2 microglial cells and **B)** ARPE-19 cell. Cells were treated with varying concentrations of free TA and D-TA with equivalent of free TA. Cell viability was measured after 24 h of treatment and compared to non-treated controls. Data represents the mean ± SEM.

2.8.2. Anti-inflammatory activity of D-TA conjugates in microglial cells.

For investigating the anti-inflammatory effect of D-TA conjugates, we used LPS induced pro-inflammatory murine BV-2 microglial cells, which play a critical role in mediatingretinal inflammation. LPS activates protein kinases in microglial cells through toll-like receptors (TLR) pathway thereby stimulating the release of immune regulated proinflammatory cytokines such as TNF-α, IL-1β, IL-6 and etc. [78,79] . We used TNF-α suppression to evaluate the anti-inflammatory properties of TA and D-TA. Upon LPS pretreatment, there was a significant increase (~15 fold) in TNF-α level at 24 hrs. We tested varying concentrations of LPS and verified that 100 µg/mL treatments did not induce any cell death at least until 72 hours after incubation (data not shown). Cells were treated with free-TA or D-TA for a 12 hour period, in the presence of LPS. The supernatant was replaced after 12 hours, with just LPS, but no D-TA and free TA. Therefore, these studies reflect the efficacy of free TA and D-TA treatment and their uptake by the cells over a limited time of 12 hours, studied at 24, 48 and 72 hours, in the

continuous presence of LPS over 72 hours. Free TA inhibited TNF-α production in a dose dependent manner, with a maximum reduction of ~28.2% at highest treatment dose of 100 µg/mL at 24 hours post treatment, whereas at low concentrations (25, 10 and 1 µg/mL) did not show any significant inhibition in TNF-α levels. In comparison, D-TA conjugate treatment, containing equivalent TA concentration (e.g. 100 µg/mL), significantly reduced the TNF-α level (~66.4%) and exhibited superior anti-inflammatory properties compared that of free TA. At 24 hours, the extent of TNF-α suppression achieved with 1 µg/mL of D-TA was better than that achieved with 100 µg/mL of free-TA. This may be attributable to the fact that the dendrimer increased the intracellular uptake of conjugated TA compared to free TA (**Figure 12A**).

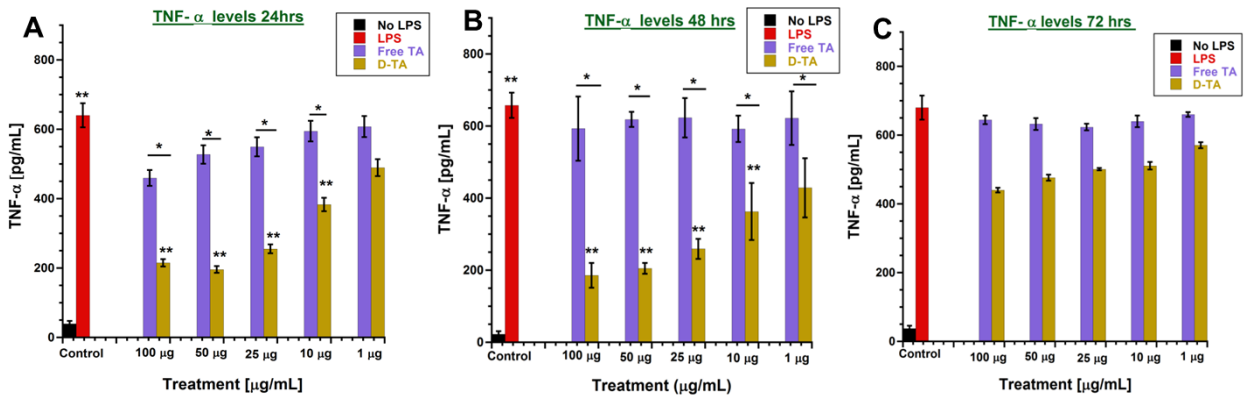

Figure 12: Anti-inflammatory activity of D-TA (TNF-α release ELISA): BV-2 cells (Passage 18) were activated using LPS (100ng/mL) and treated with indicated concentrations of free TA and D-TA containing equivalent amount that of free TA for 12 hrs and replaced with LPS medium. Five samples (medium supernatant) were used for each group at indicated time point post treatment, TNF-α was measured using mouse TNF-α ELISA Kit, **A)** 24 hrs D-TA treatment **B)** 48 hrs post D-TA treatment and **C)** 72 hrs post D-TA indicating TNF-α suppression data represents mean ± SEM *P<0.01 vs free TA and **P<0.01 vs group of LPS.

At 48 hours post treatment, with continuous LPS exposure, free TA did not inhibit TNF-α production, even at the highest concentration (100 µg/mL). In contrast, D-TA showed significant efficacy in suppressing TNF-α production in a dose dependent manner, resulting in ~35% suppression at 1 µg/mL to ~65% at 100 µg/mL (**Figure 12B**). The dose-response upon D-

TA treatment and the extent of suppression was similar to that seen at 24 hours, indicating that D-TA sustained the effect at least up to 48 hours. At 72 hours, free TA did not show any TNF-α suppression, whereas D-TA showed moderate suppression (~35% at 100 μg/mL) (**Figure 12C**). The sustained anti-inflammatory effect provided by D-TA at very low concentration promises improved therapeutic effect for inflammatory retinal diseases.

2.8.3. Anti-VEGF activity of D-TA conjugates in retinal pigment epithelium (RPE).

To examine the effects of free TA and D-TA on VEGF production, we assessed the protein and mRNA expression by ARPE-19 cells after hypoxia. We used hypoxia-reoxygenation in order to induce oxidative stress, resulting in the upregulation and secretion of VEGF in RPE, which is one of the most important causes of retinal neovascular diseases [45]. Upon 6 hours of hypoxia exposure to ARPE-19 cell monolayers, we saw increased VEGF levels (2107.9 ± 230.7 pg/mL). After exposure to hypoxia followed by 2 hours of re-oxygenation with fresh medium, the cells were treated with different concentrations of free TA and D-TA for 24 hours and then replaced with medium without TA or D-TA, and the VEGF ELISA was performed 24 hours after medium change. Both TA and D-TA treatments inhibited VEGF secretion in a dose dependent manner. Free TA treatment led to a maximum reduction of ~27% at 100 μg/mL concentration. D-TA treatment resulted in a significantly better inhibition of VEGF secretion (~60%) at 100 μg/mL (**Figure 13A**). D-TA inhibition of VEGF at 1 μg/mL was significantly better than that achieved at a 100-fold higher level of free TA.

For VEGF to be secreted from RPE, mRNA corresponding to VEGF has to be synthesized using transcription from DNA in the nucleus, from where they are released in to the cytoplasm translated to VEGF protein, and further secreted from cells. Corticosteroids induce their effect

via glucocorticoid receptor activation [37, 38] and suppressing the mRNA levels in the nucleus. To see if a reduced level of VEGF protein secreted by RPE cells after D-TA treatment is due to down regulation of mRNA synthesis in these cells, we performed RT-PCR analysis of mRNA isolated from the treated cells. The RT-PCR results were consistent with ELISA analysis showing VEGF protein suppression. The VEGF inhibition at the mRNA level, where 75% inhibition could be achieved with D-TA at 10-25 µg/mL, was significantly better than that for free TA (**Figure 13B**). At 100 µg/mL of D-TA, the inhibition was less than that achieved at 10 or 25 µg/mL. This suggests that D-TA at too high a concentration may actually decrease efficacy, as seen in steroids in animal models of retinal diseases [80].

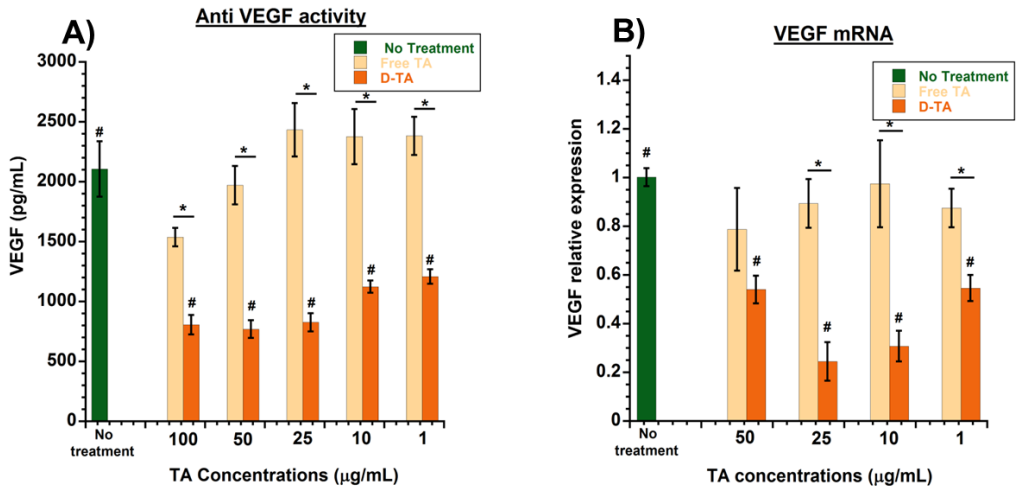

Figure 13: Anti-VEGF activity of D-TA in ARPE-19 cells: ARPE-19 (Passage 21) were subjected to hypoxia for 6hrs and treated with D-TA and free TA (equivalent drug basis) at indicated concentrations for 24 hrs and replaced with culture medium. 24 hrs post treatment VEGF was analyzed using human VEGF ELISA kit and RT-PCR for mRNA expression **A)** VEGF secretion analysis in culture medium using ELISA (n=6) and **B)** VEGF mRNA expression levels relative to GAPDH using RT-PCR (n=3) data denotes mean ± SEM, *P<0.01 vs free TA and #P<0.01 vs group with no treatment.

2.9. Cell entry and intracellular localization of D-TA conjugates.

2.9.1. Enhanced cellular uptake of D-TA conjugates:

Flow cytometry analysis was performed to assess the effect of TA conjugation on the cellular uptake of D-TA. Despite their similarity in size and surface properties, Cy5-D-TA demonstrated consistently higher uptake in ARPE cells in comparison to D-Cy5. Specifically, at 1, 3, 6 and 12 hours the percentage of the cell population that had taken up Cy5-D-TA was 1.7-, 3.7-, 3.3- and 2.2- fold higher than that of the cells that had taken up D-Cy5, respectively. The mean fluorescence intensity demonstrated a similar correlation. As expected, the cell uptake increased over time for both D-Cy5 and Cy5-D-TA treated cells (**Figure 14**).

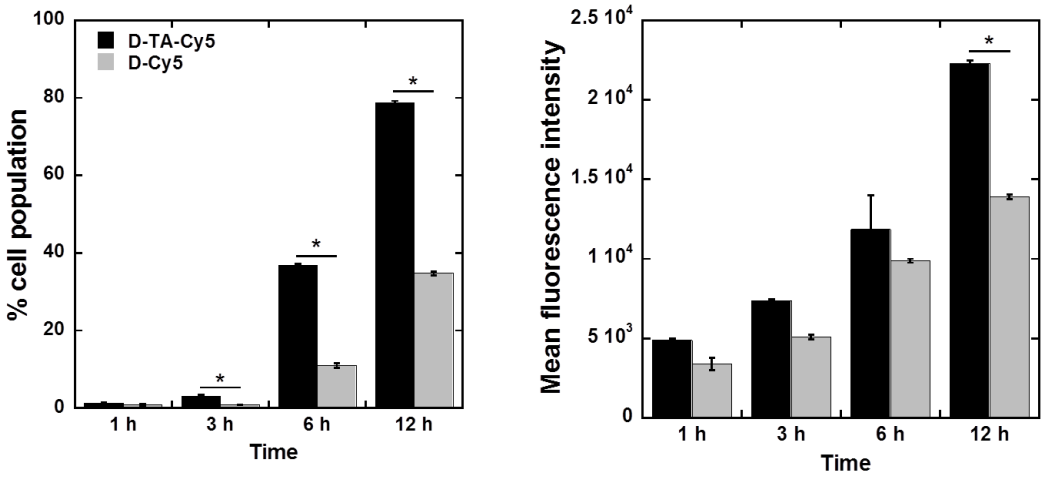

Figure 14: D-TA uptake by human ARPE-19 cells: Flow cytometric analysis of Cy5-D-TA and D-Cy5 cellular uptake by ARPE-19 cells: ARPE-19 cells were treated with Cy5-D-TA or D-Cy5 for 1 h, 3 h, 6 h and 8 h in order to assess the effect of TA-conjugation on dendrimer cell uptake. **(A)** The percentage of cell uptake at different time points demonstrated significantly higher uptake of Cy5-D-TA compared to D-Cy5 at 3h, 6h and 12 h of incubation. **(B)** The MFI of the cell population, indicating the absolute amount of dendrimer uptake, was higher following incubation with Cy5-D-TA compared to D-Cy5. Significance was only found at 12 h of incubation. *$p<0.05$

Cellular uptake constitutes an important barrier to effective delivery of anti-inflammatory therapeutics. While delivery of TA with the use of various nanocarriers has been studied, this is the first study to demonstrate that TA conjugation on the surface of dendrimers enhances cellular uptake of the conjugate. These results are in accordance with our previous work demonstrating that dendrimer–based gene vector uptake and transfection can be significantly improved

following conjugation of TA [63]. This phenomenon may be attributed to the nuclear localization of D-TA gene vectors leading to decreased exocytosis [81].

2.9.2. D-TA conjugates translocate to the nucleus via glucocorticoid receptors

Corticosteroids exert their anti-inflammatory and anti-VEGF activity via glucocorticoid receptor (GR) pathway [38, 82]. Many studies have previously reported that TA binds to GR, resulting in the activation of GR, followed by translocation to the nucleus [76]. Since D-TA conjugates exhibited enhanced therapeutic activity than free TA, we used Cy5-D-TA to visualize the intracellular localization, GR binding, and the nuclear translocation of D-TA. We used confocal microscopy at different time points (3, 6, and 12 hours) to visualize the dynamics of GR receptors in RPE cells. We used anti-GR antibody (Cy3, green) and DAPI (blue) for staining the GR and nucleus respectively. In control (**Figure 15A-D**) and free TA cells (not shown), the GR receptors were seen distributed in the cytoplasm. In contrast, at 3 hours, in the Cy5-D-TA treated cells, the GR were seen concentrated around the nucleus (**Figure 15E-H**) (indicated by white arrows) and were further co-localized with the Cy5 signal (red, **Figure 15, G**) suggesting that D-TA binds GR. Twelve hours post incubation, Cy5-D-TA and GR were co-localized in the nucleus and was confirmed by the yellow signal in merged panel (**Figure 15 K**-N). To depict the colocalization of Cy5-D-TA and GR, we digitally magnified a signal cell at 3 and 12 hours (**Figure 15,I & O**), indicating the GR concentrating around the nucleus and nuclear delivery of Cy5-D-TA respectively (white arrows).

The imaging results are in agreement with the flow cytometry results, indicating enhanced cellular uptake and nuclear localization of D-TA conjugates. The difference in the GR localization of the free TA and D-TA, and the fact that D-TA localizes with GR even at 3 hours

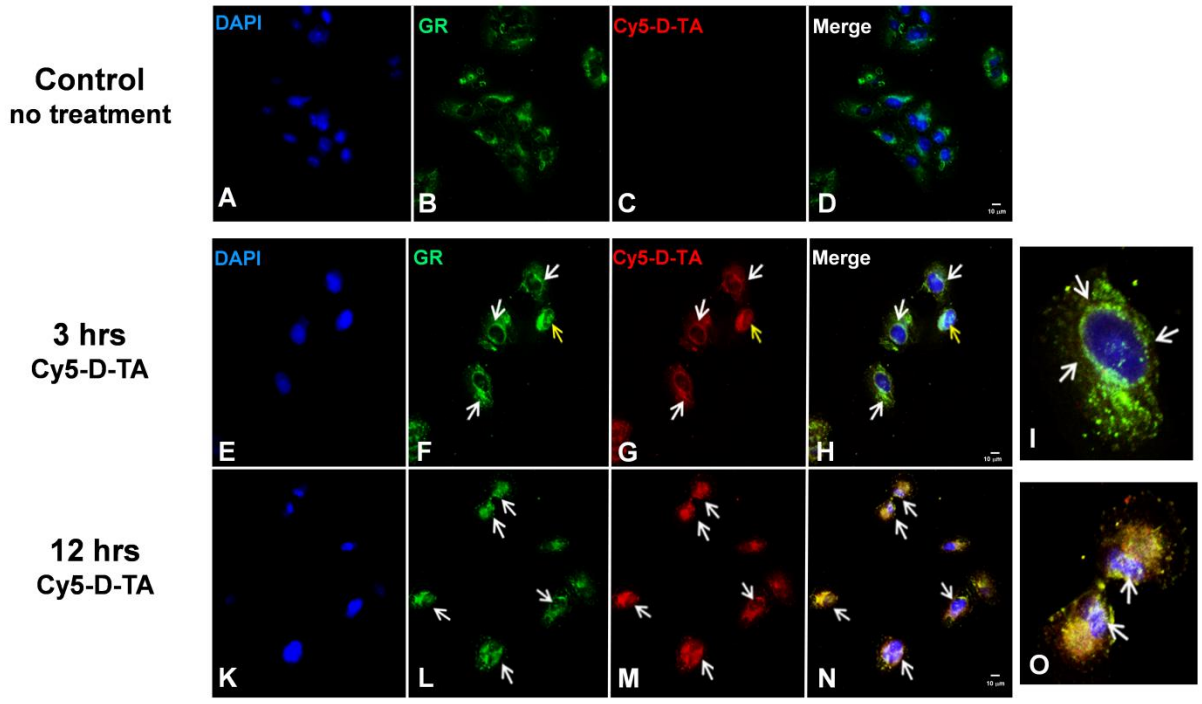

Figure 15: Cellular uptake and nuclear localization of D-TA conjugates in ARPE-19 cells using confocal imaging: Cy5 labelled D-TA (Cy5-D-TA, red) was used to probe the intracellular localization of D-TA and it's binding to glucocorticoid receptor (GR, green) and nucleus (DAPI, blue). **A-D** control cells where GR receptors are in cytoplasm, **E-H** 3 hrs post Cy5-D-TA incubation white arrows indicating GR concentrated around the nucleus **(I**, digital zoom of single cell**), K-N** 12 hrs post D-TA-Cy5 incubation white arrows indicating nuclear localization of GR along with Cy5-D-TA (yellow merge) **(O,** Digital zoom of single cell white arrows indicating the nuclear localization). The cells were imaged at 63X magnification, **bar -10 µm.**

[when we don't expect appreciable drug release (**Figure 10**)] suggest that the dendrimer conjugate is binding to the receptor. Moreover, these results also suggest that conjugating TA to dendrimer using OH group at 21st position did not alter, or perhaps enhanced the binding of TA to the GR. The D-TA formulation appears to enhance the nuclear translocation of TA-GR complex. The increased intracellular uptake of D-TA, enabled in part by TA, is in good agreement with our previous reports that D-TA based dendrimer gene carriers showed enhanced transfection in RPE cells, compared to dendrimer gene carriers [63].

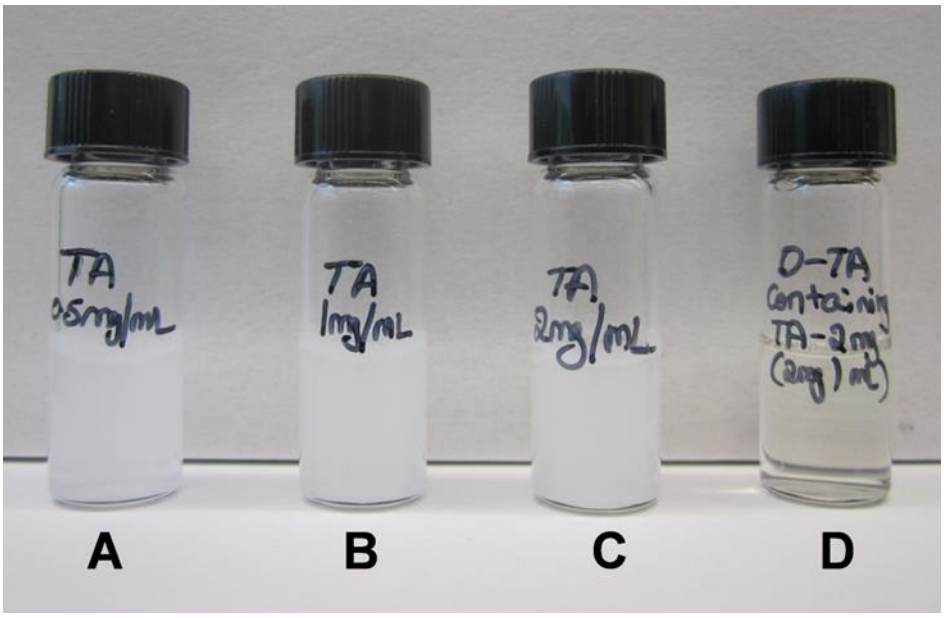

Figure 16: Solubility of free TA and D-TA in PBS. Free TA was not soluble in any of the concentrations **A)** 0.5 mg/mL, **B)** 1.0 mg/mL and **C)** 2.0 mg/mL and forms a turbid white and cloudy solution which later settles. Whereas D-TA conjugate **D)** were completely

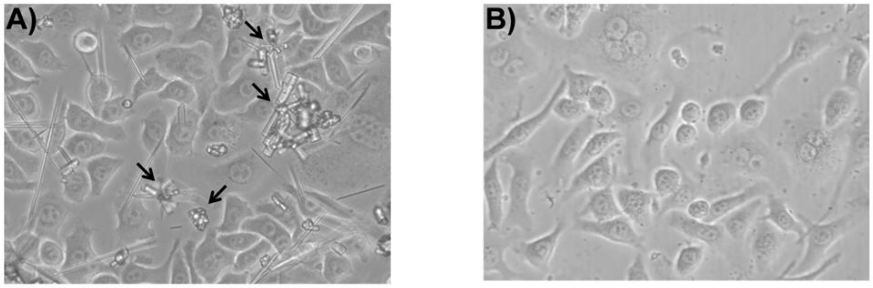

Figure 17: Light microscope images of BV-2 microglial cell culture treated with **A)** 100 µg/mL of free TA, and **B)** D-TA containing 100 µg/mL of TA. Free TA being insoluble in cell culture medium forms aggregate crystals and deposits over the cells which cause

2.10. Conclusions

Neuroinflammation and neovascularization are the two important pathological events implicated in AMD, diabetic retinopathy, CNV and other retinal diseases [83-85]. Therapies that can target both these events will be highly beneficial. Corticosteroids, particularly TA, has both anti-inflammatory and anti-angiogenic activity and has been used clinically. Improved intracellular delivery can enhance efficacy of TA and reduce its side effects [38]. In this study we synthesized hydroxyl PAMAM dendrimer based D-TA conjugate with a high payload (~21%) that were a) highly water soluble and exhibited sustained release of TA ~2% per day for a period for ~45 days, b) less toxic and enhanced cellular uptake of TA and c) significantly more efficacious in its anti-inflammatory (activated microglial cells) and anti-VEGF activity (retinal pigment epithelial cells) than free TA.

Microglial cells perform dynamic immune surveillance and are responsible in maintaining the normal retinal health [86]. However, under pathological conditions they become activated and contribute to BRB breakdown, cytokine production and stimulating RPE to produce VEGF leading to neovascularization [38, 84]. On the other hand, RPE cells are the major contributor for VEGF production [87], a factor involved in enhanced blood vessel permeability, abnormal neo-vessel formation resulting in leaky blood vessels [27]. The ability of D-TA to significantly suppress TNF-α in microglia for a period of 72 hrs, after a 12-hour treatment, suggests sustained anti-inflammatory action. In RPE cells, D-TA was fold more efficacious in inhibiting VEGF secretion, compared to a 100-fold higher concentration of free TA. In order for TA to exert its therapeutic effect, it needs to be transported into the cell, and further to the nucleus. From flow cytometry results it is evident that conjugating TA to the dendrimer enables more drug to be transported in to the cells. Interestingly, presence of TA on

the dendrimer seemed to increase dendrimer uptake. TA exerts its biological activity via glucocorticoid receptor (GR) pathway [88, 89]. In-vitro cell experiments, flow cytometry and qualitative results from con-focal microscopy suggest that D-TA enters nucleus along with GR to express its activity. Glucocorticoids down regulate VEGF by blocking up-stream of its transcription in the nucleus [38, 43, 90] which is evident from confocal images and RT-PCR studies where D-TA treatment showed low levels of VEGF mRNA.

Increased efficacy and decreased toxicity achieved with dendrimer conjugation of TA may be beneficial. TA is typically injected in relatively large doses (4 mg in human eyes) l resulting in various side-effects such as elevated IOP, retinal toxicity and blurred vision [91]. In this study we have demonstrated that both anti-inflammatory and anti-VEGF properties of TA can be enhanced by conjugating them to dendrimers resulting in efficacy at much lower concentrations (~100 fold) than that of free drug. Therefore, dendrimer-TA conjugates may be a viable formulation for targeted intracellular delivery of TA. Further evaluation of the D-TA conjugates in clinically relevant animal models can provide more insights in terms of sustained efficacy, potentially offering a potent option for fighting against numerous retinal diseases such as AMD, CNV, diabetic retinopathy and macular edema.

CHAPTER 3 "SYNTHESIS, CHARACTERIZATION AND IN-VITRO EVALUATION OF PAMAM DENDRIMER BASED GENE CARRIER FORMULATION FOR OCULAR GENE DELIVERY"

3.1. Abstract

Ocular gene therapy holds promise for the treatment of numerous blinding disorders. Despite the significant progress in the field of viral and non-viral gene delivery to the eye, important obstacles remain in the way of achieving high-level transgene expression without adverse effects. The retinal pigment epithelium (RPE) is involved in the pathogenesis of retinal diseases and is a key target for many gene-based therapeutics. In this study, we addressed the inherent drawbacks of non-viral gene vectors and combined different approaches to design an efficient and safe dendrimer-based gene delivery platform for delivery to human RPE cells. We used hydroxyl-terminated polyamidoamine (PAMAM) dendrimers functionalized with different amounts of amine groups to achieve effective plasmid compaction. We further used triamcinolone acetonide (TA) as a nuclear localization enhancer for the dendrimer-gene complex, and achieved significant improvement in cell uptake and transfection of hard-to-transfect human RPE cells. To improve serum stability, we further conjugated the dendrimer-TA with neutral polyethylene glycol (PEG). The resultant complexes showed improved stability while minimally affecting transgene delivery, thus improving the translational relevance of this platform.

3.2. Introduction.

The eye, as an immune privileged and easily accessible organ, constitutes a favorable target for gene therapy [92] The well-defined genetic targets that can alter the natural history of ocular disorders render gene therapy a promising therapeutic approach for numerous blinding disease entities such as Best's disease, Stargatdt's disease and retinitis pigmentosa [93-96] Indeed, gene therapy for Leber Congenital Amaurosis has demonstrated promising and long lasting results in clinical trials [98-101]

Significant advances in the field of ocular gene therapy have been achieved with the use of viruses such as adeno-associated virus [99-102] While relatively efficient, viral gene vectors are limited by technical difficulties in scale-up, high cost of production [103] and risk of mutagenesis [104]. Moreover, repeated administrations or prior exposures may cause neutralizing immune responses, despite the immune privileged environment of the eye [105-107]. Also, the size cut-off for the expression cassette that can be packaged in viruses excludes the delivery of large transgenes that may be effective in monogenic ocular diseases [108-110]. Non-viral gene vectors constitute an attractive alternative that can overcome most of the aforementioned limitations [111] in achieving ocular transgene delivery [112, 113] However, important issues such as vector or base-polymer cytotoxicity, instability in physiological solutions as well as low level of cellular uptake, nuclear transfer and transgene expression limit the clinical applications of nano-carriers [114]. Various cationic polymer-based gene delivery systems, such as dendrimers, have demonstrated effective transgene expression in vitro and in vivo [111]. The protonable amines of these gene vectors contribute to endosome escape and allow relatively high levels of transfection [115]. However, the same amine groups that enhance transfection lead to cytotoxicity, entrapment in physiological mesh-like barriers [116, 117] and

tendency towards nanoparticle aggregation. For these reasons, a variety of novel approaches have been used to overcome the inherent limitations of cationic polymer based non-viral gene vectors [111, 118]

Dendrimers are globular branched macromolecules with a high density of tailorable surface groups [119]. The highly precise synthesis process produces polymers with low polydispersity and allows high control over their physicochemical characteristics. Different dendrimer types have been used as non-viral gene delivery vectors, with relatively promising results [120, 121]. While amine terminated PAMAM dendrimers demonstrate high levels of transfection efficacy, they are limited by cytotoxicity due to their amine functionalized surface [111]. Hydroxyl-terminated PAMAM dendrimers demonstrate improved safety profile and have proven to be effective drug delivery vehicles [122]. However, their near neutral surface charge and lack of protonable amines impedes their use in nucleic acid compaction and transgene delivery [123].

Triamcinolone acetonide (TA) is an intermediate-acting, relatively potent corticosteroid administered intravitreally for the treatment of sympathetic ophthalmia, temporal arteritis, uveitis and other ocular inflammatory conditions not responsive to systemic corticosteroids. Due to its neuroprotective and anti-angiogenic properties, TA has also previously been used as an adjuvant therapy for diabetic macular edema (DME), retinal vein occlusion, and some forms of age related macular degeneration [125-127] TA has also been suggested to improve gene vector accumulation in the nucleus by acting as a nuclear localization signal, dilating the nuclear pores up to 60 nm when bound to its receptor [128] Ma et al. have demonstrated that TA conjugation on polyethylenimine as well as PAMAM dendrimers can significantly improve transgene expression of cationic polymer based gene vectors [129-130]

In this chapter we designed small compact gene vectors based on hydroxyl-terminated PAMAM dendrimers functionalized with a minimal number of primary amine groups [131] to allow for efficient compaction while maintaining their favorable safety profile. We further utilized TA to offset the lack of protonable amines and achieve high levels of safe transgene expression. Additionally, we used a poly-ethylene glycol surface coating to enhance colloidal stability of the aforementioned gene vectors in physiological solutions. We determined the physicochemical characteristics of the dendrimer-based gene vectors and examined the effect of the various complexation strategies on cell uptake and transfection efficiency in hard to transfect, sensitive and clinically relevant human retinal pigment epithelial cells [132-134].

3.3. Materials and methods

3.3.1 Materials and reagents.

Hydroxyl- and amine- functionalized ethylenediamine core generation four PAMAM dendrimers (G4-OH and G4-NH2; diagnostic grade; 64 end-groups) were purchased from Dendritech Inc. (Midland, MI, USA). TA, N-(3-dimethylaminopropyl)-N′-ethylcarbodiimide hydrochloride (EDC.HCl) glutaric anhydride, piperidine, N,N’-diisopropylethylamine (DIEA), trifluoroacetic acid (TFA), anhydrous dimethylformamide (DMF), dimethylacetamide (DMA), and dimethylsulfoxide (DMSO) were purchased from Sigma-Aldrich (St. Louis, MO, USA). 4-(Fmoc-amino)butyric acid (Fmoc-GABA-OH) and (benzotriazol-1-yloxy)tripyrrolidino-phosphonium hexafluorophosphate (PyBOP) were purchased from Bachem Americas Inc. (Torrance, CA, USA). Cy5-mono-NHS ester was purchased from Amersham Biosciences-GE Healthcare (Pittsburgh, PA, USA). mPEG2000 NHS ester was purchased from Creative PEGWorks (Winston Salem, NC, USA). ACS grade DMF, DMSO, dichloromethane (DCM),

diethylether, hexane, ethyl acetate, HPLC grade water, acetonitrile, and methanol were obtained from Fisher Scientific and used as received. Dialysis membrane (MW cut-off 1000 Da) was obtained from Spectrum Laboratories Inc. (Rancho Dominguez, CA, USA).

3.3.2. Preparation of FMOC functionalized bifunctional dendrimer (BiD-FMOC, 1)

Fmoc-GABA-OH (287 mg, 0.882 mmol) was dissolved in DMF (5 mL) in a 50 mL round bottom flask under nitrogen environment. PyBOP (574 mg, 1.1035 mmol) dissolved in DMF (5 mL) and DIEA (200 μL) were added, and the reaction mixture was allowed to stir for 1 hour in an ice bath. Finally, PAMAM G4-OH (309 mg, 0.022 mmol) dissolved in anhydrous DMF (10 mL) was added to the reaction mixture and was stirred for 48 hours. The mixture of solvents was evaporated at 25 °C under vacuum. The crude product was redissolved in DMF (20 mL) and subjected to dialysis in DMF (membrane MW cutoff = 1 kDa) for 26 hours by changing the solvent at least 3 times. The obtained solution was evaporated under reduced pressure at room temperature, and the final product was subjected to high vacuum overnight, to produce an off-white semi-solid Fmoc-functionalized dendrimer conjugate (BiD-Fmoc, 1, 460 mg). ^{1}H NMR (DMSO-d6) δ 1.63 (m, CH2 protons, linker), 2.27-3.39 (m, CH2 protons of G4-OH and COCH2 protons of linker), 3.99 (bs, CH2OC=O protons, G4-OH), 4.18 (bs, CH proton of Fmoc group), 4.28 (bs, OCH2 protons of Fmoc group), 4.71 (bs, OH protons of G4-OH), 7.30-7.38 (d, aromatic protons of Fmoc), 7.65 (s, aromatic protons of Fmoc), 7.86-8.13 (m, aromatic protons of Fmoc, carbamate protons, and internal amide protons of G4-OH).

3.3.3. Synthesis of Fmoc-functionalized bifunctional-Triamcinolone acetonide (BiD-Fmoc-TA, 2)

TA-21-glutarate (70.6 mg, 0.129 mmol) was dissolved in 10 mL of anhydrous DMF under nitrogen atmosphere, and PyBOP (100.5 mg, 0.193 mmol) and DIEA (0.35 mL) were added to it. The reaction mixture was stirred at 0°C for 30 min. followed by the addition of BiD-Fmoc (200 mg, 0.0086 mmol) dissolved in 10 mL of DMF, and the reaction was allowed to go to completion (48 h) under nitrogen conditions. The reaction mixture was evaporated under reduced pressure and dialyzed in DMF for 24 h, while the solvent was replaced every 6 h (Dialysis membrane cutoff 1000 Da) to remove the unreacted starting materials and byproducts. The resultant DMF was evaporated, and the conjugate was dissolved in water and re-dialyzed against water for 6 h and lyophilized to get BiD-Fmoc-TA acetonide conjugate (BiD-Fmoc-TA,3) as an off-white color solid product (220 mg). The conjugate was characterized by 1H NMR, and the drug loading was assessed using the proton integration method. ^{1}H NMR (DMSO-d6) δ 0.84 (s, -CH3 protons of TA), 1.15 (s, -CH3 protons of TA), 1.36 (s, -CH3 protons of TA), 1.47-1.55 (m, -CH3 and -CH protons of TA), 1.64 (s, -CH2 protons of linker) 1.73-1.82 (-CH proton of TA), 1.92 (m, -CH protons of TA), 2.27 (m, -CH2 protons of G4-OH), 2.67-3.40 (m, -CH protons of TA, -CH2 protons of linker and -CH2 protons of G4-OH), 4.00 (s, CH2OC=O protons, G4-OH), 4.19 (brs, -CH protons of Fmoc group), 4.29 (bs, OCH2 protons of Fmoc group), 4.70-6.25 (m, -OH protons of G4-OH, -CH and aromatic protons of TA), 7.29-8.05 (m, carbamate protons, aromatic protons of Fmoc, aromatic protons of TA and amide protons of G4-OH).

3.3.4. Synthesis of bifunctional-Triamcinolone acetonide (BiD-TA, 4)

BiD-Fmoc-TA dendrimer (220 mg) was dissolved in anhydrous DMF (10 mL) and piperidine/DMF (2:8; 10 mL) was added to it under nitrogen. The reaction mixture was stirred for 30 min. and solvent was evaporated under vacuum at room temperature. The resultant crude product was subjected to dialysis in DMF (membrane MWCO = 1 kDa) for 24 h. The solvent

was evaporated and the conjugate was re-dialyzed against water for 3-4 h and lyophilized to get BiD-TA, 4(145 mg) as off-white solid product. The BiD-TA has some free amine groups and TA molecules on the surface. ^{1}H NMR (DMSO-d6) δ 0.83 (s, -CH3 protons of TA), 1.15 (s, -CH3 protons of TA), 1.35 (s, -CH3 protons of TA), 1.50 (s, -CH3 protons of TA), 1.54-2.07 (m, -CH protons of TA, -CH2 protons of linker), 2.21 (bs, -CH2 protons of G4-OH), 2.29-2.48 (m, -CH protons of TA, -CH2 protons of linker and -CH2 protons of G4-OH), 2.65 (bs, -CH2 protons of G4-OH), 3.10-3.12 (t, -CH2 protons of G4-OH), 3.28-3.29 (d, -CH2 protons of G4-OH), 3.28-3.41 (t, -CH2 protons of G4-OH), 4.01-4.02 (d, CH2OC=O protons, G4-OH), 4.20-7.31 (singlet and doublet, -CH and aromatic protons of TA), 7.82-8.07 (m, amide protons of G4-OH).

3.3.5. Synthesis of bifunctional dendrimer (BiD, 5)

The whole batch of above BiD-Fmoc dendrimer was dissolved in anhydrous DMF (10 mL) and 10 mL of piperidine/DMF (2:8) was added to it under nitrogen. The reaction mixture was stirred for 1 hour and the mixture of solvents was evaporated under vacuum. The crude product was co-evaporated with 10 mL of DMF under high vacuum and subjected to dialysis against DMF (membrane MWCO = 1000 Da) for 24 h. The solvent was evaporated and the product was triturated with diethylether to take out traces of DMF. Finally, the semi-solid product was re-dialyzed with pure DI water for 2-3 hours and subjected to freeze dryer to get bifunctional dendrimer (BiD, 280 mg). ^{1}H NMR (DMSO-d6) δ 1.24-1.53 (m, CH2 protons, linker), 2.21 (bs, CH2 protons of G4-OH), 2.29 (m, COCH2 protons of linker), 2.43 (bs, CH2 protons, G4-OH), 2.65 (bs, CH2 protons, G4-OH), 3.09-3.12 (t, CH2 protons, G4-OH), 3.27-3.28 (d, CH2NH protons, linker), 3.38-3.41 (t, CH2 protons, G4-OH), 3.99-4.01 (t, CH2OC=O protons, G4-OH), 7.84-8.11 (m, NHCO protons of G4-OH).

3.3.6. Synthesis of amine dendrimer-mPEG2000 conjugate (G4-NH2-PEG, 6)

The G4-NH2 dendrimer (100 mg, 0.007 mmol) was dissolved in borate buffer (10 mL) and EDC●HCl (134.5 mg) was added to it at 0°C. After 10 min mPEG2000 NHS ester was added and stirred the reaction mixture for 2 h. Finally the reaction mixture was dialyzed against water for 48 h (membrane cutoff: 8 kDa) and lyophilized to get PEG-functionalized dendrimer (G4-NH2-PEG, 6). The final product was characterized by ^{1}H NMR, (DMSO-d6) δ 2.15-2.65 (-CH2 protons of G4-OH), 3.08-3.10 (-CH2 protons of G4-OH), 3.25 (-OCH3 protons of PEG), 3.36-3.66 (-OCH2 protons of PEG), 8.02-8.24 (amide protons of G4-OH).

3.4. Characterization of the conjugates

3.4.1. Proton NMR Characterization

Proton NMR spectra of the final conjugates as well as intermediates were recorded on a Bruker (500 MHz) spectrometer using commercially available DMSO-d6 solvents. Proton chemical shifts were reported in ppm (δ) and tetramethylsilane (TMS) used as internal standard. All data were processed using ACD/NMR processor software (Academic Edition).

3.4.2 High performance liquid Chromatography (HPLC)

The purity of the dendrimer conjugates was analyzed by HPLC (Waters Corporation, Milford, Massachusetts) equipped with a 1525 binary pump, a 2998 photodiode array (PDA) detector, a 2475 multi-wavelength fluorescence detector, and a 717 auto sampler (kept at 4°C) interfaced with Empower software. The HPLC chromatograms were monitored at 210 (G4-OH) and 240 nm (TA conjugated dendrimers) using PDA detector. Fluorescence detector was used for the detection of Cy5-conjugated dendrimer (excitation: 645 nm and emission: 662 nm). The

water/acetonitrile (0.1% w/w TFA) was freshly prepared, filtered, degassed, and used as mobile phase. Symmetry C18 reverse-phase column, TSK gel ODS-80 Ts (250 X 4.6 mm, i.d., 5 μm) and TSK gel guard column were used for the study (Tosoh Bioscience LLC, Japan). A gradient flow was used with initial condition of 100:0 (H2O/ACN), gradually increasing to 90:10 (H2O/ACN) in 10 min to 50:50 (H2O/ACN) in 20 min and returning to 100:0 (H2O/ACN) in 50 min with flow rate of 1 mL/min for all conjugates.

3.4.3. Fluorescence spectroscopy

Fluorescence spectra of the Cy5-conjugated dendrimer (BiD-TA-Cy5) were recorded in phosphate buffer (0.1M) using a Shimadzu RF-5301 spectrofluorometer with excitation at 645 nm and emission at 662 nm. To measure the fluorescence quantum yield of BiD-TA-Cy5 the absorbance at a wavelength of 645 nm and integrated fluorescence intensity following excitation at 645 nm of Cy5-conjugated dendrimer (BiD-TA-Cy5) and free Cy5 solutions at various concentrations were measured using the Synergy Mx Monochromator-Based Multi-Mode Microplate reader (Biotek, Winooski, VT). The quantum yield was calculated using the previously described comparative method47.

3.4.4 Measurement of size and zeta potential of the conjugates

Dendrimer conjugates were dissolved at 1mg/mL in 10 mM NaCl at pH 7.0. The ζ-potential was measured by laser Doppler anemometry using a Nanosizer ZS90 (Malvern Instruments, Southborough, MA).

3.4.5 Buffering capacity of dendrimer conjugates

Dendrimer conjugates were dissolved at a concentration of 0.2 mg/mL in 5 mL of ultrapure DI water. Ultrapure water and PEI were used as a control. The initial pH was adjusted to 12.0 using 1.0 M NaOH and the solutions were titrated at 5 μL steps of 0.1 M HCl. The pH was measured using a microprocessor-based pH meter (Hanna instruments, Woonsocket, RI).

3.5. Formulation and characterization of gene vectors

3.5.1. Gene vector complexation

The pBAL was produced by Copernicus Therapeutics Inc. (Cleveland, OH) and pEGFP plasmid was purchased by Clontech Laboratories Inc. (Mountain View, CA). The plasmids were expanded and purified as previously described.26 Plasmid was fluorescently labeled with Cy5 or Cy3 using Mirus Label IT® Tracker™ Intracellular Nucleic Acid Localization Kit (Mirus Bio, Madison, WI). The gene vector complexation was achieved by the drop-wise addition (1mL/min) of 10 volumes of plasmid DNA at a concentration of 0.1 mg/ml to 1 volume of a swirling polymer solution. Different polymer solutions were prepared with one or more dendrimer conjugates at nitrogen to phosphate (N/P) ratio of 5 unless otherwise specified. For the formulation of gene vectors with varying amounts of TA, blends of BiD-TA and BiD with a varying percentage of amine groups contributed by the BiD-TA polymer (100%, 75%, 50%, 25%, 10%, 5%) were used. For the formulation of PEGylated gene vectors, blends of BiD-TA and D-NH2-PEG with a varying percentage of amine groups contributed by D-NH2-PEG (75%, 50%, 25%) were used. The plasmid-polymer solutions were incubated for 30 min at room temperature to allow the formation of gene vectors. PEI and PEG-poly-L-lysine (PEG-PLL) gene vectors were formulated as previously described26 and used as controls in the following experiments.

3.5.2. Gene vector characterization

Zeta potential and particle size

The ζ-potential of the dendrimer complexes was measured in 10 mM NaCl at pH 7.0 by laser Doppler anemometry using a Nanosizer ZS90 (Malvern Instruments, Southborough, MA). The hydrodynamic diameter and polydispersity of the gene vectors were measured in an ultrapure water solution by dynamic light scattering using a Nanosizer ZS90.

Transmission electron microscopy (TEM)

In order to confirm their shape and size, the dendrimer-based gene vectors were imaged using transmission electron microscopy at 60,000x magnification (TEM, Hitachi H7600, Japan). Stability was assessed over time in ultrapure water at 4^{o}C as well as in PBS buffer in room temperature by dynamic light scattering using a Nanosizer ZS90. Gel retardation assay was preformed to assure efficient compaction of the plasmid DNA at different N/P ratios.

Stability of gene vectors

All the gene carriers were investigated for their stability in biological fluids by dispersing them in 1X PBS and measuring their size at appropriate time points such as 10mins, 30mins, 1hr, 2hrs, 4 hrs and 12 hrs. At each time point 10μL of the sample was drawn and diluted with 990μL of PBS and immediately sized for their stability.

3.6. In vitro experiments in human retinal pigment epithelial cells

3.6.1. Cell culture

The human retinal pigment epithelial cell line (ARPE-19) was a kind gift from Dr. Gerard Lutty, Wilmer Eye Institute. Cells were cultured in Dulbecco's modified Eagle's medium, low glucose, pyruvate (DMEM, Life technologies, Grand Island, NY) supplemented with 1% penicillin/streptomycin (Invitrogen Corp., Carlsbad, CA) and 10% heat inactivated fetal bovine serum (FBS, Invitrogen Corp., Carlsbad, CA).

3.6.3. Evaluation of gene vector toxicity

For the assessment of gene vector toxicity, cells were seeded in 96-well plates at an initial concentration of 1.0×10^4 cells/well and incubated at 37 °C. After 24 h, cells were incubated with a range of doses of DNA gene vectors in media for 24 h at 37 °C. Cell viability was assessed using the Dojindo cell counting kit-8 (Dojindo Molecular Technologies, Inc., Rockville, MD). Absorbance at 450 nm was measured using the Synergy Mx Multi-Mode Microplate Reader (Biotek, Instruments Inc., Winooski, VT).

3.6.3. Transfection studies in RPE cells

To assess cell transfection, cells were seeded in 24-well plates at an initial concentration of 5.0×10^4 cells/well. After 24 h, cells were incubated with different dendrimer-based gene vectors carrying pBAL plasmid (2 μg of DNA/well) in media for 5 h at 37°C. Subsequently, culture media was replaced with fresh media. After additional 3 days of incubation at 37°C, media was removed and 0.5 mL of 1X Reporter Lysis Buffer was added. Cells were subjected to two freeze-and-thaw cycles to assure complete cell lysis, and supernatants were isolated by

centrifugation. Luciferase activity in the supernatant was measured using a luciferase assay kit (Promega, Madison, WI) and a 20/20n luminometer (Turner Biosystems, Sunnyvale, CA). The relative light unit (RLU) was normalized to the total protein concentration of each well measured by the BCA protein assay kit (Thermo Scientific, Rockford, IL). Similarly, for image-based assessment of transfection cells were incubated with different dendrimer-based gene vectors carrying pEGFP plasmid. Two days after additional incubation at 37°C, cells were stained with NucBlue® Fixed Cell ReadyProbes® Reagent (Life Technologies, Grand Island, NY) and immediately imaged for fluorescence originated from NucBlue® and eGFP using confocal LSM 710 microscope (Carl Zeiss, Hertfordshire, UK).

3.6.4. Cell uptake studies by flow cytometry

Cell uptake was assessed via flow cytometric analysis. Cells were seeded in 24-well plates at an initial concentration of 5.0×10^4 cells/well. After 24 h, cells were incubated with various dendrimer-based gene vectors carrying Cy5-labeled plasmid (2 μg DNA/well). After 5 h of incubation, the media was removed and cells were washed 3 times with 1x PBS and incubated with 1 volume of 0.25 % Trypsin with EDTA for 5 min at 37 °C. Two volumes of DMEM medium with 10% FBS were added to neutralize trypsin. The cellular uptake of gene vectors was measured using the Accuri C6 flow cytometer (BD Biosciences, San Jose, CA) with an FL4 band-pass filter with emission detection wavelength of 675/25 nm. Data were analyzed using the BD Accuri C6 software. The thresholds were set using untreated samples; cellular uptake of dendrimer-based gene vectors was compared to that of free plasmid uptake.

3.6.5. Cell uptake evaluation by con-focal microscopy

Similarly, for image-based analysis of gene vector cellular uptake; gene vectors formulated from BiD-TA-Cy5 and Cy3-labeled plasmid were administered to cells cultured in a 35 mm glass bottom culture dish (MatTek Corporation, Ashland, MA) stained with NucBlue® Fixed Cell ReadyProbes® Reagent and imaged using confocal LSM 710 microscope over 12 h in a live cell imaging chamber.

3.7. Results and Discussion

3.7.1 Preparation and characterization of the bifunctional dendrimer (BiD, 2)

The preparation of the bifunctional dendrimer (BiD, 2) was prepared using Fmoc protection/deprotection chemistry as shown in **Figure 18A** [134]. Our aim was to functionalize the dendrimer with approximately 20 amine groups out of the 64 hydroxyl end groups, so that it could be efficiently complexed with plasmid DNA. In brief, Fmoc-GABA-OH was reacted with the G4-OH dendrimer using PyBOP as a coupling reagent, to get Fmoc-functionalized intermediate (BiD-Fmoc, 1). A multiplet at 1.63 ppm for GABA-linker CH2 protons and multiplets between 7.30-7.86 for aromatic Fmoc protons in NMR confirmed the formation of the bond (**Figure 19**). The characteristic peak at 3.99 ppm for internal CH2 protons of G4-OH confirmed the formation of an ester bond with the linker. We calculated the loading of the linker by comparing the amidic protons of the dendrimer with aliphatic methylene protons of the linker, which suggested that 33 molecules were attached to the dendrimer (**Figure 19**). We carried out the deprotection step with piperidine (20% in DMF) without further purifying the intermediate, to get free bifunctional dendrimers (BiD, 2). Absence of Fmoc aromatic proton peaks in NMR

confirmed the deprotection of Fmoc groups. Using the proton integration method, we calculated that 18-20 linker molecules were attached to the dendrimer.

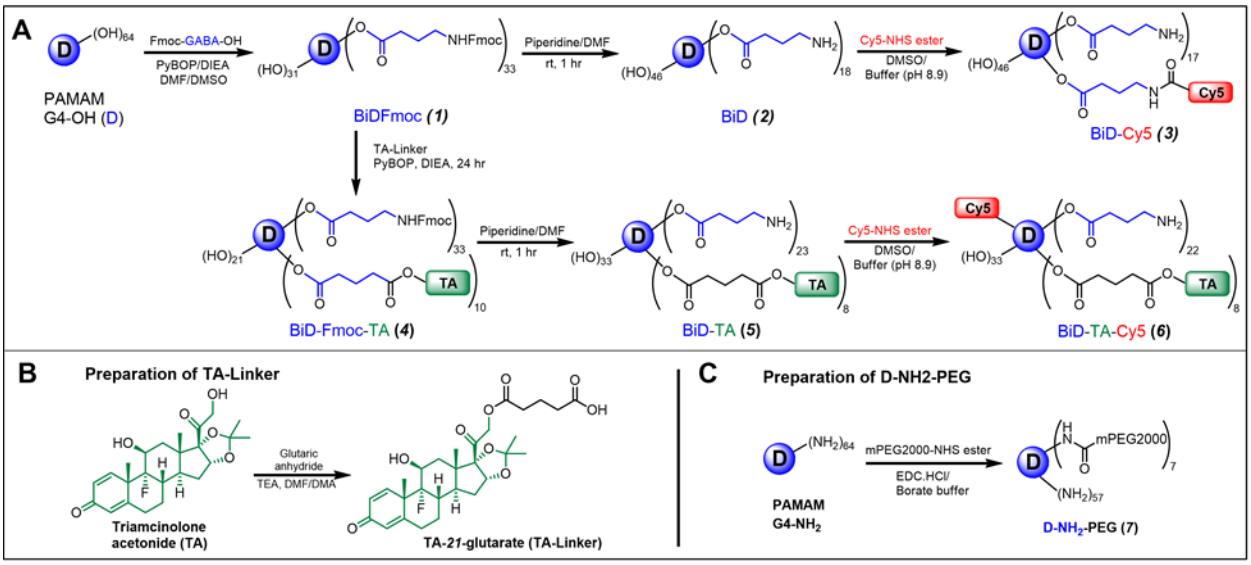

Figure 18: Preparation of the dendrimer conjugates. **(A)** Preparation of the amine functionalized bifunctional dendrimer (**BiD, *2***); Bifunctional triamcinolone acetonide (**BiD-TA, *4***); and Cy5-labeled bifunctional triamcinolone acetonide (**BiD-TA-Cy5, *5***). **(B)** Preparation of triamcinolone acetonide-21-glutarate (**TA-Linker**). **(C)** Preparation of PEGylated amine functionalized PAMAM dendrimer (**D-NH_2-PEG, *6***).

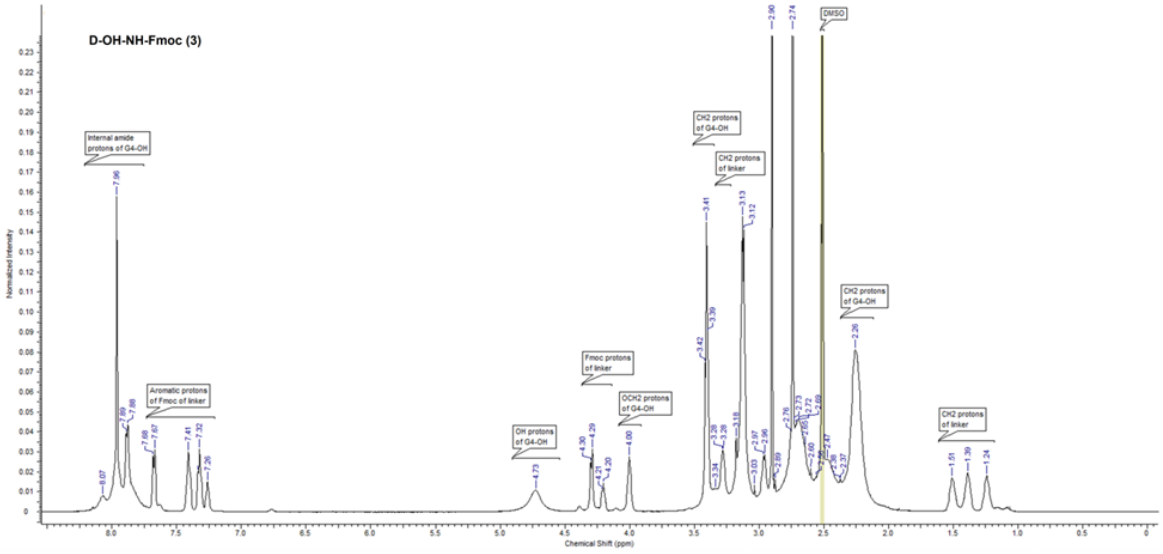

Figure 19: Proton NMR characterization of BiD-FMOC conjugate

3.7.2 Preparation of bifunctional-TA conjugate (BiD-TA, 4)

Synthesis of BiD-TA was performed using a three-step process with glutaric acid as a spacer, starting from G4-OH (**Figure 18A**). The Fmoc-functionalized dendrimer was reacted with TA-linker using PyBOP as the coupling reagent and DIEA as the base to get BiD-Fmoc-TA (3). The conjugate was characterized by ^{1}H NMR and reverse phase HPLC. In the 1H NMR spectrum, peaks at 0.84-1.50 ppm represent methyl protons of TA, and peaks at 4.75-6.25 ppm represent aromatic protons of TA and along with dendrimer peaks confirmed the formation of the conjugate. Four multiplets belonging to Fmoc aromatic protons still remained in the spectrum between 7.29 to 7.86 ppm, confirming the presence of Fmoc-linker molecules. The payload of TA to the surface of the dendrimer was calculated by comparing the proton integration of the amide protons of the G4-OH to the aromatic proton of TA; approximately 10 molecules of TA were conjugated (**Figure 20**). Finally, the Fmoc groups were deprotected with piperidine (20% in DMF) to get bifunctional-TA dendrimer (BiD-TA, 4) and the structure was established in proton NMR. Absence of aromatic Fmoc protons signal in NMR and presence of all signals related to TA confirmed the formation of the product with free amines on the surface. In the final BiD-TA conjugate, 8 molecules of TA and 23 free amine groups were confirmed using the proton integration method (**Figure 21**). The lower number of TA and amine groups in the conjugate were due to hydrolysis of the ester bond with prolonged exposure to dialysis in DMF under basic conditions (presence of piperidine in the reaction mixture and traces of water in DMF). The BiD-TA conjugate was readily soluble in PBS buffer and saline solution, in contrast to TA which has poor water solubility. The retention time of BiD-TA in HPLC chromatogram at

20.1 min (monitored at 240 nm, PDA detector) confirms the conjugation of the TA to the dendrimer. At the same time, the retention time of BiD was 9.5 min (monitored at 210 nm).

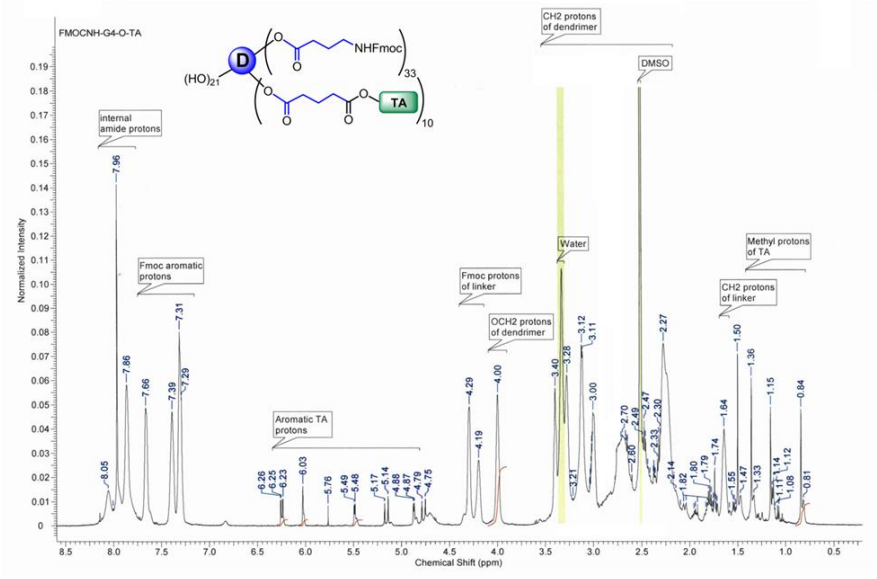

Figure 20: ^{1}H NMR spectrum of Fmoc-functionalized bifunctional-triamcinolone acetonide (BiD-Fmoc-TA, ***3***) in DMSO-d_6.

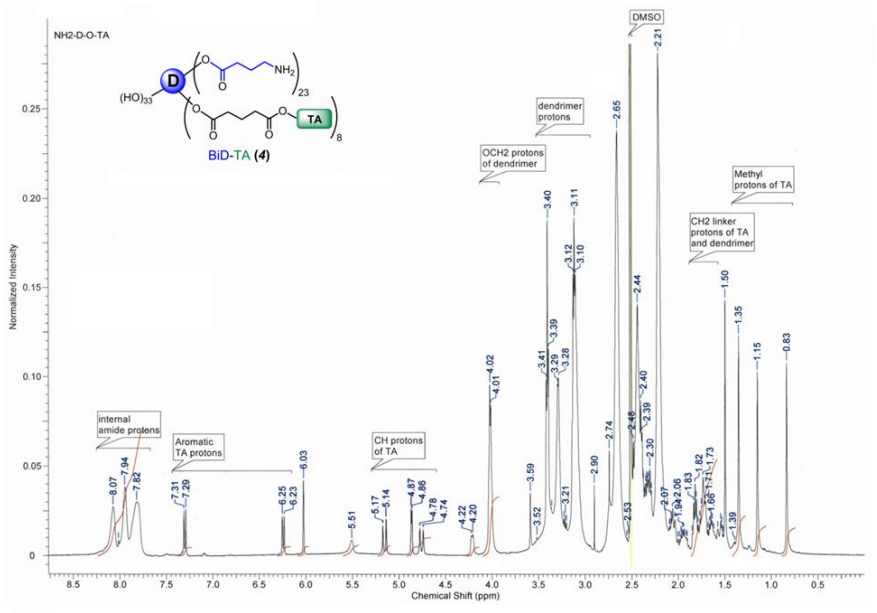

Figure 21: ^{1}H NMR spectrum of bifunctional-triamcinolone acetonide (BiD-TA, ***4***) in DMSO-d_6.

3.7.3. Preparation of BiD-TA-Cy5 (5) conjugate

The BiD-TA (4) was labeled with Cy5, a near IR imaging agent, to study the internalization of the conjugate in RPE cells. We have previously reported the preparation of the dendrimer-Cy5 and characterized extensively using HPLC/GPC, NMR and fluorescence spectroscopy.49 In brief, Cy5-mono-NHS ester was reacted with TA-functionalized bifunctional dendrimer (BiD-TA) in borate buffer to get Cy5-labeled dendrimers BiD-TA-Cy5 as shown in Fig. 1A. The final conjugate was purified by dialysis followed by GPC fractionation and characterized by reverse-phase HPLC and fluorescence spectroscopy. The HPLC trace showed a peak at 20.4 min. for BiD-TA-Cy5 (monitored at 645 nm excitation) different from BiD-TA and Cy5, confirming the formation of the conjugate. The fluorescence spectrum showed peaks at 648 nm (for excitation) and 663 nm (for emission) which follow a similar pattern to Cy5 also suggesting the conjugation of Cy5 to the dendrimer. Only one mole equivalent of Cy5 was used in each reaction and the percentage payload of the Cy5 to the dendrimer is ~4-5 wt%. The fluorescence quantum yield for the final conjugate was calculated to be 0.18, demonstrating a slight decrease compared to free Cy5 (~0.28).

3.7.6 Preparation of D-NH2-PEG (6) conjugate

The amine functionalized dendrimer (D-NH2) was partially functionalized with 2K PEG to enhance the transfection efficiency of the dendrimer. In brief, NHS-ester of mPEG2000 was reacted with D-NH2 dissolved in borate buffer to get the PEG functionalized dendrimer and was characterized by proton NMR. In the NMR chart, a peak at 3.25 ppm corresponds to OCH3 peak of the PEG and multiplets between 3.36-3.66 ppm (methylene protons of PEG) along with dendrimer protons peaks in between 2.15-3.10 ppm confirm the formation of the conjugate. The

loading of the PEG to the dendrimer was calculated by comparing the amidic protons of the dendrimer (8.02-8.24) to the backbone methylene protons of the PEG and found out that 7 molecules of the PEG were conjugated to the dendrimer.

3.7.7. Surface charge of dendrimer conjugates

BiD-TA and BiD ζ-potential were measured to be 13.9 mV and 12.9 mV, respectively. Their surface charge was significantly lower than the ζ-potential of D-NH2 (22.2 mV). D-NH2-PEG demonstrated significant shielding of the D-NH2 positive surface charge resulting in a ζ-potential of 11.7 mV.

3.7.8. Dendrimer conjugates buffering capacity

As expected, BiD-TA and BiD demonstrated significantly lower buffering capacity in comparison to D-NH2 and PEI, suggesting limited ability to buffer the lysosome environment and achieve endosome escape through the proton buffer effect, hence, underlying the importance of the incorporation of TA in order to improve the nuclear localization and transfection efficiency (**Figure 22**).

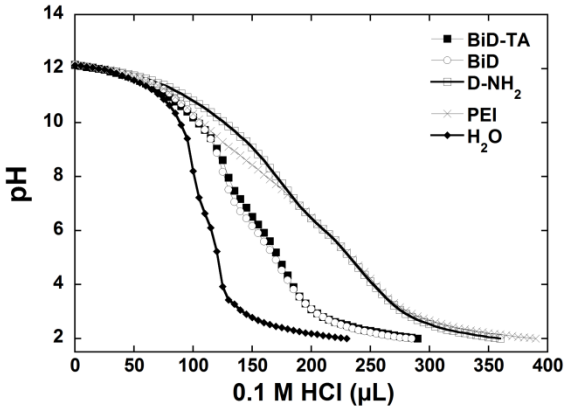

Figure 22: Buffering capacity. Measurement of buffering capacity of dendrimer base polymers by acid titration; PEI and ultrapure water were used as a control and solutions were titrated from pH 12 to pH 2 using 0.1 M HCL.

3.7.9. Gene vector formulation and characterization

Using BiD as a base, we were able to formulate compact ~50 nm gene vectors with a nearly homogeneous size distribution (PDI: 0.16) (**Figure 23A**). Similarly, the conjugation of 8 TA molecules did not appear to affect the complexation efficiency of these gene vectors, resulting in BiD-TA particles of similar size (~44 nm). We compared these gene vectors with conventional amine-terminated PAMAM dendrimer-based gene vectors at the same N/P ratio. This formulation resulted in particles with similar physicochemical characteristics (**Figure 24 and Table 2**). We confirmed the spherical morphology and efficient plasmid compaction of these gene vectors using TEM (**Figure 23B**). The gene vectors were stable in an aqueous solution for at least 10 days (**Figure 25A**). However, once added into a high ionic strength solution (phosphate buffered saline, PBS), the particles rapidly aggregated and lost their colloidal stability. After one hour of incubation in PBS, BiD and BiD-TA reached a size of ~500 nm. D-NH2 gene vectors aggregated at a slower rate and were ~300 nm in size at 1 hour (**Figure 25B**). To achieve successful transgene expression the gene vectors need to reach the target cells intact; the lack of stability and rapid aggregation imposes a serious obstacle to in vivo gene therapy.

In order to improve nanoparticle stability we formulated gene vectors using a blend of BiD-TA and D-NH2-PEG.26 This technique resulted in gene vectors of similar size (~50 nm) but a significantly lower ζ-potential of ~6 mV in comparison to that of non-coated nanoparticles (BiD-TA: ~11.4mV, BiD: ~13.3 mV, D-NH2: ~14.5 mV). The ratio of BiD-TA to D-NH2-PEG did not affect the physicochemical characteristics of the gene vectors. Gene vectors formulated by 100% D-NH2-PEG had size of 42 nm and ζ-potential of 5.2 mV. In comparison, BiD-TA/ D-NH2-PEG based gene vectors formulated with 25%, 50% and 75% of amines contributed by BiD-TA had sizes of 51 nm, 51 nm and 43 nm, respectively and ζ-potential of 7.3 mV, 6.1 mV

and 5.9 mv, respectively. The 'shielding' of the gene vectors ζ-potential suggests effective PEG coating. PEG significantly improved stability in high ionic strength solutions, as PEG coated gene vectors retained their physicochemical properties for at least 18 h. Interestingly, gene vectors with higher than 25% of amines contributed by D-NH2-PEG slightly increased in size, whereas gene vectors with only 25% of amines contributed by D-NH2-PEG retained their size over 18 h (**Figure 25C**).

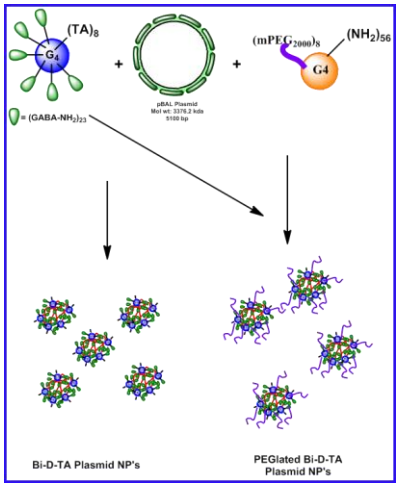

Figure 23: A schematic representation of gene vector formulations

Gene vectors	Hydrodynamic diameter (nm) ± SEM	PDI	Zeta Potential (mV) ± SEM
BiD-TA	43.6 ± 4.7	0.20	11.4 ± 2.7
BiD	54.1 ± 3.6	0.16	13.3 ± 1.1
D-NH_2	43.7 ± 0.5	0.29	14.5 ± 1.8
D-NH_2-PEG	42.1 ± 4.7	0.24	5.2 ± 1.0
BiD-TA 75% + D-NH_2-PEG 25%	51.1 ± 2.1	0.26	7.3 ± 0.6
BiD-TA 50% + D-NH_2-PEG 50%	51.1 ± 2.7	0.24	6.1 ± 0.5
BiD-TA 25% + D-NH_2-PEG 75%	43.5 ± 6.3	0.25	5.9 ± 1.1

Table 2: Physicochemical characteristics of respective dendrimer-based gene vectors Size and polydispersity (PDI) were measured by dynamic light scattering (DLS). ζ-potential was measured by Laser Doppler anemometry. Measurements were performed in 10mM NaCl at pH 7.0 and are presented as average of at least 3 measurements ± standard error (SEM).

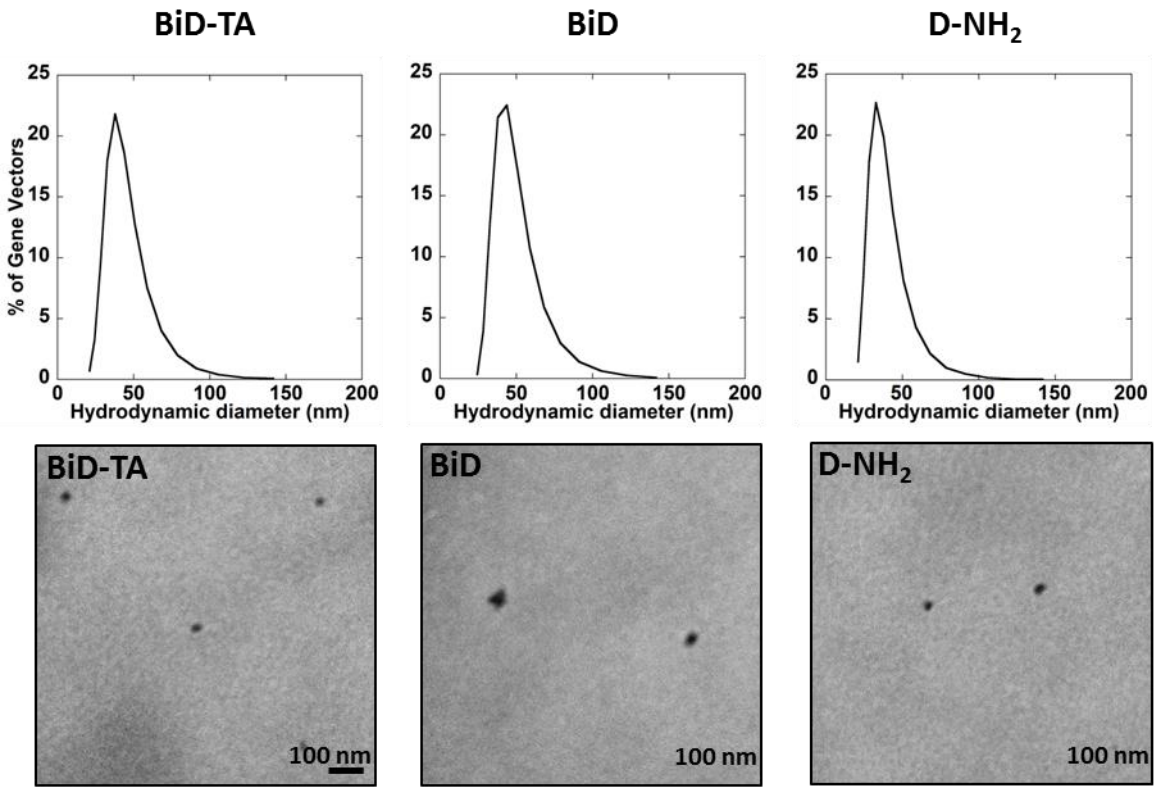

Figure 23: Gene vector characterization. (A) Hydrodynamic diameter distribution of respective gene vectors. **(B)** Transmission electron microscopy images of respective gene vectors in ultrapure water.

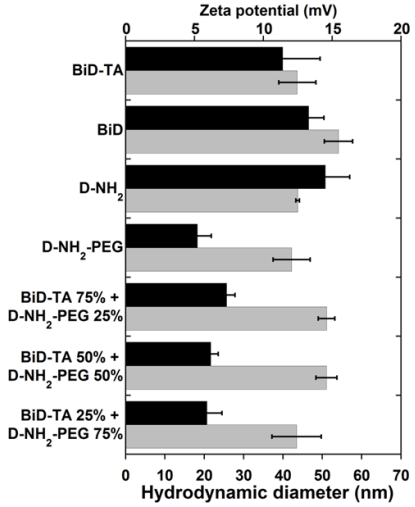

Figure 24: Size and Zeta-potential of respective gene vectors measured by dynamic light scattering (DLS) method, data represents average of 3 measurements mean ±standard error.

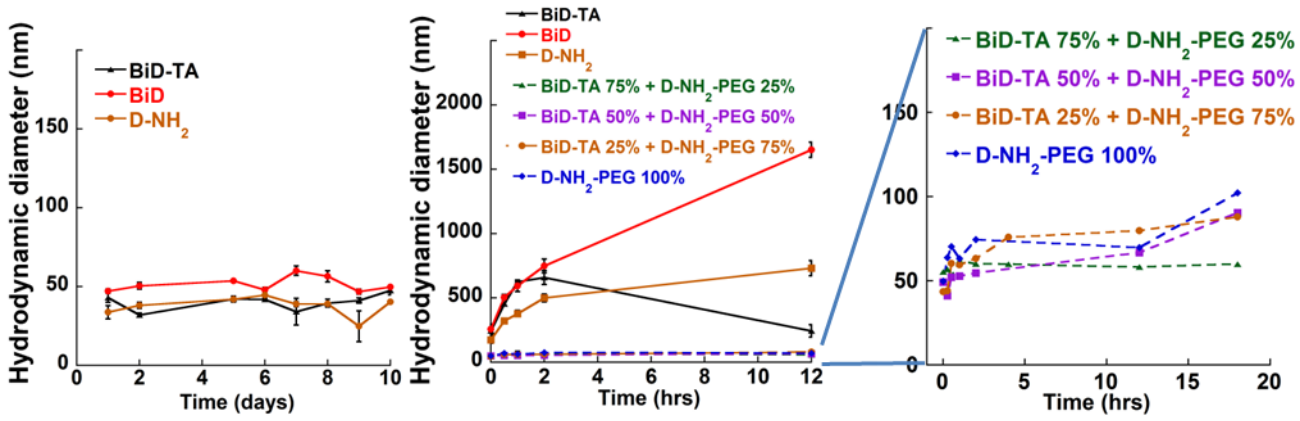

Figure 25: Gene vector stability in ultrapure water (A) at high ionic strength solution (B) using DLS to measure hydrodynamic diameter. Data are presented as average of at least 3 measurements ± (SEM).

3.9.10. Gene vector cell uptake and transfection efficiency in retinal pigment epithelium

Transfection of BiD and BiD-TA was compared to D-NH2 gene vectors as well as PEI and PEG-PLL gene vectors, which are widely used and are considered to be gold standards for non-viral gene delivery [111, 141-143]. The use of BiD resulted in approximately 59-, 59000- and 29000- fold lower transfection efficiency in comparison to PEG-PLL, PEI and D-NH2 respectively, in primary RPE cells. In contrast, incubation of BiD-TA gene vectors resulted in ~1700- fold higher transfection in comparison to PEG-PLL, and no statistically significant difference in transgene expression in comparison to PEI or D-NH2. BiD-TA transfection efficiency was 100000-fold higher than BiD (**Figure 24A**), underlying the important role of TA in improving transfection efficiency. These results were qualitatively confirmed using eGFP plasmid in combination with fluorescence microscopy (**Figure 24 C-D**), which suggested that BiD-TA and D-NH2 were comparable.

TA binds to the cytosolic glucocorticoid receptor (GR), which dilates the nuclear pores and translocate itself into the nucleus along with the gene carrier [132, 133]. Here, we take

advantage of the high concentration of GR in human ARPE cells to achieve high-level transgene expression using hydroxyl terminated PAMAM dendrimer-based gene vectors.

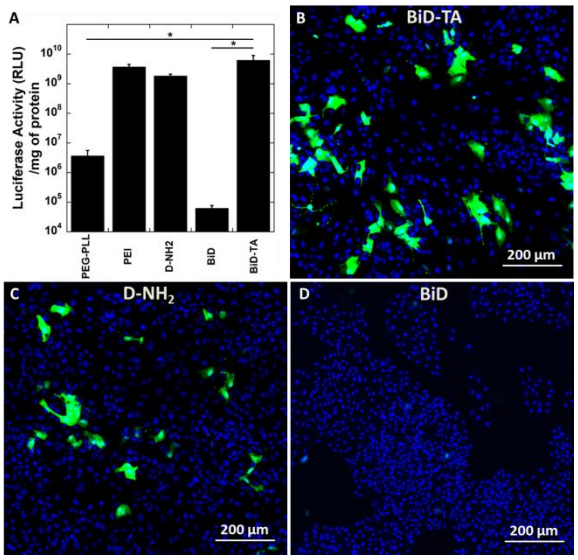

Figure 24: Transfection of human ARPE-19 cells by cationic polymer based gene vectors. (A) Luciferase activity following *in vitro* delivery of the luciferase gene to human ARPE 19 cells with respective gene vectors. Data represents mean ± SEM. * denotes statistical significance; $p<0.05$ **(B-D)** *In vitro* eGFP expression by ARPE cells following eGFP plasmid delivery using respective gene vectors.

Flow cytometry analysis was performed to assess the effect of different dendrimer types as well as the addition of TA on the gene vector cell uptake. BiD did not efficiently penetrate ARPE cells, with only ~30% of cell population taking up the fluorescently labeled plasmid, ~2.4-fold lower than D-NH2. The mean fluorescence intensity (MFI) of the BiD treated cells was 100-fold lower than D-NH2 treated cells. In contrast, BiD-TA based gene vectors achieved high level cell uptake of ~80%, comparable to D-NH2. However, the MFI, indicative of the absolute amount of plasmid taken up, was 5-fold lower than D-NH2 treated cells (**Figure 25A-E**). This is the first study to demonstrate not only improved transfection but also enhanced cellular uptake of TA conjugated gene vectors.

In order to confirm that the nanoparticles were able to enter the cells intact, we formulated BiD-TA gene vectors with 5% of amines contributed by Bi-D-Cy5 and Cy3-labeled plasmid. Fluorescence confocal microscopy and differential interference contrast (DIC) microscopy were combined to observe co-localized Cy3-plasmid and Cy5-dendrimer in the cell cytoplasm as well as the cell nucleus, indicating that dendrimer nanoparticles were able to be taken up and localize in the nucleus intact (**Figure 25F**), without disintegration during the endocytotic, and endosomal-lysosomal-nucleus transport.

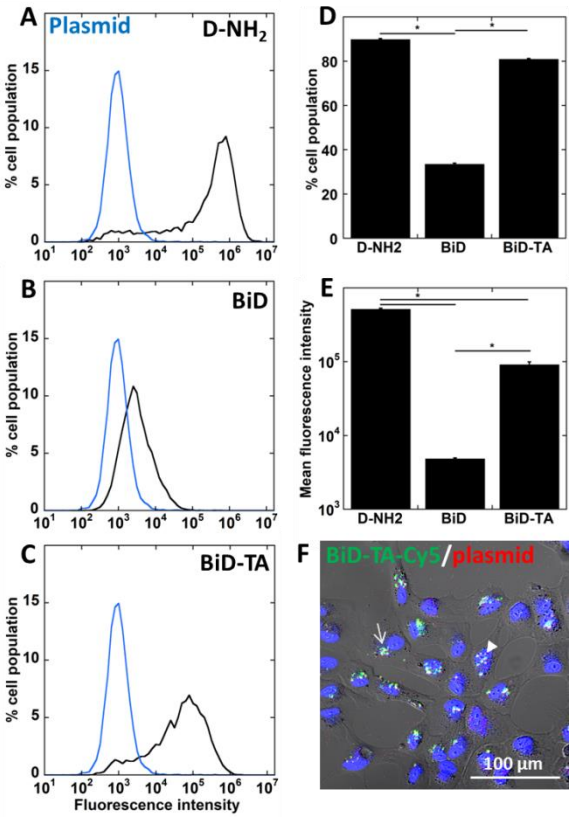

Figure 25: Gene vector uptake by human ARPE cells. (A-E) Flow cytometric analysis of fluorescently labeled gene vector cell uptake after 4 h of incubation with respective gene vectors. Data represents mean ± SEM. * denotes statistical significance; $p<0.05$ **(F)** Confocal imaging of BiD-TA gene vector cell uptake using dual fluorescent labeling. Dendrimer (Green), Plasmid (Red), Co-localization (Yellow). White arrow indicates gene vectors in the cytoplasm; white arrow head indicates gene vectors in the nucleus.

3.7.11. Role of TA and PEG in cell uptake and transfection efficiency

In order to further understand the amount of TA required for effective cell uptake and transgene delivery, we repeated the cell uptake and transfection studies using dendrimer nanoparticles formulated from a blend of BiD-TA and BiD at a decreasing percent of amines contributed by BiD-TA (**Figure 26A-H**). Varying the BiD-TA to BiD ratio did not result in significant change of the gene vector physicochemical characteristics. More specifically, formulation of nanoparticles with 100%, 75%, 50%, 25%, 10% and 5% of amines contributed by D-TA resulted in sizes of 42.9 nm, 34 nm, 34.5 nm, 38.8 nm, 46.2 nm and 45.8 nm, respectively. Also, the ζ-potentials were 16.5 mV, 9.92 mV, 15.8 mV, 13.6 mV, 15.3 mV, 16.9 mV, respectively.

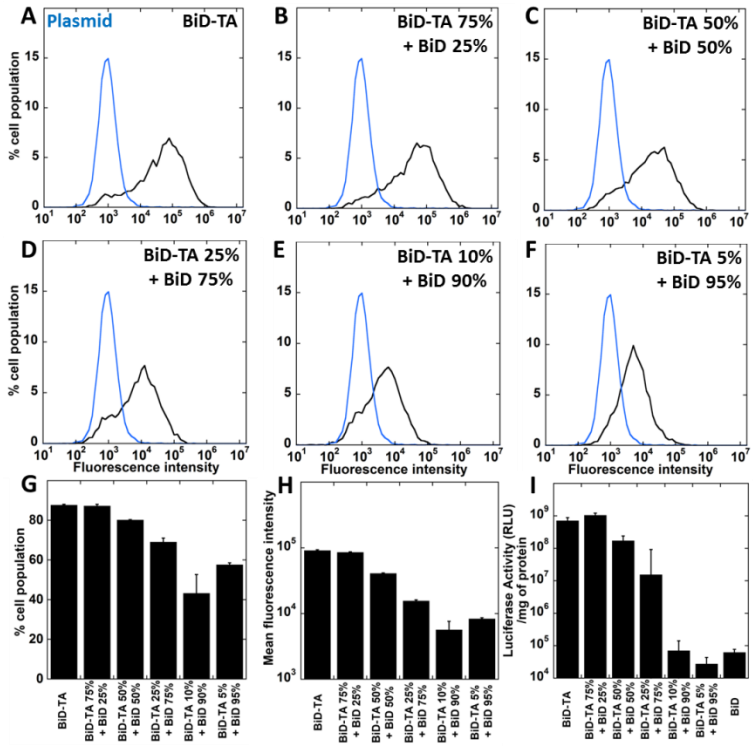

Figure 26: Effect of conjugated TA on gene vector cell uptake and transgene expression. (A-H) Flow cytometric analysis of cell uptake of fluorescently labeled gene vectors with varying ratios of BiD-TA/BiD. **(I)**

Luciferase activity following *in vitro* delivery of luciferase gene to human ARPE 19 cells with respective gene vectors of varying BiD-TA/BiD ratios. Data represents mean ± SEM.

Both the percentage of cell uptake as well as MFI demonstrated a positive correlation with the percentage of BiD-TA in the gene vectors (R2: 0.842, $p<0.01$; R2: 0.923, $p<0.01$; respectively). The transgene expression demonstrated a similar positive correlation (R2: 0.765, $p<0.01$). Importantly, the inclusion of BiD-TA equal to or lower than 10% did not seem to improve transfection over BiD gene vectors. This underlines the importance of achieving a significant TA concentration on the gene vector surface in order to allow for improvement of cell uptake and transgene expression.

Having established the role of a PEG coating in drastically improving the stability of these gene vectors we attempted to determine the effect of formulating a gene vector with a blend of D-NH2-PEG and BID-TA on cell uptake and transfection efficiency. We used a previously established blending technique, with different percentages of amines contributed by D-NH2-PEG, and achieved effective PEG coating of the gene vectors as demonstrated by the significant shielding of the positive surface charge and stability of the gene carriers. Flow cytometric analysis determined no significant difference in percentage of cell uptake or MFI between PEG coated gene vectors with varying ratios of D-NH2-PEG to BiD-TA (**Figure 27A-E**). The percentage of cell uptake of the PEGylated dendrimer gene vector did not differ significantly from BiD-TA and D-NH2 gene vector uptake (~80%). However, the MFI was significantly lower for the PEGylated gene vectors ($p<0.05$), indicating lower absolute amount of gene vector uptake. No difference in transfection efficacy was observed between the PEGylated gene vectors. The transgene expression following incubation with PEGylated gene vectors was significantly decreased compared to BiD-TA and D-NH2 ($p<0.05$) but still significantly higher

than BiD-based gene vectors ($p<0.05$) (**Figure 17F**). These findings are in good agreement with previous studies demonstrating that relatively small nanoparticles can be efficiently taken up regardless of their PEGylation profile. However, the improved stability of PEG coated cationic polymer based gene vectors impedes endosome escape and reduces transfection [143].

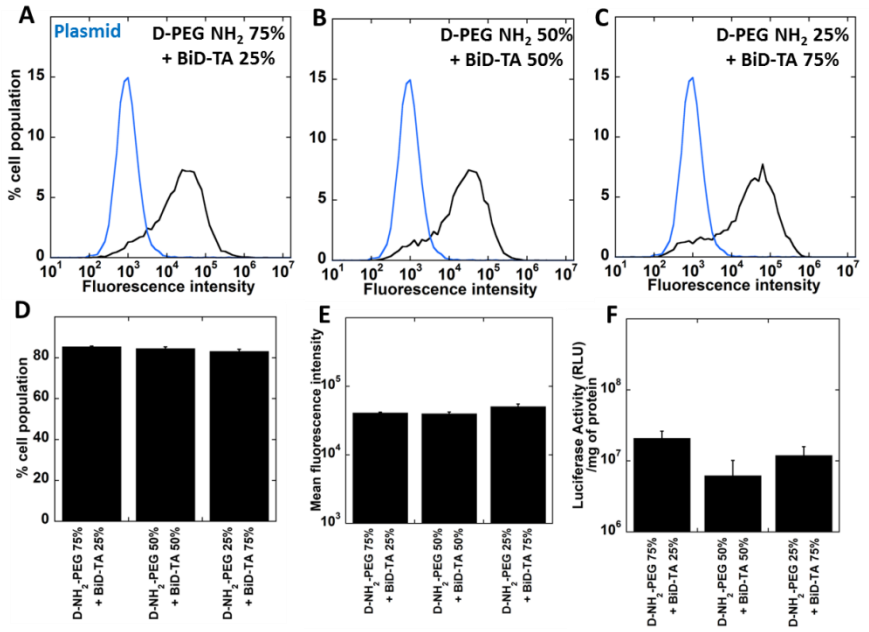

Figure 27: Effect of BiD-TA gene vector PEG coating on uptake and transgene expression. (A-H) Flow cytometry analysis of cell uptake of fluorescently labeled gene vectors with varying D-NH_2-PEG/BiD-TA ratio. **(I)** Luciferase activity following *in vitro* delivery of luciferase gene to human ARPE 19 cells with respective gene vectors of varying D-NH_2-PEG/BiD-TA ratio. Data represents mean ± SEM.

3.7.12. Cytotoxicity profile

ARPE cell transfection has been greatly limited by the cytotoxic effect of different gene vector systems. Importantly, cell incubation with varying concentrations of BiD-TA, BiD and BiD-TA/D-NH2-PEG blend did not result in significant toxicity. However, incubation with D-NH2, D-NH2-PEG and BiD-TA/D-NH2 blend resulted in statistically significant toxicity, presumably due to the increased positive surface charge and cytotoxicity of the base polymers

(**Figure 28**). Therefore, partial PEGylation and the hydroxyl groups improves the toxicity profile of the delivery vectors.

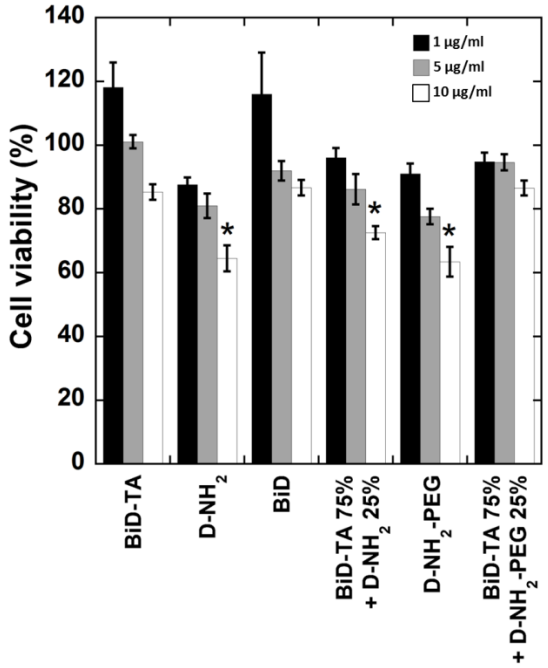

Figure 28: Cytotoxicity of dendrimer-based gene vectors to human aRPE cells. Cells were treated with varying concentrations of respective gene vectors. Cell viability was measured after 24 h of treatment and compared to non-treated controls. Data represents the mean ± SEM. * Denotes statistically significant ($p < 0.05$) difference from 80%.

3.8. Conclusions

In this study we attempted to address the inherent limitations of cationic-polymer based non-viral gene vectors. Using hydroxyl-functionalized PAMAM dendrimers, we achieved effective plasmid compaction, resulting in relatively small complexes using (a) a base-polymer with minimal amount of primary amine groups to minimize cytotoxicity, (b) TA as a nuclear localization signal to improve transfection and (c) a hydrophilic and near neutral PEG coating to improve stability in physiological solutions. We demonstrated efficient transgene delivery in hard to transfect human retinal pigment epithelial cells.

Cationic polymers with a high number of amine groups, such as PEI and amine-terminated PAMAM dendrimers, have traditionally been used for efficient complexation [112]. We establish a new approach in which we minimally functionalized a hydroxyl PAMAM dendrimer, with or without the conjugation of TA, in order to achieve efficient compaction while retaining a reduced cytotoxicity profile in primary RPE cells [144]. These complexes demonstrate physicochemical characteristics similar to conventional D-NH2 gene vectors. However, the lack of stability of both conventional and BiD based gene vectors in high ionic strength solutions somewhat limits their translational relevance. For this reason, we adapted a previously established blending technique [113]. to introduce a hydrophilic PEG coating which substantially reduces aggregation of the particles and increases the possibility of reaching the target cells intact [117,118] allowing for protection of the plasmid cargo [154] and more efficient cell uptake.

TA has previously demonstrated the ability to improve transgene expression and nuclear localization in human embryonic kidney and human hepatocellular carcinoma [132-133]. In this study we used this attribute in order to offset the lack of buffering capacity, endosome escape and nuclear localization of BiD-based gene vectors and improve transgene expression in primary RPE cells, an important group of cells in retinal function and retinal diseases. Indeed, BiD-TA based gene vectors were observed to enter the nucleus intact and achieved high level transgene expression similar to conventional D-NH_2 based gene vectors. We demonstrate for the first time that TA can drastically enhance transfection of hard to transfect retinal pigment epithelial cells. We further show that the effect of TA is dose dependent and that at least 25% of base-polymer needs to be conjugated to TA to significantly improve transgene delivery.

The ability of gene vectors to enter the cells constitutes an important limiting factor for non-viral gene delivery for slowly replicating cells. We found that BiD based gene vectors are taken up significantly less than D-NH_2 gene vectors, presumably due to reduced electrostatic interaction with the cell membrane. Interestingly, TA seems to be involved in the endocytosis process as there was a significant improvement in cell uptake for BiD-TA based gene vectors. In fact, there was a positive correlation between the amount of TA on nanoparticles and cell uptake. This phenomenon may be attributed to the nuclear localization of BiD-TA gene vectors leading to decreased exocytosis [146].

PEG coating has been suggested to reduce particle uptake by cells [147-148]. However, in good agreement with previous studies on PEGylated cationic polymer based gene vectors [143], we found that PEGylation did not affect cellular uptake. Their small particle size may contribute to effective uptake in spite of PEGylation [149-150]. The reduced transfection efficacy of the PEGylated gene vectors may be explained by their improved stability that impedes DNA unpackaging and endosome escape [143, 151]. The stability in physiological solutions, favorable safety profile and relatively high transfection efficiency of these PEGylated gene vectors renders them a promising vehicle for the delivery of therapeutic transgenes to retinal pigment epithelial cells in vivo.

CHAPTER 4 "EVALUATION OF RETINAL MICROGLIA UPTAKE AND BIODISTRIBUTION OF DENDRIMERS IN MICE ISCHEMIC-REPERFUSION (I/R) MODEL"

4.1. Abstract

Microglial activation occurs in many diseases of the retina including viral infection, diabetes, and retinal degeneration. It was shown previously that hydroxyl-terminated polyamidoamine (PAMAM) dendrimers are taken up and retained in microglia during retinal degeneration. The purpose of this study was to develop a nanoparticle formulation that targets activated retinal microglia and can be delivered safely intravenously as well as intravitreally. The dendrimers were conjugated to Cy5 (D-Cy5) and were evaluated by intravenous (femoral vein) or intravitreal injection in normal BALB/c mice and in a murine model of ischemia/reperfusion (I/R). Uptake of the dendrimer by microglia was determined with immunofluorescence using rabbit Iba-1 antibody with Cy3-goat anti-rabbit secondary antibody (microglia) and GSA lectin-FITC (blood vessels and microglia). Clearance of the D-Cy5 from the normal eyes appeared almost complete by 24 hours after injection. In eyes with activated microglia after I/R injury, the D-Cy5 appeared to be retained by microglia (IBA+) up to 21 days after intravenous administration. The nontoxic PAMAM dendrimers appeared to be an excellent drug delivery system to activated microglia. This approach may yield an intravenous dendrimer-based therapy to decrease inflammation in diseases associated with retinal microglia activation like age-related macular degeneration.

4.2. Introduction

Microglia cells are the resident inflammatory cells of the brain and retina [152]. They become activated in diseases such as diabetes and retinal degeneration where photoreceptors die, causing microglia to scavenge dead cells. Activation of retinal microglia occurs in a mouse model of Ischemia reperfusion (I/R) which is a model of branch vein occlusion. Retinal vascular occlusion, be it by high intra-ocular pressure in I/R model or thrombus in BVO, causes a decrease in blood flow to the eye or ischemia. This causes death of photoreceptors initiating further activation of inflammatory microglia [153].

Dendrimers are a group of molecules that have the potential to deliver drugs and small molecule therapies to intracellular domains because of the large number of functional groups. Previously our group have shown utility of a dendrimer-based therapeutic can be used to treat a rabbit model cerebral palsy (CP. This rabbit model replicates the neuroinflammation seen in the adult brain. Using microglia as a target for attenuation of inflammation may be an alternative way for treating a number of diseases of the brain and eye such as age related macular degeneration (AMD) where inflammation plays a large part in the degeneration of photoreceptors which destroys the delicate environment of the retina and choroid [27].

Therefore, we in this chapter investigated the ability of dendrimers to target activated microglia in retina. We evaluated dendrimeric transport into normal murine retina as well as retina following ischemia reperfusion injury in which microglia activation occurs. This study also aimed to characterize the transport and retention of dendrimer by microglia in the retina after local intravitreal delivery as well as systemic intravenous delivery. Systemic delivery would have many advantages to current treatments as there are at present no systemic treatments

available for ischemic retinopathies and AMD. These advantages include less frequent injections due to retention in microglia and ability to delivery systemically, avoiding monthly intraocular injections as in current anti-VEGF therapies.

4.3. Materials and methods

4.3.1. Synthesis of D-Cy5 conjugates:

D-Cy5 was synthesized in 3 steps reaction. 1st step is synthesis of bifunctional dendrimer using FMOC-NH-Caproic acid to G4-OH dendrimer using PyBOP as coupling reagent with DIEA as base. The FMOC groups are deprotected using piprideine in the 2nd step and reacted with Cynine due Cy5-NHS ester. The resulted conjugates were purified using dialysis against DMA and then against water. The purified conjugate solution was lyophilized and then passed through GPC to remove traces of unreactive dye.

4.3.2. High Performance Liquid Chromatography (HPLC) analysis

The purity of the dendrimer-Cy5 conjugates (D-Cy5) were analyzed using Waters HPLC instrument equipped with Waters In-line degasser, binary pump, photodiode array (PDA) detector, multi fluorescence λ detector and auto sampler (maintained at 4ºC) interfaced with Empower software. The HPLC chromatogram was monitored simultaneously for absorbance at 210 nm for dendrimer and 650nm for Cy5 using Waters 2998 PDA detector and fluorescence with excitation at 645 nm and emission at 662 nm using Waters 2475 fluorescence detector. The water/acetonitrile (0.1% w/w TFA) was freshly prepared, filtered, degassed, and used as a mobile phase. TSK-Gel ODS-80 Ts (250 X 4.6 mm, 25 cm length with 5 µm particle size) connected to TSK-Gel guard column was used. A gradient flow was used with initial condition of 90:10 (H2O/ACN) and gradually increasing the acetonitrile concentration at 10:90

(H2O/ACN) by 30 min and returning to original initial condition 90:10 (H2O/ACN) in 60 min with flow rate of 1 ml/min.

4.3.3. Dynamic light scattering and Zeta potential analysis:

The particle size and ζ-potential of G4-OH and D-Cy5 conjugates were determined by dynamic light scattering (DLS) using a Zetasizer Nano ZS equipped with a 50 mW He-Ne laser (633 nm). For sizing the samples were dissolved in deionized water (18.2 Ω) to make the solution with the final concentration of 50 μg/mL. The solution was filtered through a cellulose acetate membrane (0.45 micron, PALL Life Science) and DLS measurements were performed at 25°C with a scattering angle of 173°. Zeta potentials were calculated using the Smolokowsky model and measurements were performed in triplicate.

4.3.4. Animals & Ischemia reperfusion (I/R) injury:

All procedures involving the animals conformed to the ARVO Statement for the Use of Animals in Ophthalmic and Vision Research. BALB/c albino mice, each weighing ~25 grams, housed in wilmer animal facility at johns hopkins were used for transport as well as I/R studies. All surgeries were performed under anesthesia using ketamine (100mg/Kg) and Xylazine (10mg/Kg) injected into the peritoneal space. Six mice were used in each group at each time point. I/R injury was performed in left eye by following the procedure described elsewhere [7]. Briefly, the anterior chamber was cannulated with 30 gauze needle attached with line infusing saline system. The saline system is mounted on to a custom made saline reservoir and elevated to certain height (calibrated to 90mm Hg). The IOP was elevated to 90mm Hg for 90mins and I/R injury and shut off of choroidal circulation was evidenced by blanching of the posterior segment

via fundus examination. After ischemia the needle is immediately withdrawn for immediate blood reperfusion. The right eye with no injury serves as control.

4.3.5. Routes of Administration, Injections and Time points for Sacrifice

Dendrimer-Cy5 (D-Cy5), free Cy5 (free dye) or PBS was injected 6 days after Ischemia reperfusion injury (I/R) by intravitreal administration or intravenous administration. For intravenous injections, 100 µl of D-Cy5, Cy5 or PBS was injected into the femoral vein of the mouse using a 1ml syringe. Each mouse injected via femoral vein on a D-Cy5 basis in 100 µL of sterile PBS (600 µg). For intravitreal injections, 2 µl (20 µg) of D-Cy5, Cy5 or PBS was injected with a Harvard compression injector using a glass needle. A 30 gauge metal needle was used to pierce a hole to allow the glass needle into vitreous chamber. Animals were sacrificed at 24 hours, 72hours or 21 days after injection of D-Cy5. Control animals (Cy-5 and PBS) were sacrificed at 24 hours post administration. Animals were sacrificed with a lethal dose of pentobarbital intracardially after ketamine/Xylazine anesthesia.

4.3.6. Biodistribution analysis of D-Cy5 in vital organs and posterior eye cups

Twelve BALB-C mice weighing ~ 25 gr BW were used for this study. Four animals were sacrificed at each time point: 24hrs, 72hrs and 21 days. Each mouse was injected via femoral vein with 600 µg of D-Cy5 in 100 µL of sterile PBS. At respective time point, the animals were euthanized and vital organs (heart, lungs, spleen, kidney, liver and eyes) were harvested immediately and respective wet organ wet weights were noted, organs snap frozen on dry ice, and stored at -80ºC until analysis. Upon analysis, the tissues were thawed and approximately 100-150 mg of tissue were measured and homogenized with 1 ml of MeOH in low DNA binding using stainless steel bead and tissue homogenizer resulting in a pulpy tissue suspension. The

suspension was sonicated for 30 minutes and appropriate volumes containing 100mg of tissue were placed in different low DNA binding vials and diluted with methanol to 1 ml so that the same amount of tissue and same volume was analyzed for each sample. The samples were centrifuged at 10,000 rpm for 10 mins at 4ºC resulting in supernatants, which were subjected to fluorescence spectroscopy (FLS).

4.3.7. Analysis of cryopreserved tissue sections and microglia localization

Eyes were enucleated and fixed in 2% paraformaldehyde (PFA). The anterior chamber of the eye was removed and eye cup cryopreserved using previously established protocols. The eyes were frozen with dry ice in isopentane in 20% sucrose with optimum cutting temperature compound (OCT) in a 1:2 ratio respectively. Cryoblocks are stored at -80°C until sectioned. 8um sections were cut from previously frozen blocks using a cryostat. Sections were incubated in rabbit anti-Ionized Calcium Binding Adapter 1 molecule (IBA-1), which is a microglia cell marker, and a goat anti-rabbit-Cy3 secondary antibody applied. Sections were analyzed on a Zeiss 510 confocal microscope. Excitation and emission wavelengths and laser settings were identical to analyze all tissue in Intravitreal injected animals and IV injected animals. A z-stack of the sections were taken and collapsed to give an image through the depth of the whole section.

To quantify the amount of D-Cy5 accumulation in retina and choroid upon intravenous and intravitreal injections were determined as follows. The anterior chamber along with the lens were removed from the enucleated eyes and the posterior eyecups were frozen using liquid nitrogen and immediately homogenized using disposable micro pestles (Bel-art, NJ, USA.) and reconstituted with 100µL of 0.05M Methanolic tichloroacetic acid (TCA) and sonicated for 15mins. The methanol was evaporated using vacuum and the homogenized tissue was

reconstituted with 100µL of PBS and freezed at -80ºC and lyophilized. The white powder obtained was reconstituted with 100µL of HPLC grade methanol and sonicated for 20 mins and centrifuged at 20,000 rpm for 20 mins. The supernatant was collected and subjected to FLS measurements using low volume quartz cuvette (starna cells. Inc., CA, USA). The fluorescent emission values were obtained with a slit width 10-10 at 665nm and the background was subtracted from PBS injected samples. The amount of D-Cy5 was calculated from calibration graph ranging from 0.5 to 20ng at same slit width.

4.4 Results

4.4.1. Synthesis of D-Cy5 Conjugates

Ethylenediamine-core poly-(amidoamine) [PAMAM] hydroxyl-terminated generation-4 (G4-OH) were labelled with near IR fluorescent dye Cy5 which was already reported in our previous publications [72]. Briefly, G4-OH was partially functionalized by 6-amino caproic acid using FMOC protection/deprotection chemistry resulting in bifunctional dendrimers with ~5-6 NH2 groups on their surface. The resulting bifunctional dendrimers with reactive amine groups were reacted with N-hydroxysuccinimide monoester Cy5 dye to obtain the D-Cy5 conjugate (**Figure 29**). The resulting conjugates were purified using dialysis and GPC and characterized using ^{1}H NMR. The HPLC chromatogram of bifunctional dendrimer showed elution time of 14.84 min from the column which is different from the elution time of G4-OH dendrimer (elution time 14.42 min) (**Figure 30**). This indicates formation of new compound and there is a minor shift in elution time indicating that the structural property of G4-OH dendrimer has not changed significantly.

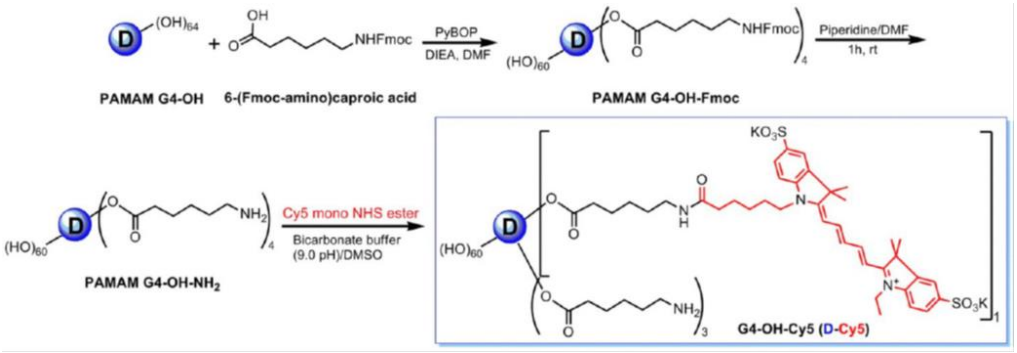

Figure 29: Preparation of Cy5 labelled PAMAM G4 dendrimer (D-Cy5)

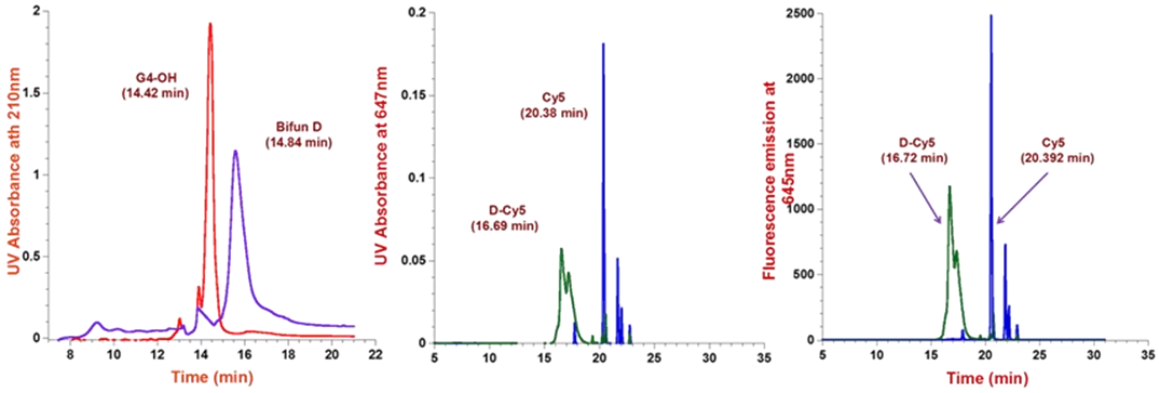

Figure 30: HPLC chromatrograms of G4-OH, Bifunctional dendrimer, D-Cy5 and free Cy5 eluted from the columns. Appearance of different peaks at varied time points assures the purity of the conjugates.

This is also congruent from the DLS results where the approximate size and Zeta potential of G4-OH dendrimer 4.36±0.18nm and +4.59±0.11mVrespectively. Whereas, the size and Zeta potential values of bifunctional dendrimer were 4.87±0.20 and 6.63±0.24mV respectively indicating no significant change in size and surface properties of dendrimers. Appearance of new peak simultaneously in 16.69min at 647nm (UV λmax for Cy5) and 645nm (fluorescence emission of Cy5) which is different from the Cy5 peaks (20.39min) confirms successful conjugation of dye to the dendrimers.

4.4.2. Changes in retinal microglia and retinal structure

In normal retina Iba-1+ve resident microglia/macrophages were found to be lesser in number and have ramified morphology with distinctive dendritic structures. The heterogeneous populations of microglial cells were predominately found in choroid and inner nuclear layer (INL) and very few of them were found scattered in outer plexiform layer (OPL). The retinas were structurally intact with all the layers compacted to one other. I/R injury led to a marked activation of microglia in the retina and choroid. In I/R retinas the microglial/macrophage cells showed marked changes in morphology, increased number and retinal distribution. 6 days post IR the retinal resident microglial/macrophages were devoid of their dendritic structures, became amoeboid with smaller cell bodies. Increased numbers in activated microglial cells were found distributed in all retinal layers such as IPL, INL, ONL and subretinal layers. Interestingly we found decreased number choroidal microglia/macrophages suggesting their infiltration in to retina. The IR injury caused collapse of inner retinal layers and retinal detachment from choroid and RPE layers. We also observed thinning of retina especially the nuclear layers in IR injured retinas when compared to normal retina suggesting neuronal and ganglionic cell atrophy (**Figure 31**).

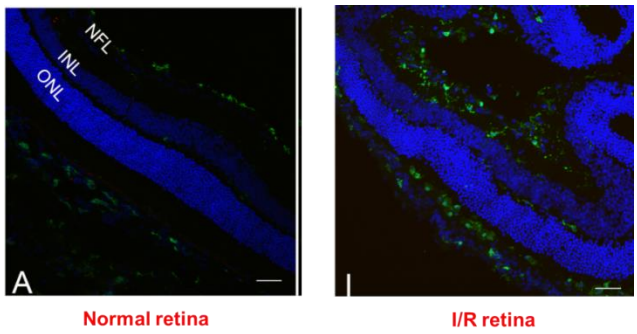

Figure 31: Confocal images of normal and I/R retina. **A)** Normal retina with regular retinal layers and less microglial cells (Green). **B)** I/R retina showing pathology related structural alterations and damage with increased microglial population. (**NFL**- Nerve fiber layer, **INL**- Inner nuclear layer, **ONL**-Outer nuclear layer).

4.4.3. Retinal biodistribution of D-Cy5 upon intravitreal & intravenous administration:

Upon, Intravitreal administration D-Cy5 showed differential biodistribution between normal and I/R retinas. In normal retinas 24hrs post Intravitreal injection of D-Cy5 yielded very minimal fluorescence in retina and choroid and we did not notice any fluorescence signal from D-Cy5 beyond 24 hrs time point indicating that dendrimers were cleared intact from retinas in later time points (72hrs and 21days). In the case of I/R injured retinas we observed significant fluorescence signal from D-Cy5 in retinal sections. At 24hrs post injection dendrimers (D-Cy5) were found co-localized in Iba-1 +ve microglial in subretinal space, outer nuclear layer (ONL), inner nuclear layer (INL) and in near vicinity of internal limiting membrane (ILM) in retina. We have also observed dendrimers entrapment in vitreous network (yellow arrows) and localized in other cells throughout all retinal layers. At 72 hours post intravitreal injection of D-Cy5 were cleared out from other cells and vitreous network in I/R eyes (**Figure 33 A-H**). D-Cy5 was found co-localized and retained in microglia/macrophages near ILM, in inner retina, and sub-retinal space. This demonstrated by co-localisation of D-Cy5 (red) with IBA1 labelled cells (green) Interestingly, 21 days post injection D-Cy5 were found specifically retained and co-localized in microglial cells in photoreceptor layer, IPL and near ILM. However, in the case of free Cy5 injected animals, both I/R and normal eyes Cy-5 can be seen in outer and inner retina and appears to be concentrated in blood vessels near the ILM be were completely cleared out after 24hrs post injection (**Figure 34**).

D-Cy5, Free Cy5 or PBS were injected intravenously through femoral vein 6 days later in age matched mice under gone I/R injury in one eye. At respective time points (24hrs, 72hrs and 21 days) post injection the eyes were enucleated for qualitative assessment of differences in

retinal biodistribution of dendrimers between I/R injured and normal retina at different time points using IHC. In I/R eyes at 24 hours post intravitreal D-Cy5 administration, D-Cy5 has made their entry in to retina from systemic circulation and was found co-localized concentrated in microglia posterior to the internal limiting membrane (ILM) in retina, outer nuclear layer (ONL) and subretinal space. IBA-1+ cells in the subretinal space, posterior to the outer nuclear layer (ONL) also had D-Cy5, However, both in normal and I/R eyes 24 hours post free Cy5 dye administration, Cy-5 appears to be blood vessels specific and seen concentrated & entrapped in choriocapillaries posterior to RPE layer and were cleared at later time points, suggesting that dendrimers can cross the outer retinal barrier were as free Cy5 cannot. Interestingly, we did not find any fluorescence signal from D-Cy5 indicating the intact blood retinal barrier.

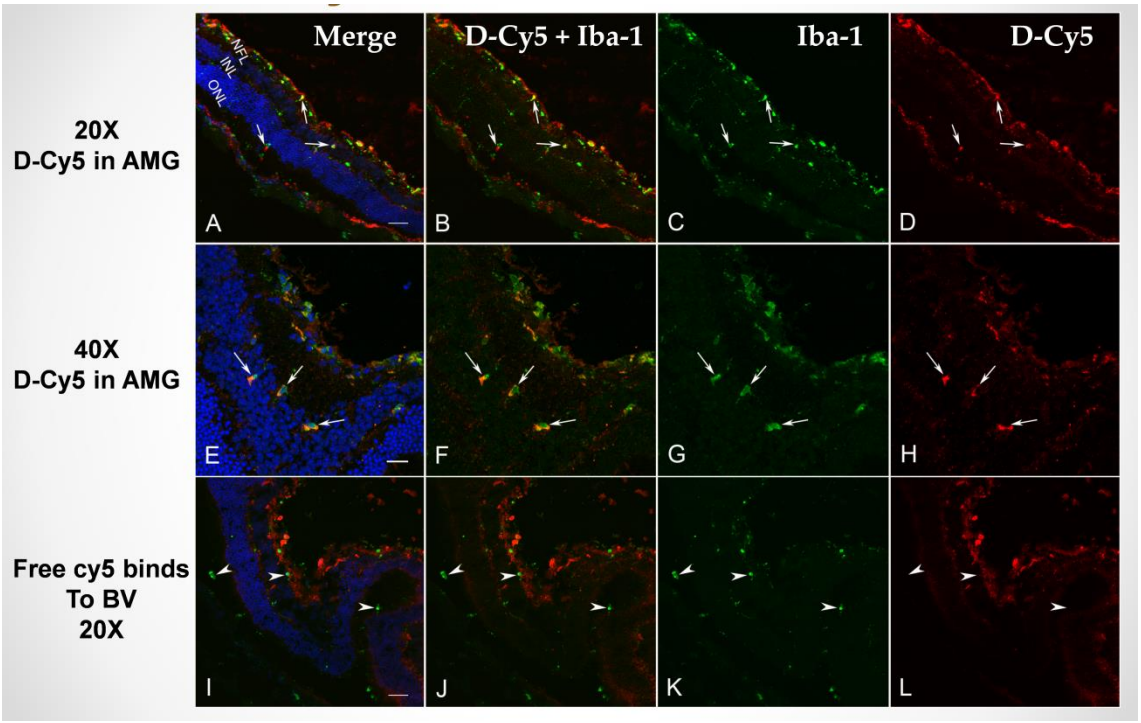

Figure 32. Sections from ischemia/reperfusion eyes 24 hours after intravitreal injection. **A-D**. Dendrimer-Cy5 (red) is present in Iba-1+ microglia (green)(arrows). **E-H**. Higher magnification of D-Cy5 (red) in Iba-1+ microglia. **I-L**. Cy5 or free dye (red) is throughout inner retina and not associated with only Iba-1+ microglia (green). It appears to be associated with blood vessels in inner retina (arrows).

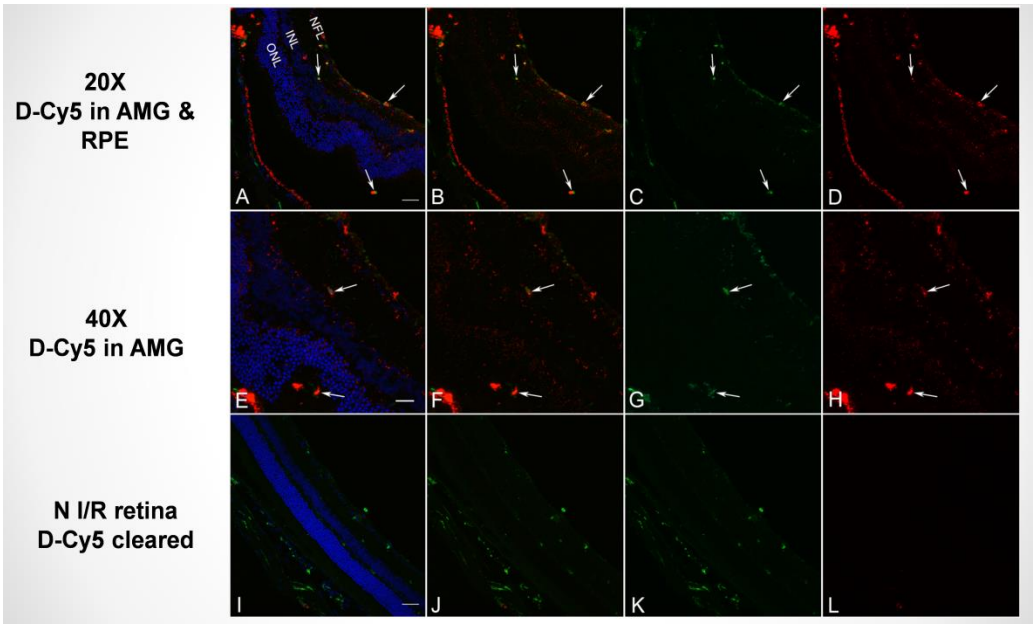

Figure 33: 72 hrs after intravitreal injection. **A-D.** D-Cy5 is still present in microglia in I/R eyes. **E-H**. Higher magnification of D-Cy5 in microglia (arrows) and RPE cells (arrowheads). **I- L.** D-Cy5 was not present in non-I/R control eyes. [DAPI nuclear counterstain (blue). Dendrimer-Cy5 (red). A-D and I-L 20X magnification; E-H 40X magnification]

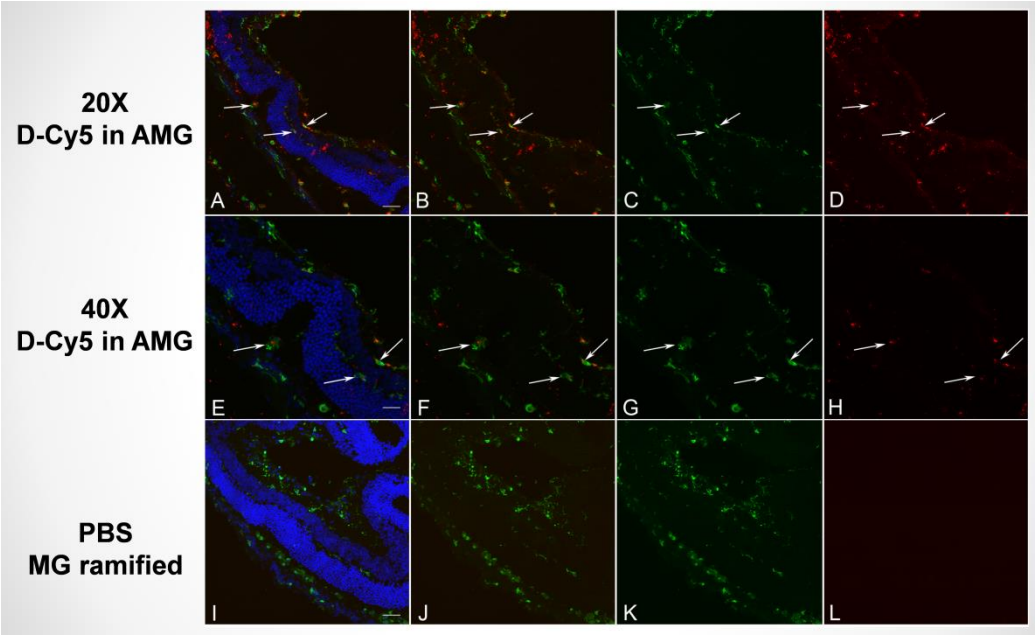

Figure 34: Twenty one days after intravitreal injection. A-D. D-Cy5 remains in Iba-1+ cells in I/R eyes (arrows). Some appear to be subretinal macrophages (left arrows). E-H. Retina of D-Cy5 injected eyes after I/R at higher magnification. I- L, D-Cy5 is not present in non-I/R control eyes. [DAPI nuclear marker (blue). Dendrimer-Cy5 and Cy5 (red). Iba-1 microglia cell marker (green). A-D and I-L 20X magnification; E-H 40X magnification]

72hrs post D-Cy5 injection intravenously, D-Cy5 were selectively localized and retained in microglia/macrophages in I/R retinas Even though activated microglial cells were scattered and distributed in all retinal layers but dendrimers were found retained only in microglial cells in choroid, subretinal/photoreceptor layer and inner nuclear layers (INL) At 21 day post injection D-Cy5 were retained in microglial cells which are present adjacent to inner limiting membrane (ILM), there was relatively less microglial cells and D-Cy5 co-localization than compared to 24hrs and 72hrs time point retinas.

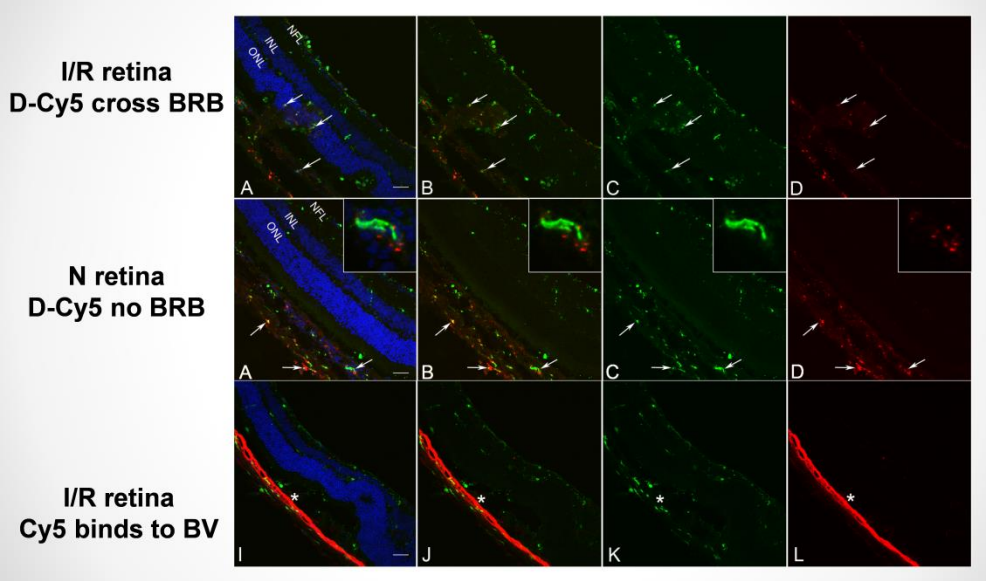

Figure 35: Sections of retinas from I/R eyes 24 hr after intravenous injection. **A-D**. D-Cy5 colocalizes Iba-1 labeled cells (green) in retina and also appears to be in RPE cells. **Panel 2 A-D retinal** section of non I/R eye showing D-Cy5 uptaken by cgoroidal circulating macrophages but did not cross the BRB. **I-L**. Free Cy5 dye is still present in choroid after 24 hrs. M-P. There is no fluorescence in the Cy wavelength in eyes receiving PBS intravenously. [DAPI nuclear counterstain (blue); D-Cy5 and Cy5 (red); Iba-1 microglia cell marker (green). A-D and I-P 20X magnification; E-H 40X magnification]

The microglial cells were seemed to revert back to their ramified morphology but also uptake and retention of D-cy5 in them continued to be concentrated in microglia in the choroid, sub-retinal space in I/R eyes at 72 hours post intravenous administration. In these areas, IBA1 labelled cells (green) colocalized with D-Cy5 (red).There was little fluorescence at Cy5

wavelength in control non-I/R eyes 72 hours after intravenous injection of D-Cy5. D-Cy5 appeared to have been cleared from the retina by 72 hrs.

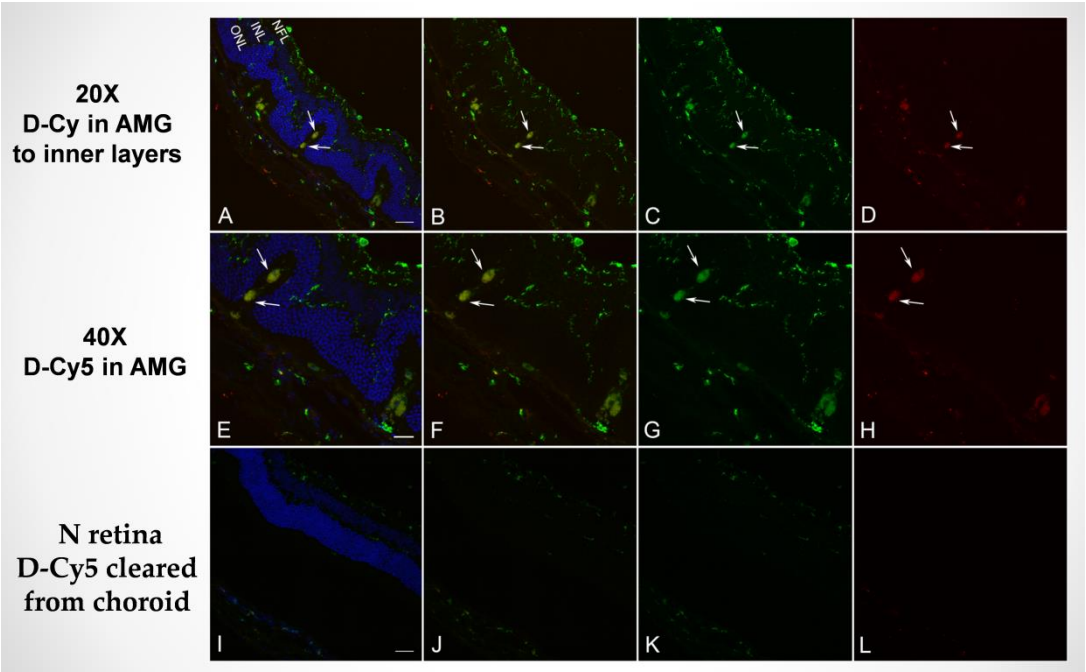

Figure 35: Retina 72 hours post intravenous D-Cy5 administration. A-D. There are many Iba-1+ cells in I/R retinas and a few in this field have D-Cy colocalized. E-H. Colocalization is shown at higher magnification. I- L, No cells have D-Cy5 in non-I/R control eyes. [DAPI nuclear counterstain (blue). Dendrimer-Cy5 and Cy5 (red). Iba-1 microglia cell marker (green). A-D and I-L 20X; E-H 40X].

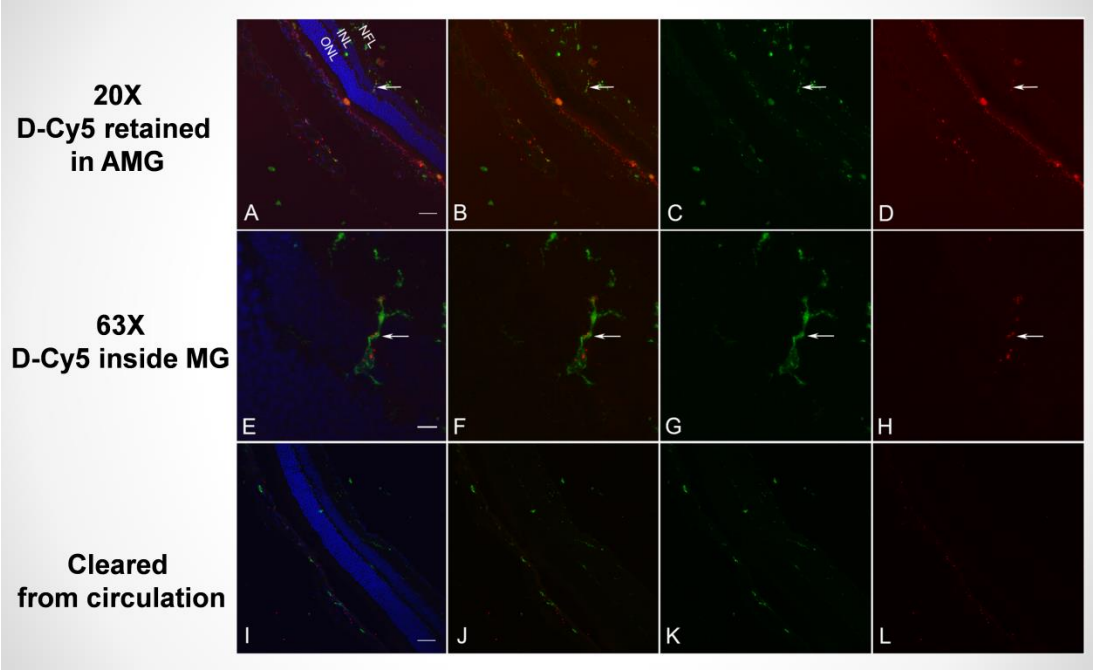

Figure 36: Retina and choroid 21 days after D-Cy5 injection. A-D. I/R retina still has Cy-5 colocalized with an Iba-1+ cell (arrow).. E-H. D-Cy5 colocalization with Iba-1 shown at higher magnification. I-L. D-Cy5 administration with non-I/R control eyes. **A-H** arrows mark colocalization of D-Cy5 (red) and Iba-1 labelled cells (green). [DAPI nuclear marker (blue). Dendrimer-Cy5 and Cy5 (red). A-D and I-L 20X magnification; E-H 63X]

4.4.4. Quantitative biodistribution of D-Cy5 in vital organs

Quantitative biodistribution in vital organs (liver, kidney, spleen, heart, lungs and serum) and kinetics of D-Cy5 injected intravenously into animals with I/R injury was assessed using FLS method [154]. For analysis, weight of tissues was measured before being homogenized and D-Cy5 was extracted using methanol as described previously by Wojciech et al. [154]. The D-Cy conjugates were intact stable in human plasma at 37ºC and in vivo and also the applied methanol extraction protocol yielded best recovery of 96%. The methanol extracts were subjected to fluorescence measurements for emission values using fluorescence spectrophotometer. The amount of D-Cy5 accumulated in each organ was calculated by incorporating the emission values (subtracted background from emission values of respective organs injected with PBS) into

the calibration graphs and the values were then back calculated to % of injected dose (ID)/organ using whole organ wet weights.

Upon intravenous injection, some percentage of D-Cy5 was immediately cleared out from circulation via urine. We observed that the animals injected with D-Cy5 or free Cy5 urinated deep blue urine within ~5-7 mins. Twenty four hrs post injection, the majority of D-Cy5 was cleared from blood plasma but retained in differential amounts in vital organs (**Figure 37A**). At 24 hrs

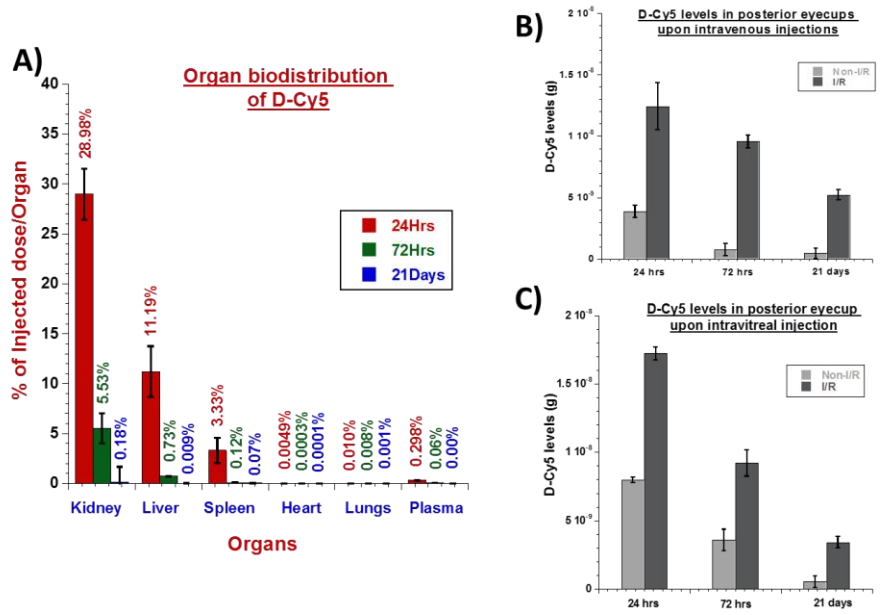

Figure 37: Biodistribution and accumulation of intravenously injected dendrimers. **A)** Biodistribution in vital organs. **B)** D-Cy5 fluorescence levels in posterior eyecup in I/R and non I/R eyes via intravenous injection **C)** D-Cy5 levels in posterior eye cup via intravitreal injections.

according to FLS analysis ~0.18% of the injected dose was still in blood. The total blood volume for BALB/C mice is 10.35 ±0.16 ml/g of tissue. The injected D-Cy5 conjugates were cleared but some accumulated in the kidneys. This is in good agreement with the previous results based on fluorescence measurements and radiolabelling. The D-Cy5 biodistribution and accumulation is

as follows: kidney (29.98±2.5%), liver (11.19±2.2), and spleen (3.33±1.26) (**Figure 37A**). Heart and lungs had minimal accumulation of D-Cy5 (0.0049% and 0.01% respectively). Free Cy5 on other hand was found to be rapidly cleared from blood and had significantly lower accumulation of 0.82±2.93% of the injected dose (ID) in kidneys in 24 hrs. Moreover, we could not detect any fluorescent signals in other organs indicating the free Cy5 has rapid clearance. At 72 hrs post injection, D-Cy5 was cleared from heart, lungs, and spleen but found predominately and persistently retained in kidneys (5.53±1.5%) and to very little extent in liver (0.73±0.026%). Free Cy5 was not detectable in any of the organs indicating that they were either cleared from the body or the amount was below limits of detection (LOD). Twenty one days post injection, dendrimers were completely cleared from all organs examined.

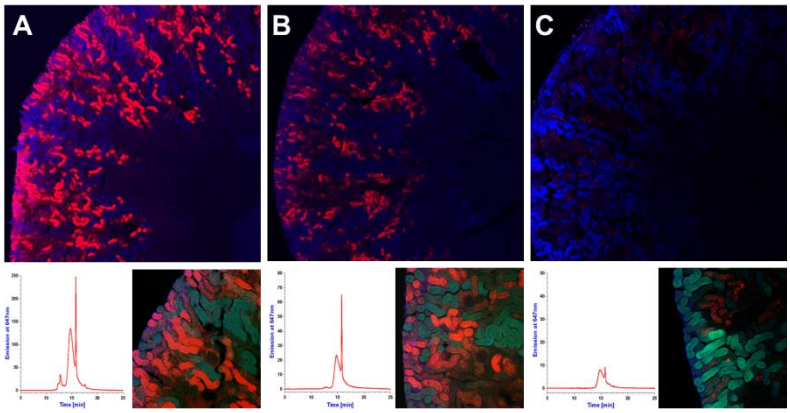

Figure 38: Qualitative assessment of D-Cy5 levels in the kidney as a function of time, using confocal microscopy. **A-C**. (top panel) cross sections of kidneys at 24 hrs, 72 hrs and 21 days respectively post D-Cy5 injection intravenously. D-Cy5 (red) upon intravenous injection were rapidly cleared from systemic circulation and found predominately accumulated in the proximal tubules of the kidney cortex and were excreted at later time points (72 hrs & 21 days). Below are the HPLC chromatograms of the kidney extract proving the fluorescence signals from kidney cortex are from intact D-Cy5 (based on the retention time 14.92 min). Whereas the time increases the peak signal decreases indicating D-Cy5 excretion via urine and is in good agreement with the confocal images.

Because there was predominant accumulation of D-Cy5 in kidneys, a qualitative microscopic analysis was done using confocal microscopy. At 24 hrs the signal intensity of D-Cy5 channel was high in proximal tubules (**Figure 28**) of the kidney cortex but the signal

intensity was decreased in 72 hrs kidneys, which is in good agreement with the biodistribution data. The kidney extracts were also analysed using HPLC to confirm that the fluorescence emission is from D-Cy5 or free Cy5 species. The HPLC chromatograms of the kidney extracts at 24 and 72 hrs showed a small peak from free Cy5 but the major fraction of the peak was D-Cy5 Twelve % of the conjugated Cy5 was released, based on the calibration graphs of free Cy5, suggesting that the conjugates are somewhat intact in-vivo up to 72 hrs and is in good agreement with our previous studies [152]. The H and E analysis on these kidney sections show no neutrophil or monocyte infiltration, no structural damage or any signs of toxicity suggesting that the injected D-Cy5 dose did not inflict any toxic effects to organs

4.4.5. Ocular biodistribution of D-Cy5 in retina and choroid

In terms of the amount of D-Cy5 injected per animal, the intravenous dose was 30-fold higher than that of the intravitreal dose. Interestingly, the qualitative uptake and retention pattern in retina was similar after both modes of administration (**Figure 39**). This demonstrates a relatively low uptake in the healthy control eye, followed by rapid clearance, and a much higher uptake in the fellow I/R eye, and then sustained retention in the I/R eye. In fact, even the quantitative uptake/retention pattern was similar (with intravitreal administration showing a 30-fold higher eye uptake, on an injected amount basis). Even though there is some choroidal presence of the intravenous dendrimer in normal eye, it appears to be mostly cleared within 72 hours. Following intravenous administration, in the I/R eye, ~40% of the DCy5 uptake observed after 24 hours is retained up to 21 days. For intravitreal administration, ~16% of the D-Cy5 level from 24 hours is retained up to 21 days.

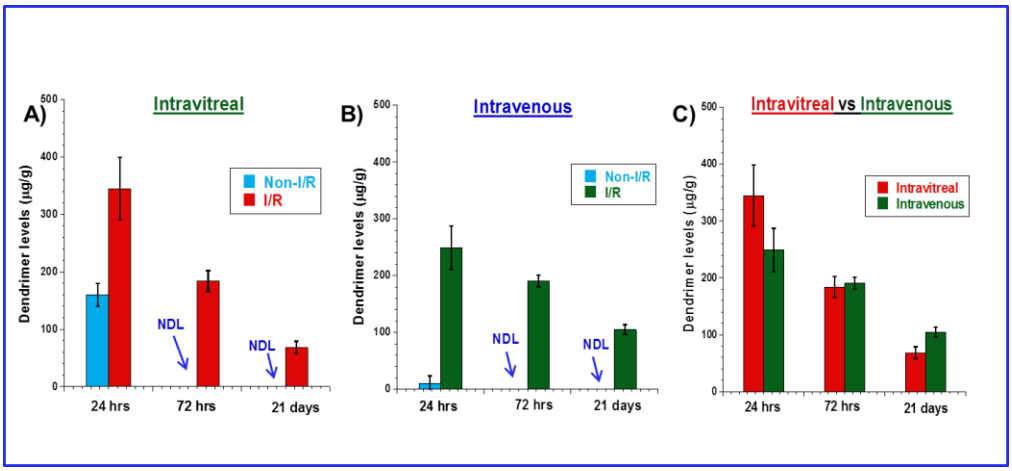

Figure 39: Quantification of dendrimer (D-Cy5) levels in posterior eye cups by fluorescence spectroscopy (FLS) method. **A)** dendrimer levels in eye cups upon single intravitreal injection of 20µg of D-Cy5 showing significant difference in dendrimer uptake between non I/R and I/R eyes. **B)** dendrimer levels in eye cups upon single intravenous injection of 600µg of D-Cy5 via femoral vein. **C)** Comparison of dendrimer levels in I/R eyes in both intravitreal and intravenous administration routes showing not much significant differences. n=8, student t test.

4.5. Discussions

The current study demonstrates the ability of PAMAM dendrimers to target one key cell type in retinal neuroinflammation, activated microglia. Retention by activated microglia occurred whether the dendrimer was delivered intravenously or intravitreally. Furthermore, the microglia retained dendrimer while other cell types did not take up the dendrimer. The dendrimers remained in microglia for an extended period of time, 21 days, the longest time point evaluated in this study. Activated microglia/macrophages have been associated with retinal diseases such as macular degeneration, diabetic retinopathy, glaucoma, and retinopathy of prematurity [151, 154-157]. Ischemia-reperfusion (I/R) injury has been used to model certain aspects of chronic glaucoma, diabetic retinopathy and branch vein occlusion (BVO). I/R injury causes occlusion of both retinal and choroidal blood vessels, resulting in reduced blood flow and

tissue hypoxia [152]. The above conditions were reported to cause disruption of blood retinal barriers (BRB) 152, 153], activation of resident microglia/macrophages, infiltration of microglia and macrophages from choroid and systemic circulation, elevated production of cytokines (TNF-α, INF-α, TGF-β. IL-1β and IL-6) [154], and death of retinal ganglion cells (RGCs) [155].

Hydroxyl terminated generation 4 PAMAM dendrimers (G4-OH) conjugated with near IR dye Cy5 (D-Cy5) used in this study were well characterized in our previous study [150]. 1H NMR confirmed that one molecule of Cy5 was successfully conjugated to each dendrimer and it is sufficient to measure the amount of dendrimers at low levels of detection of 0.1ng. HPLC analysis demonstrated the high purity of D-Cy5 conjugates and successful synthesis. PAMAM dendrimer conjugated with fluorescent dyes we used in previous studies as diagnostic probes to investigate the biodistribution and cellular localization of dendrimers in central nervous system [156, 157]. We used cyanine Cy5 dye, which is near IR to avoid tissue auto-fluorescence from retinal cells, especially microglia and RPE cells. In order to investigate the biodistribution, dendrimer–retinal cell interactions, and differences in retinal distribution upon different mode of administration, we used both intravitreal and Intravenous route of delivery.

Dendrimers after intravitreal and intravenous injection showed pathology-dependent retinal distribution. Upon intravitreal injection, dendrimers were mostly cleared from normal retina within 24 hrs, whereas in I/R retinas, they were found specifically localized in activated microglia (round or fusiform and Iba-1+) in INL, ONL and in near vicinity of ILM. This can be attributed to the increased phagocytic activity of activated microglial cells. Moreover free Cy5 was not localized in Iba-1+ cells in I/R retina and were completely cleared after 24 hrs. Activated microglia. Macrophages were present at 72 hrs but appear to have migrated towards the photoreceptor layer. In normal retina, microglia is restricted to inner retinal layers but under

pathological conditions such as I/R injury exhibit dynamic behavior like migration to the injury site and engulfment of dead cells. In I/R injury there reported a ganglionic and photoreceptor cell death and RPE atrophy and accumulation of microglia in INL, ONL and subretinal space. At 21 days post intravitrial injection in I/R eyes, dendrimers were still retained in microglia, but the amount of D-Cy5 had decreased compared to 24 and 72 hrs. This corresponded to a decline in the number of activated microglia and a return to their quiescent ramified morphology. Such changes in microglia morphology are in agreement with previous studies by Zhang et al. [153].

Retina has a blood retinal barrier, so entry of dendrimers into retina in normal animals must be from the choroidal vasculature. Although the capillary system of choroid has tight junctions, it also has fenestrations. It appears that the D-Cy5 in normal choroid must have traversed the fenestrations. However, after I/R injury, the retinal barriers are breached so systemic D-Cy5 passes through leaky retinal blood vessels and perhaps through injured RPE from choroid. As in intravitreal injection, activated microglia after injury take up the D-Cy5 and retain it for 21 days, the longest time point in this study

It was striking that the majority of the D-Cy5 was cleared quickly from the body whether injected intravitreally or intravenously, yet activated microglia retained it. Clearance studies demonstrated that kidney and liver retained the largest percentage of the intravenous D-Cy5 dose. All organs showed complete clearance of D-Cy5 by 72 hrs except kidney, which had a small 0.0008% uptake. This is clear evidence that D-Cy5 is cleared intact from the body after intravenous administration and only remains in cells spanning injured retina at 21 days. Clearance after intravitreal administration was visually apparent at 24 hrs (daa not shown, when the blue color of the D-Cy5 had disappeared from the normal globe. Furthermore, there was no indication of toxicity from the D-Cy5.

The ischemia reperfusion (I/R) model selected for these studies represents some aspects of branch vein occlusion. It also represents a retinal injury in which there is hypoxia, then tissue injury, followed by activation of microglia. This I/R model causes cell death and an inflammatory response. This model was used in a study by Zhang et al to create a short term model of some events in diabetic retinopathy: creation of acellular capillaries, death of neurons, and increased vascular permeability. They also demonstrated significant activation of microglia in the model [159]. In non-I/R retinas, microglia are ramified or quiescent but, following I/R, the cells are round or fusiform, indicating they are activated and phagocytosing . There were also less microglia in non-I/R retina compared to I/R retinas.

An important observation was that the D-Cy5 was retained almost exclusively in activated microglia, whether they were delivered intravenously or intravitreally. Intravenous administration is safer than intravitreal, but intravitreal is currently the standard of care for anti-VEGF therapies used in treating exudative age-related macular degeneration (wet AMD) and diabetic macular edema. D-Cy5 retention in microglia at 21 days post femoral injection is also very significant in that repeated injections like current anti-VEGF therapies would not require intravitreal injection. Femoral administration of the dendrimer resulted in less Cy5 fluorescence in the retina than intravitreal administration but still a substantial number of microglia had D-Cy5. Both intravitreal and intravenous non-I/R controls with D-Cy5 at 24 hours post activated injection showed no fluorescence of Cy5 indicating that the dendrimer was cleared from the eyes at 24 hours post administration; these healthy controls had no microglia. With intravenous administration it could be argued that D-Cy5 would not traverse the blood brain barriers. In I/R injury and in our cerebral palsy (CP) model, the blood barriers are compromised as part of the pathology, Cy5 alone administered intravenously or intravitreally was not localized to microglia.

This difference in distribution of unconjugated Cy5 proves that dendrimer retains its cargo and has a favorable distribution in diseased and healthy retina (retention and clearance respectfully). Furthermore, Cy5 was not ever present in microglia, indicating that it is the dendrimer that is targeted to activated microglia, not the dye.

In chronic diseases like diabetes, microglia are activated in human diabetic retinopathy and undoubtedly they contribute to the neuroinflammation and death that occurs in diabetic retina. Because diabetic retinopathy is a chronic disease, it is not possible to repeatedly inject therapeutics intravitreally as this can lead to further damage to vision. With intravenous injections of dendrimer, repeated injections would be possible as this leads to no secondary damage to the eye. The retention of dendrimers in activated microglia cells at 21 days post intravenous injection indicated that drugs bound to dendrimers could be released slowly over a prolonged period of time decreasing the need for multiple injections in a short period of time.

This is a great advantage as it decreases the need for regular PAMAM dendrimers because they target only activated microglia after intravenous administration. These attributes suggest that these dendrimers could be used to treat diabetic retinopathy where retinal blood vessels leak and retinal microglia are activated. Another potential target would be AMD where the outer retinal barrier is lost and activated microglia/macrophages are thought to contribute to the pathology. Kannan et al used dendrimers with N-acetyl cysteine (D-NAC) in a rabbit model of CP and observed attenuated activation of brain microglia and astrocytes. Kits treated with D-NAC had an improved muscle tone from day 1 to 5 compared to kits treated with PBS ($P<0.001$).

Therefore, the current study demonstrates the potential for intravenous delivery to target activated microglia in retina and choroid in many inflammatory diseases in the eye. Attenuation of the microglia activation in AMD and diabetes would decrease the degeneration of photoreceptors and other neurons. The only therapies currently available require monthly intravitreal injections. If it is possible to give drugs systemically that can target the desired cells and release therapies slowly, injections will be needed less frequently and the complications of injections into the eye will not occur.

4.6. Conclusions:

We investigated the retinal biodistribution of dendrimers, upon intravitreal and systemic administration, in a mouse model where one eye was healthy and the other eye had I/R injury. The qualitative biodistribution was somewhat similar after intravitreal and systemic administration of the dendrimer after I/R injury. There was a differential retinal biodistribution of dendrimers between the healthy eye, and the injured fellow eye, with D-Cy5 localizing selectively in activated microglia/macrophages in the injured eye. Once localized in activated microglia, the dendrimers appeared to be retained to an appreciable extent, up to 21 days. The ability of the dendrimer to selectively target activated microglia, even upon systemic administration may offer significant opportunities for targeted, sustained, systemic therapies for retinal degeneration. The relatively rapid clearance of the dendrimers from the healthy eye, and off-target organs suggests that dendrimers may reduce side effects associated with current ocular drugs.

CHAPTER 5 "IN-VIVO EVALUATION AND EFFICACY OF THE PREPARED DENDRIMER DRUG CONJUGATES IN RAT MODEL OF CNV"

5.1. Abstract

Choroidal neovascularization (CNV) is a major complication of age-related macular degeneration (AMD) resulting in devastating damage to the retina. Increasing evidence suggests microglia/macrophages may play a critical role in the development and the progression of AMD. When injected, polyamidoamine (PAMAM) dendrimers have been shown to be taken up in activated microglial cells in brain and retina in response to inflammatory stimuli. The purpose of this study was to investigate whether intravenously injected dendrimers would accumulate and deliver drugs in a lipid-induced CNV rat model. Dendrimer-Cy5 (D-Cy5) and dendrimer-N-acetyl-L-cysteine (D-NAC) conjugates were evaluated in lipid-induced rat CNV model. A single dose of D NAC+D-Cy5 was administered intravenously on day 3 post lipid injection. Rats injected with D-Cy5 alone and PBS served as controls. Rats were sacrificed 7 days post dendrimer injections, and then retina and choroids were prepared for flat mount IHC. Flat-mounts were imaged under Zeiss 710 confocal microscope. The co localization of D-Cy5 was assessed using IBA-1 antibody (macrophage/microglia) and GSA lectin-FITC (blood vessels and microglia). The CNV areas and the microglial counts in the CNV and RNV areas were assessed. Sub-retinal lipid injection stimulated the migration of IBA-1 positive microglial/macrophages and formation of CNV. Intravenous administration of D-Cy5 was colocalized predominantly in activated microglia/macrophages in the CNV/RNV areas. Image analysis showed that D-NAC+D-Cy5 treated rats had a ~30% reduction in the CNV area and a significant reduction in microglial cell counts associated with the CNV/RNV compared to controls, following just one dose of D-NAC. D-Cy5 was selectively taken up by activated microglia/macrophage cells and, therefore, is promising for delivering anti-inflammatory drugs to retina/choroid via systemic

administration. The efficacy of D-NAC in reduction of microglia numbers and CNV regression opens a new therapeutic window for delivering a combination of intravenous anti-angiogenic and anti-inflammatory drugs as an effective treatment option for early stages of AMD and perhaps other ocular inflammatory diseases.

5.2. Introduction

Age related macular degeneration (AMD) is one of the leading causes of blindness in the western world often affected in individuals between 65 and 75 years of age [160]. AMD causes decline in central vision due to the photoreceptor loss in the macular area. This photoreceptor atrophy is often result of accumulation of drusen (lipid and photoreceptor fragments accumulated in the subretinal layer) (dry form) leading to onset pathological events. The slow progression of events includes neuroinflammation, microglial & monocyte accumulation and infiltration, increased production cytokines, growth factors such as HIF-1 &2, VEGF 1 & 2 and etc. causing formation of new blood vessels leading to neovascularization and disruption of blood retinal barrier resulting in decline of retinal homeostasis [161]. Inflammation, mediated by activated microglia/macrophages, plays a key role pathogenesis of neovascularization and multiple early disease alterations involving retinal pigment epithelium and photoreceptor atrophies. It has been reported in many previous research studies that resident microglia have primary responsible in clearing up the accumulated drusen by phagocytosis and there by digesting them and hence avoiding toxic effects [162]. Under overwhelming circumstances of continuous pathological stimulation these resident microglial cells become activated to pro-inflammatory cells completely changing their function causing devastating effects [163]. Activated microglial cells have multiple effects such as increased production of cytokines, angiogenesis growth factors and chemokine for macrophage infiltration from systemic circulation, oxidative stress and endothelial dysfunction [164]. Current treatment options for AMD are intravitreal injections of antiVEGF agents, monoclonal antibodies such as pegatanib, bevabizumab, ranibizumab and vitriprofin. The above therapies are effective only for short term and repeated injections are required and often have severe side effects [165]. Focus towards attenuating neuroinflammation

and neovascularization as a combined treatment option will be beneficial. A drug delivery system that can target choroid and retina neovascularization upon systemic delivery via intravenous route achieves patience compliance and avoids the incidence of intraocular infections.

Polyamidoamine (PAMAM) dendrimers have been shown to localize in cells associated with neuroinflammation. Dendrimer-drug conjugates showed significant efficacies in retinal degeneration models upon intravitreal delivery, and in cerebral palsy model upon intravenous delivery. NAC is used as an antioxidant agent in various disease conditions such as photoreceptor dystrophies, CNV and AMD [161]. NAC is proved to have protective effects and facilitates long-term survival of cone photoreceptors which are responsible for central and clear vision [161]. NAC is required to be delivered at high concentrations in order to achieve a therapeutic efficacy because of its low stability and clearance. Moreover it causes retinal toxicity and ganglionic atrophy. Dendrimer N-Acetyl cysteine conjugates (D-NAC) have been reported to attenuate neuroinflammation in cerebral palsy rabbit model and improves motor function in rabbit pups.

Triamcinolone acetonide (TA) is a potent angiostatic steroid, which can exert multi-pronged effects on many complications of AMD, including neuroprotective and anti-angiogenic properties[166-172]. It has shown promise against CNV in multiple animal models [171, 172]. TA has been used clinically in combination with other approaches, mostly as an intravitreal formulation, for diabetic macular edema (DME), retinal vein occlusion, and some forms of AMD [171] The side effects associated with intravitreal TA include elevated intra-ocular pressure and cataract [173].

In chapter 2, we have shown that dendrimer-triamcinolone conjugates (D-TA) show sustained anti-inflammatory and anti-VEGF activity in activated microglia and hypoxic retinal pigment epithelium. D-TA has overcome the solubility issue and was better in terms of efficacy at 100 fold lower concentration that free drug. The above studies indicate that D-TA treatment will overcome the toxicity and elevated IOP. Chapter 4 results suggest that upon intravenous injection dendrimers can target activated microglial cells and RPE, indicating their intrinsic targeting ability. By combining the targeting ability of dendrimers and using dendrimers as drug carriers for two above mentioned drugs (NAC and TA) as a potential treatment option fpr intravenous therapies for AMD.

In this chapter, we evaluate the efficacy of dendrimer-N-Acetyl cysteine conjugates (D-NAC) as an intravenous treatment option for treating early AMD stages (dry AMD) and a combination therapy (D-NAC + D-TA) as a treatment option for late stages of AMD (wet AMD with CNV) via intravenous route. Upon systemic administration, dendrimer crosses blood retinal barrier (BRB) and accumulated only in the activated microglia/macrophage of choroids and retina. Moreover, D-NAC and D-TA treatments both individually and combined resulted in significant reduction in choroidal and retinal inflammation by decreasing the microglia/macrophage accumulation in CNV areas. In the case of CNV growth the dendrimer formulations suppressed significantly whereas, the free drug did not show significant reduction in microglia/macrophage accumulation and CNV suppression. Upon further evaluation of these conjugates for various parameters may result in profound insights that can be helpful in developing dendrimer based delivery of various different drugs via intravenous rout as an effective and potential treatment option for treating various retinal diseases such as AMD, CNV, diabetic retinopathy and etc.

5.3. Materials and methods

5.3.1. Synthesis & characterization of Dendrimer-NAC conjugates (D-NAC)

Dendrimer-NAC (D-NAC) conjugates were synthesized using 4 steps protection and deprotection reactions. In the 1st step G4-OH is reacted with Fmoc-GABA acid using PyBOP as coupling agent in the presence of DIEA as base. The resultant bifunctional dendrimer is deprotected using pypridine to obtain bifunctional dendrimer with amine groups. In the 3rd step the amine groups were reacted with SPDP for 6hrs and NAC is added to get D-NAC. The conjugates were purified and characterized using ^{1}H NMR, and HPLC for purity and drug loading.

5.3.2. HPLC analysis of D-NAC conjugates

The purified dendrimer NAC conjugate (D-NAC) was analyzed by Waters HPLC instrument (Waters Corporation, Milford, Massachusetts) equipped with binary pump, photodiode array (PDI) detector, and auto sampler interfaced with Empower software. The HPLC chromatogram was monitored at 210 and 205 nm simultaneously using PDI detector. The water/acetonitrile (0.1% w/w TFA) was freshly prepared, filtered, degassed, and used as a mobile phase. Symmetry C-18 reverse phase column with 5 μm particle size, 25 cm length, 4.6 mm internal diameter was used. A gradient flow was used with initial condition of 100:0 (H2O/ACN) and gradually increasing the gradient condition of 90:10 (H2O/CAN) till 10min to 50:50 (H2O/ACN) in 20 min and returning to 100:0 (H2O/ACN) in 40 min with flow rate of 1 mL/min.

5.3.3. Animals and CNV model

In this study, male Sprague-Dawley rats from Harlan Laboratories Inc. (Frederick, MD) were used. The ages of the animals were between 6-8 weeks and they each weighed approximately 200-250 g. The animals were housed in the Johns Hopkins Animal facility and all animal care and experimental procedures complied with the Association for Research in Vision and Ophthalmology (ARVO) statement for the Use of Animals in Ophthalmic and Vision Research and the Johns Hopkins University guidelines for Care and Use of Laboratory Animals.

Rat CNV model is established in Dr. Gerard lutty's Lab at Wilmer eye institute, Johns Hopkins University. Briefly, HpODE (lipofuscin extracted from human AMD patients) were dissolved in sterile borate buffer at a concentration of 20μg/2μL. SD rats of 8 weeks age and ~250grams of weight were chosen and anesztied using ketamine (100mg/Kg) and Xylazine (10mg/Kg) injected into the peritoneal space. 2μL of HpODE solution was given as subretinal injection using nano-injector and glass needle. Bleb formation is confirmed upon injection using an optical microscope funds examination. HpODE injection causes inflammation resulting in accumulation of inflammatory resident choroidal and retinal microglia in and around the bleb area, retinal thinning, RPE dystrophy, and choroidal and neovascularization [61].

5.3.4. Dendrimer conjugates injections:

For biodistribution studies, 6mg of Cy5 labelled conjugates (D-Cy5) (20 mg/Kg on dendrimer basis) were injected intravenously via penile vein. Linear polymer dextran-FITC (Mol wt 15,000 daltons) (Sigma-Aldrich) and 20 nm polystyrene nanoparticles (red nanoparticles, Cy3 wavelength) were injected on equimolar basis same as D-Cy5. For efficacy studies D-NAC (20mg/Kg on NAC basis) were injected intravenously on day 3, 5 and 7 for early AMD

treatment and sacrificed on day 10. For late AMD treatment, the animals were not treated until day 9 but on day 10, a combination therapy of D-NAC (20 mg/Kg on NAC basis) and D-TA (10mg/Kg on TA basis) were dissolved together in 300 μL of PBS and injected intravenously on day 10, 13 and 15 and on day 19 the were sacrificed with an overdose of sodium pentobarbital (50mg/ml) intraperitoneally. The eyes were enucleated immediately and placed in distilled water with 1X Tris-buffered saline (TBS) (pH 7.4).

5.3.5. Tissue Processing and Immunohistochemistry

After one hour on wet ice to allow for post-mortem time, using a micro-dissection vannas scissors the anterior segment was removed using a circumferential cut near ora serrata. the anterior segment of the eye was removed and the retina was separated from the choroid. The retina and choroid with retinal pigment epithelial (RPE) cells and sclera attached were fixed for 24 hours at 4°C, in 2% paraformaldehyde in 0.1 mol/L cacodylate buffer, pH 7.4. The next day, the tissue was washed in 1XTBS for 30 minutes. Both retina and choroid were blocked for 6 hours at 4°C using 5% normal goat serum (Jackson ImmunoResearch, PA) in 1XTBS, 1% bovine serum albumin (BSA) and 0.1% Triton X-100 (Sigma Aldrich, MO). After the tissue was washed for 10 minutes at 4°C in 1XTBS with 0.1% Triton, it was incubated with the primary antibody Anti-IBA1, Rabbit (1:500, Wako Pure Chemicals, Japan) in 1XTBS, 1% BSA and 0.1% Triton, for 20 hours at 4°C. The next day, the tissue was washed in 1XTBS with 0.1% Triton for 30 minutes at 4°C and the secondary antibodies Goat anti-Rabbit Cy3 (1:200, Jackson ImmunoResearch, PA) and Isolectin GS-IB4 AF488 (1:100, Thermo Fisher, MA)were applied to the tissue and incubated for a further 20 hours at 4°C. After application of antibodies, all tissue was washed for 30 minutes in 1XTBS at 4°C.

5.3.6. Choroidal and Retinal flatmounts imaging by confocal microscopy:

Choroid & retinal flat mounts were performed on glass slides. To make them flat 3 to 4 relaxing radial cuts are performed using vannas scissors and the flattening was stabilized using micro slide cover slips. The flat mounts were imaged under Zeiss 710 confocal microscope. 3 channels are used Cy3 channel for Iba-1, FITC 488 channel for lectin blood vessels and Cy5 channel for D-Cy5. Choroids flat mounts were imaged at 5X magnification, Tiled Scan of 9X9 with overlap 10%. The images showed here are collapsed; tile stitched using Zen confocal software. Retinal flat mounts were imaged at 20X magnification, 6X6 tiled Z scan with overlap 10%. The images shown here are collapsed; tile stitched using Zen confocal software.

5.3.7. Image analysis and cell counting and morphology analysis

CNV areas were analyzed using Image-J software morphometric analysis. Choroidal whole mount images were magnified 20 times using magnifier option and using a digital pen the CNV borders were delineated and using area analysis. Macrophage/microglial counts in choroid and retina were performed using Imaris software. Three areas of interest (3x3 tile zone) were chosen from the bleb area and the cell count analysis were done using Imaris (Bitplane) software using surface function with smoothing factor and cell size threshold of 8-12 μm diameter with split function. Activated and resting microglia in retinas was counted based on cell shape using cell surface function. The function ‘surfaces’ was used and the individual Iba1+ microglia/macrophages were analyzed for surface and volume of each cell in bleb area and area away from the bleb, approximately 150 cells were included for each region. The threshold settings were based on the diameter of cells, cell surface to volume ratio with sphericity of 0.758 add ellipiticity function 0.298 as threshold.

5.3.8. RT-PCR analysis of cytokines in retina and choroids

The retinas and choroid of rats were collected at day 10 post D-NAC treatment to evaluate the mRNA levels using quantitative RT-PCR (qRT-PCR). Total mRNA was extracted using triZol for cDNA synthesis (SuperScript III First-Strand Synthesis SuperMix, Invitrogen, CA, USA). The procedures of mRNA extraction and cDNA synthesis followed those provided by the manufacturers and the primers are listed in Table 3. Reactions were performed in a 25 μL eppendorf tube with 2 μL of cDNA, 0.3 ml of forward and reverse primer (10 pmol/μL), 10 μL of 26Mix (full velocity SYBR greenqPCR master mix, Stratagene) Taq and 7.4 ml of ddH2O. The procedure for real-time qRT-PCR included 5 min at 99ºC, followed by 40 cycles of 15 s at 94ºC, 30 s at 59ºC, and 45 s at 72ºC (Roche LC480, Roche Applied Science). All the qRT-PCR reactions were run in triplicate to yield averaged Ct values. Expression (evaluated as fold change for each target gene) was normalized to GAPDH.

5.4. Results and discussions

5.4.1. Synthesis and Characterization of D-NAC conjugates

D-NAC was synthesized using 4 step reaction process. Bifunctional dendrimer was synthesized using FMOC protection and de-protection resulted in 21 primary amine groups on the dendrimer surface (^{1}H NMR analysis). These amine groups were reacted with SPDP, a bifunctional linker which has NHS ester on one side and PDP group for disulfide bonds on other side. The NHS group reacts with amine group to form an amide bond. This reaction will be completed by stirring them at nitrogen atmosphere overnight and NAC was added. The PDP group will react with thiol (SH) group of NAC to for disulfide bond that is cleavable only in intracellular glutathione levels.

^{1}H NMR analysis confirms 18 molecules of NAC were conjugated to each dendrimer which corresponds to 20% of the payload. HPLC analysis confirms the purity and successful completion of the reaction and devoid of small molecule and side products impurities. A release experiment was carried out in PBS with different varying concentrations of glutathione ranging from plasma concentrations (2μM) to intracellular concentrations in microglial cells (500μM). The conjugates released NAC on increased glutathione levels where as significantly low amount was released in extracellular plasma glutathione levels. On other hand the conjugates released NAC almost ~60% of payload within 2hrs.

5.4.2. CNV formation induced by subretinal injection of HpODE

Blood vessel vasculature was observed by confocal microscopy using GS Isolectin (red) in flat-mounted choroids 10 days after borate or HpODE injection. Rats injected with borate only, did not show development of CNV in the bleb site or in the surrounding area of the choroid (**Figure 40A**). A higher magnification of the bleb area with GS Isolectin (red) only, does not show CNV formation, however there appears to be some degeneration of the chorio-capillaris (CC) in the bleb area (**Figure 40E**). The mean CNV area of borate injected eyes was 0 mm^2. In contrast, HpODE injected rats showed distinct formation of CNV in the bleb area (**Figure 40B**). In all cases of HpODE injected eyes, CNV formation was present with a high area of CC degeneration in the bleb area (**Figure 40F**). The mean CNV area of HpODE injected eyes was 0.24±1.64 mm^2. Statistical analysis shows a significant difference between the CNV areas of HpODE compared to borate injected rats ($P<0.0001$). Interestingly, there was onset of microglial accumulation in the bleb area and around the CNV.

5.4.3. Biodistribution of dendrimers in choroid and retina

Delivering drug to targeted cells is critical and important in-order to have significant efficacy. We used model dendrimer conjugates, D-Cy5 as a marker to know the targeting capability and delivery of drug to the retina and choroid upon intravenous injection. D-Cy5 was injected via penile vein and ocular biodistribution was investigated using flat-mount imaging. Seven days post injection flat-mounts of choroid and retina were imaged using 710 confocal microscopy. D-Cy5 were found accumulated in microglia/macrophages in the choroid bleb area ~80.25% (**Figure 42**) of total microglial cells in the bleb area were activated [based on their shape (amoeboid, elliptical and circular with short and few dendrite process)] and almost all of the activated population of microglia/macrophages were uptake with dendrimers (red signal, **Figure 41A**). Such specific co-localization of dendrimers in microglia/macrophages suggests that intravenous therapies for targeting ocular inflammation are possible. The specific localization and retention of dendrimers both in retinal and choroidal activated macrophages can be attributed to its size, shape and phagocytic activity microglia/macrophages when activated.

To understand the influence of shape and size; we used a linear dextran molecule and a larger nanoparticle polystyrene 20 nm particles to compare and to know if the same fashion of biodistribution is observed. Interestingly, in the case of linear dextran, did not exhibit such pathology dependent biodistribution. Moreover, dextran was found in only in large retinal blood vessels and did not get co-localized in activated microglia/macrophages. In the case of 20 nm polystyrene nanoparticles did not show any sign of retention and seemed to be excreted, suggesting the influence of size and shape of the dendrimers.

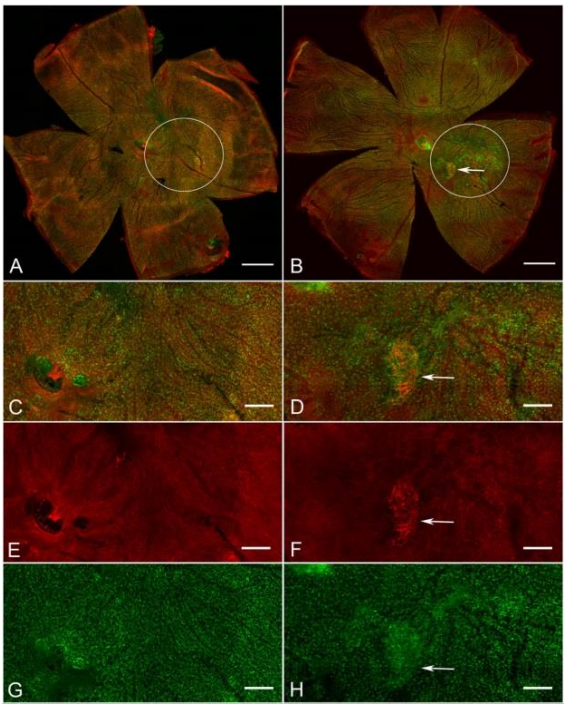

Figure 40: Flat mount images of choroids representing the changes and CNV growth after subretinal HpODE injections **A)** Borate injected choroid showing no CNV formation whereas **B)** HpODE injection showing formation of CNV (white arrow) and microglial/macrophage accumulation (green). The CNV formed is indicated by arrow in panel **F** (red). Scale bar 100µm.

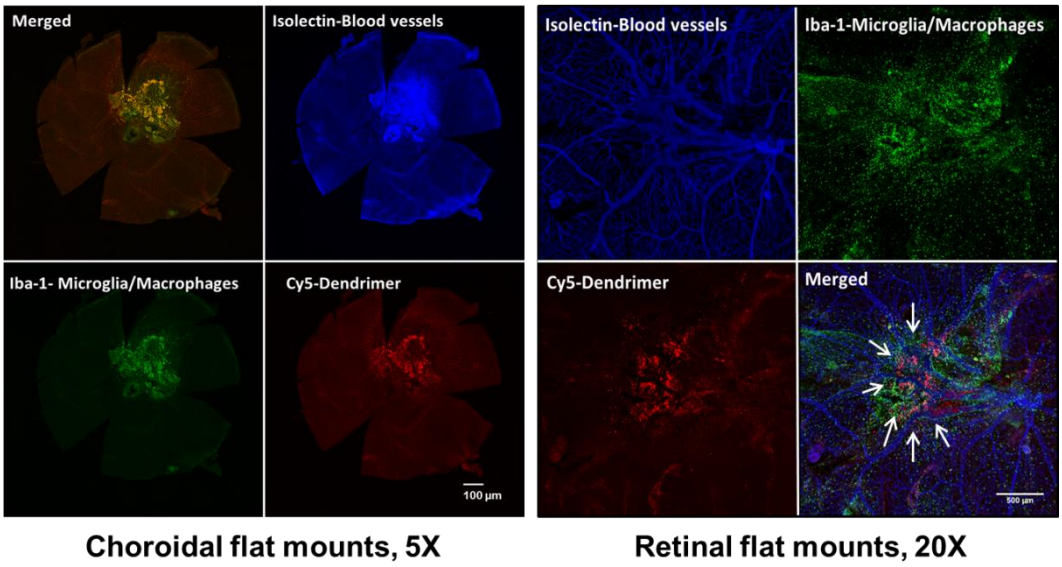

Figure 41: A) Choroidal flat mounts from lipid-injected eyes, imaged 7 days after D-Cy5 (red) administration (Day 10), stained for blood vessels (isolectin), macrophages (IBA-1, green). The D-Cy5 localizes in the IBA-1 macrophages. Minimal D-Cy5 uptake is seen in the IBA-1 labeled 'ramified' macrophages in healthy choroids. See Figure 7 later. Scale bar is 100µm **B)** Retinal flatmounts depicting microglial migration and accumulation in the bleb area corresponding to choroid with dendrimer co-localization and retention in activated microglia.

5.4.4. D-NAC treatment suppresses CNV in early AMD period

D-NAC was administered on Day 3 (two days after lipid administration), and on day 5 and day 7 at 20 mg/kg on a NAC basis. D-NAC caused significant suppression of CNV when assessed on Day 10 compared to free NAC at equivalent doses, and untreated controls (PBS injected). Untreated controls have irregular choriocapillaries that are enlarged with outgrown blood vessels. The mean area of CNV in untreated choroids were 0.24±1.64 mm^2, and D-NAC treated choroids showed significant reduction in CNV area 0.08±2.43 mm^2 which corresponds to ~78% suppression (**Figure 42A & B**). Free NAC treatment showed little reduction of CNV but not significant than compared to D-NAC treatment. The CNV suppression after D-NAC treatment is in good agreement with biodistribution studies where dendrimers were found localized and retained in activated microglial cells suggesting that D-NAC delivers NAC to the inflammatory cells in the area of pathology.

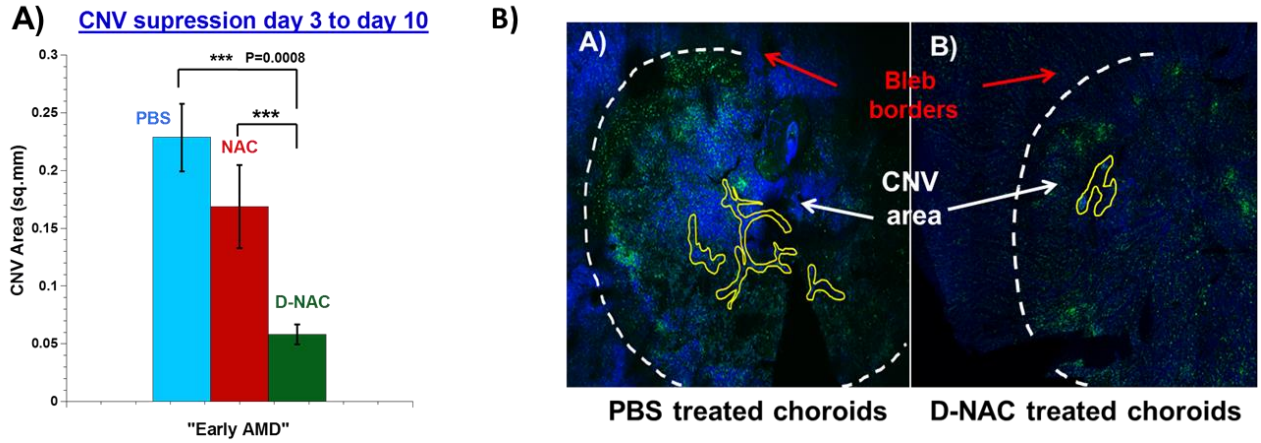

Figure 42. Effect of intravenous injections of free NAC, D-NAC or PBS, on CNV. D-NAC treated animals showed significant decrease in CNV areas when compared to PBS. Free NAC showed some decrease that was not significant. CNV areas were assessed using morphometric analysis (yellow delineation) in Image-J software. **Panel A** shows the PBS choroid with larger CNV and increased population of macrophages (green) in the bleb area, whereas **panel B** shows the efficacy of D-NAC with reduced CNV and macrophage accumulation. The vasculature was stained with GSA lectin (blue), and macrophages are stained with IBA-1 (Green).

5.4.5. D-NAC treatment reduces macrophage migration and accumulation to CNV area

The extent of macrophage depletion in the CNV region, upon systemic D-NAC therapy at 20 mg/kg NAC was assessed on Day 10, using IBA-1 staining. A significant reduction in total macrophages accumulation (~63%) was seen upon D-NAC therapy. Previous studies by *Ambati and coworkers* showed that macrophage depletion correlated with CNV reduction [174]. Interestingly, morphological analysis using Imaris [175] suggested that there was a 80% reduction in activated macrophages, and ~90% of the these activated macrophages contained D-Cy5 (in both PBS and D-NAC treated animals), indicating selectivity (**Figure 43C**).

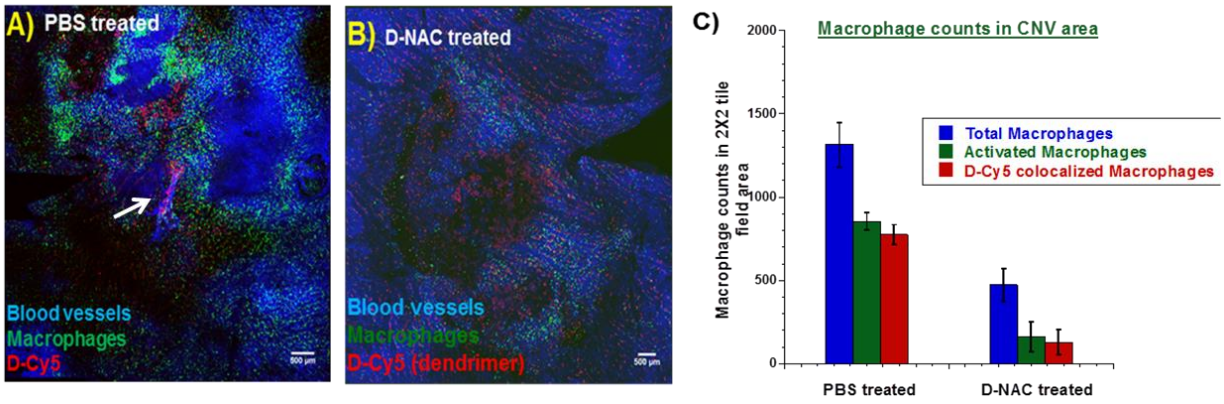

Figure 43: Flat mount image analysis of choroids for macrophage accumulation in the bleb area surrounding the CNV. Macrophages were stained with IBA-1 (Green) and D-Cy5 is red. Macrophage cell count analysis showed a ~63% reduction in number of macrophages cells, and a ~60% reduction in activated macrophages upon D-NAC compared to PBS treatment, with near 90%+ colocalization of activated macrophages and dendrimers. The cell count analysis was done using Imaris (Bitplane) software.

5.4.6. D-NAC treatment suppressed choroidal and retinal inflammation

The effect of D-NAC treatment on choroidal and retinal inflammation was accessed using RT-PCR, by measuring proinflammatory (IL-1β, IL-6, MCP-1-monocyte chemo-attractant, and TNFα) and anti-inflammatory cytokine levels (IL-10) [167-178]. There was a significant

reduction in all the proinflammatory cytokines, which returned to levels seen in healthy controls, whereas free NAC was not effective (**Figure 43A,B,D & E**). This can be attributed to reduced microglial/macrophage accumulation in bleb area of choroid and retina, suggesting the suppression of inflammation and neovascularization. Interestingly, D-NAC appeared to enhance the anti-inflammatory cytokine IL-10 both in retina and choroid (**Figure 44C & F**). This suggests that selective attenuation of proinflammatory response can be achieved with D-NAC.

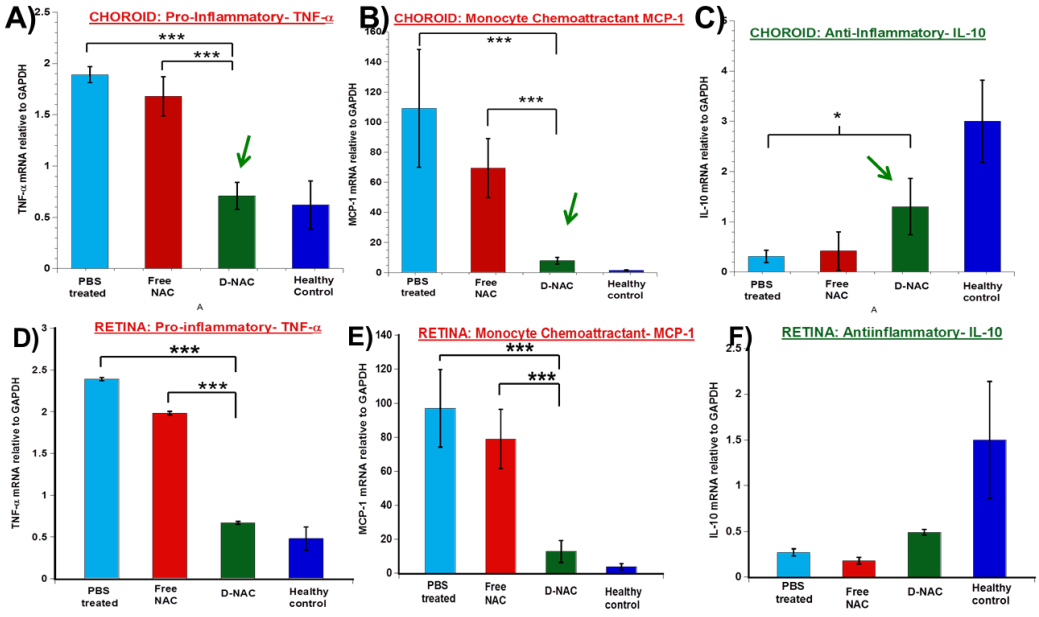

Figure 44: RT-PCR analysis of inflammatory and anti-inflammatory cytokines in choroid (A-C) and retina (D-F). The choroids and retinas of free NAC, D-NAC and PBS treated rats were subjected to trizol treatment and RNA was extracted and subjected to RT-PCR analysis. The expression was compared to healthy control with not pathology and relative to GAPDH.

Similar to the biodistribution pattern seen in the CNV area, the D-Cy5 localized selectively in the activated microglia/macrophages in the bleb area (**Figure 45B**), but did not localize in the unaffected areas of the same retina (**Figure 45A**). In D-NAC treated retina, there was a reduction in the number of microglia/macrophages in the bleb area, and which were more

ramified with less D-Cy5 uptake. Suggesting that D-Cy5 treatment reversed activated microglia to resting and ramified microglia (**Figure 45C**).

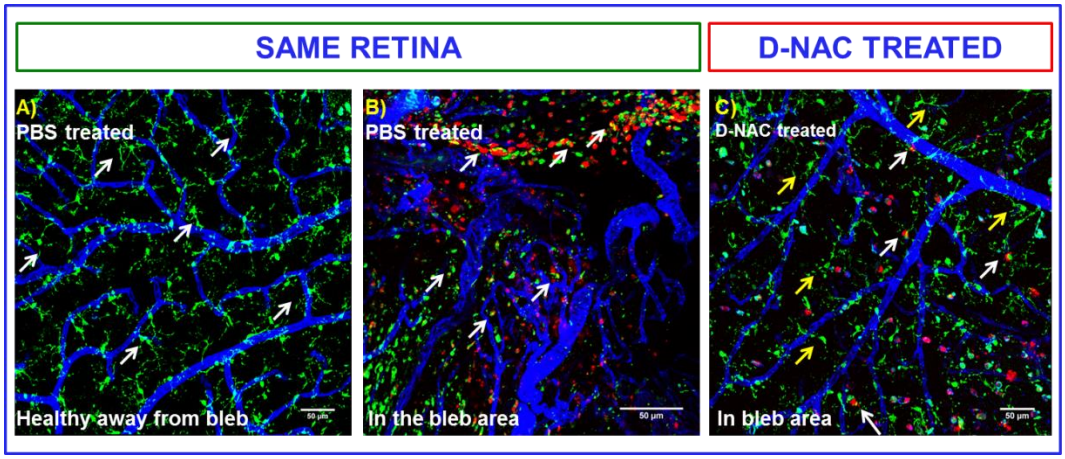

Figure 45: Flat mount retinas (40X magnification) with GSA-stained blood vessels, IBA-1 for mi/ma, and dendrimer (D-Cy5); **A)** 'Healthy', non pathlologic area of same retina with regular blood vessel structure and resting mi/ma (ramified) (white arrows), and no D-Cy5; **B)** Pathological area of the same retina near the bleb showing abnormal vessels, activated mi/ma ('round' and amoeboid) and 'spiked' dendrimers co-localized in activated mi/ma (white arrows); **C)** D-NAC treated retina showing both populations (i) resting microglia (ramified) (yellow arrows) and (ii) activated mi/ma (amoeboid) with dendrimer (white arrows) suggesting the therapeutic effect of D-NAC in quieting microglial activation.

5.4.7 A combination therapy of D-NAC and D-TA promotes CNV regressing in later stages of AMD.

A combination of D-NAC (20 mg/kg on NAC basis) and D-TA (10 mg/kg on TA basis) was administered systemically at a later stage (on Day 11, Day 13 and Day 15) to assess the efficacy when significant CNV has already occurred: (1) On Day 19, there was a 72% reduction in CNV in dendrimer-treated animals, compared to PBS controls, suggesting that late treatment is effective (**Figure 46**); (2) Compared to the extent of CNV area on Day 10, there was a ~45% reduction in dendrimer-treated animals on Day 19, showing strong suggestions of CNV regression. These results (n=6) suggests that, significant CNV suppression may be possible with systemic therapies delivered with dendrimers. In this CNV model the time period from day 10 to

day 20 the formed CNV grows with larger blood, leaky and irregular blood vessels and are entirely different from regular choriocapillaries (**Figure 47**). A combination of anti-inflammatory and anti-oxidant formulation (D-NAC) and an anti-angiogenic and anti-VEGF formulation (D-TA) treatment resulted in suppression of CNV growth further and regression. Regression can be attributed to the effect of TA delivered to microglia and RPE cells. D-NAC targets activated microglial cells and attenuate inflammation both in choroid and retina. A combine effect of D-NAC and D-TA may be necessary for treating late AMD where the CNV progress to retina forming retinal neovascularization (RNV) thereby, affecting the normal function retina, retinal and intravitreal hemorrhage.

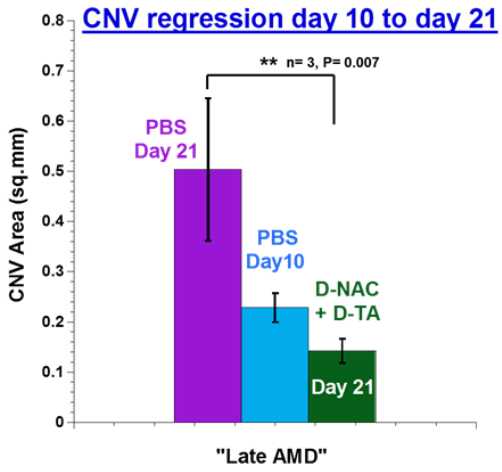

Figure 46: CNV area analysis of D-NAC + D-TA treated choroids showing significant regression (~52%) than compared to PBS treated choroids. At day 19 the PBS treated choroids showed significantly larger area neovascularization. ** indicates $p<0.01$. Scale bar at 100 µm.

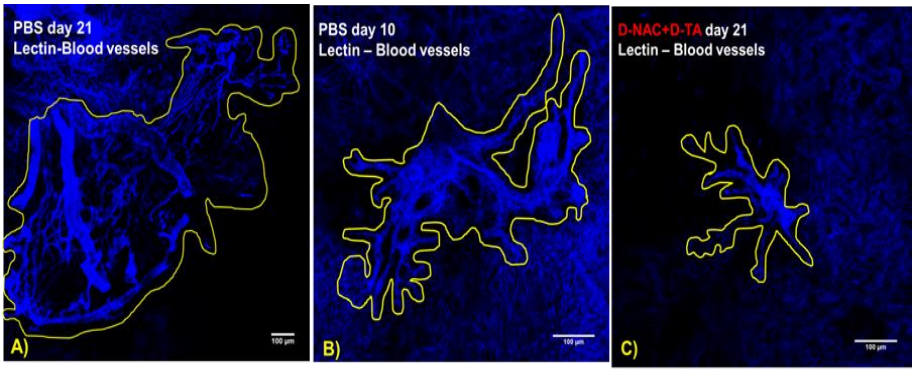

Figure 47: Confocal images of CNV in choroid, the blood vessels are stained using lectin (blue) and the CNV borders are delineated using Image-J software (yellow lines). Representative images showing CNV of PBS-Day 21**(A),** and PBS-Day 10**(B),** and D-NAC+D-TA-Day 21**(C).** ** indicates $p<0.01$. Scale bar at 100 µm.

5.5. Conclusions:

This study has demonstrated for the first time that D-NAC and D-TA administered intravenously can drastically reduce CNV formation in an HpODE induced CNV rat model. At early stages of AMD (combination of lipid accumulation and growth of CNV) it was demonstrated by D-NAC treated eyes having a minute amount of CNV formation compared to HpODE control eyes that had obvious CNV growth. A very important observation is that the microglial accumulation and activation was significantly reduced in D-NAC treated retina choroids strongly suggesting that targeting inflammation may have impact on CNV growth. At later stages of AMD a combination therapy of D-NAC and D-TA showed significant effect in promoting CNV regression and attention of inflammation by reversing the microglial conformation to resting stage. There was no increase in IOP levels or cataract formation after combination therapy making this an extremely promising therapy for wet AMD. Targeted therapy using dendrimers would mean that wet AMD patients can avoid invasive treatments such as intravitreal injections which would increase patient compliance. The long retention time of dendrimers in microglia/macrophages may also suggest less frequent treatments needed, therefore lowering the number of hospital trips needed and further reducing healthcare costs. In

future studies, it would be appropriate to vary the number of injections given, to vary the dosage of D-TA and to study animals for a longer period after HpODE injection, to ensure that treatment is effective for different stages of CNV development. Furthermore, D-TA and D-NAC toxicity should be carefully studied in addition to further experiments analyzing the mechanism of action of D-TA on retinal and choroidal endothelial cells (expression of ICAM and PCAM) and retinal blood vessel leakage. Nevertheless, this study has contributed to the advancement of medicine by demonstrating the potential therapeutic benefits of an intravenous dendrimer-based therapy for wet AMD.

REFERENCES

1. Paul P. Lee; Zachary W. Feldman; Jan Ostermann; Derek S. Brown; Frank A. Sloan Longitudinal Prevalence of Major Eye Diseases Arch Ophthalmol. 2003;121(9):1303-1310.
2. Americans, Eye Health, and Eye Disease National Survey, Greenberg, Quinlan & Rosner Research Inc., June, 2007 (needed to be modified).
3. Dutton, G. Ocular therapeutics target the retina. Genet. Eng. Biotechn. N. 32:18–19, 2012.
4. MILLER D, PECZON JD, WHITWORTH CG. CORTICOSTEROIDS AND FUNCTIONS IN THE ANTERIOR SEGMENT OF THE EYE. Am J Ophthalmol. 1965 Jan;59:31-4.
5. Manzouri, B.; Wyse, R. K.; Vafidis, G. C. Pharmacotherapy of fungal eye infections. Expert Opinion on Pharmacotherapy 2001, 2, 1849-1857.
6. HULL, D. S.; HINE, J. E.; EDELHAUSER, H. F.; HYNDIUK, R. A. Permeability of the Isolated Rabbit Cornea to Corticosteroids. Investigative Ophthalmology & Visual Science 1974, 13, 457-459.
7. Loftsson, T.; Sigurdsson, H.; Hreinsdóttir, D.; Konrádsdóttir, F.; Stefánsson, E. Dexamethasone delivery to posterior segment of the eye. Journal of Inclusion Phenomena and Macrocyclic Chemistry 2007, 57, 585-589.
8. Tombran-Tink, J.; Barnstable, C. J.; Gunda, S.; Hariharan, S.; Mandava, N.; Mitra, A. K. Barriers in Ocular Drug Delivery. In Ocular Transporters In Ophthalmic Diseases And Drug Delivery, Eds. Humana Press: 2008; pp 399-413.
9. Hughes, P. M.; Olejnik, O.; Chang-Lin, J.-E.; Wilson, C. G. Topical and systemic drug delivery to the posterior segments. Advanced Drug Delivery Reviews 2005, 57, 2010-2032.

10. S. Duvvuri, S. Majumdar, and A. K. Mitra. Drug delivery to the retina: challenges and opportunities. Expert. Opin. Biol. Ther. 3:45–56 (2003)
11. Saffar Mansoor, Baruch D. Kuppermann, and M. Cristina Kenney."Intraocular Sustained-Release Delivery Systems for Triamcinolone Acetonide". PharmaceuticalResearch, Vol. 26, No.4, April 2009.
12. Gaudana, R., Jwala, J., Boddu, S., & Mitra, A. (2009). Recent Perspectives in Ocular Drug Delivery. Pharmaceutical Research, 26(5), 1197-1216.
13. Edelhauser, H. F. (2010). Ophthalmic Drug Delivery Systems for the Treatment of Retinal Diseases: Basic Research to Clinical Applications. Investigative ophthalmology & visual science, 51(11), 5403-5420.
14. Diebold, Y., & Calonge, M. (2010). Applications of nanoparticles in ophthalmology. Progress in Retinal and Eye Research, 29(6), 596-609.
15. Campbell, M. (2010). Retinal Degenerative Diseases Reversible and Size-Selective Opening of the Inner Blood-Retina Barrier: A Novel Therapeutic Strategy. Advances in experimental medicine and biology, 664, 301-308.
16. Tomalia, D. A., Baker, H., Dewald, J., Hall, M., Kallos, G., Martin, S., Roeck, J., Ryder, J., Smith, P., 1985. A new class of polymers: starburst-dendritic macromolecules. Polym. J. (Tokyo, Japan) 17, 117-132.
17. Sk, Ugir Hossain, et al. "Enhancing the Efficacy of Ara-C through Conjugation with PAMAM Dendrimer and Linear PEG: A Comparative Study." Biomacromolecules 14.3 (2013): 801-810.

18. Esfand, Roseita, and Donald A. Tomalia. "Poly (amidoamine)(PAMAM) dendrimers: from biomimicry to drug delivery and biomedical applications." Drug discovery today 6.8 (2001): 427-436.
19. Mintzer, Meredith A., and Mark W. Grinstaff. "Biomedical applications of dendrimers: a tutorial." Chemical Society Reviews 40.1 (2011): 173-190.
20. Perumal, O.P. Inapagolla, R. Kannan, S. Kannan, R.M. The effect of surface functionality on cellular trafficking of dendrimers. Biomaterials. 2008; 29: 3469-3476.
21. Bravo-Osuna, I. Noiray, M. Briand, E. et al. Interfacial Interaction between Transmembrane Ocular Mucins and Adhesive Polymers and Dendrimers Analyzed by Surface Plasmon Resonance. Pharm. Res. 2012; 29: 2329-2340.
22. Yao, C. Wang, W. Zhou, X. et al. Effects of Poly(amidoamine) Dendrimers on Ocular Absorption of Puerarin Using Microdialysis. JOPT. 2011; 27: 565-569.
23. Holden, C.A. Tyagi, P. Thakur, A. Kadam, R. et al. Polyamidoamine dendrimer hydrogel for enhanced delivery of antiglaucoma drugs. Nanomedicine: Nanotechnology, Biology and Medicine. 2012; 8: 776-783.
24. Kambhampati, Siva P., and Rangaramanujam M. Kannan. "Dendrimer Nanoparticles for Ocular Drug Delivery." Journal of Ocular Pharmacology and Therapeutics 29.2 (2013): 151-165.
25. Bourges, J.L. Gautier, S.E Delie, F. et al. Ocular Drug Delivery Targeting the Retina and Retinal Pigment Epithelium Using Polylactide Nanoparticles.IOVS. 2003; 44: 3562-3569.
26. Sakurai, E. Ozeki, H. Kunou, N. Ogura, Y. Effect of particle size of polymeric nanospheres on intravitreal kinetics. Ophthalmicres. 2001; 33: 31-36.

27. Iezzi, R. Guru, B.R. Glybina, I,V. Mishra, M.K. et al. Dendrimer-based targeted intravitreal therapy for sustained attenuation of neuroinflammation in retinal degeneration. Biomaterials. 2012; 33: 979-988.
28. Marano, R.J. Toth, I. Wimmer, N. et al. Dendrimer delivery of an anti-VEGF oligonucleotide into the eye: a long-term study into inhibition of laser-induced CNV, distribution, uptake and toxicity. Gene therapy. 2005; 12: 1544-1550.
29. Luganini, A. Giuliani, A. Pirri, G. Peptide-derivatized dendrimers inhibit human cytomegalovirus infection by blocking virus binding to cell surface heparan sulfate. Antiviral research. 2010; 85: 532-540.
30. Kang, S.J. Durairaj, C. Kompella, U.B. Subconjunctival Nanoparticle Carboplatin in the Treatment of Murine Retinoblastoma. Arch Ophthalmol(1960). 2009; 127: 1043-1047.
31. McCarthy CA, Widdop RE, Deliyanti D, Wilkinson-Berka JL. Brain and retinal microglia in health and disease: An unrecognized target of the renin–angiotensin system. Clinical and Experimental Pharmacology and Physiology. 2013;40:571-9.
32. Schuetz, Erik, and Solon Thanos. "Microglia-targeted pharmacotherapy in retinal neurodegenerative diseases." Current drug targets 5.7 (2004): 619-627.
33. Zheng L, Gong B, Hatala DA, Kern TS. Retinal Ischemia and Reperfusion Causes Capillary Degeneration: Similarities to Diabetes. Investigative Ophthalmology & Visual Science. 2007;48:361-7.
34. Checchin, Daniella, et al. "Potential role of microglia in retinal blood vessel formation." Investigative ophthalmology & visual science 47.8 (2006): 3595-3602.

35. Li S-Y, Yang D, Yeung C-M, Yu W-Y, Chang RC-C, So K-F, et al. Lycium barbarum polysaccharides reduce neuronal damage, blood-retinal barrier disruption and oxidative stress in retinal ischemia/reperfusion injury. PloS one. 2011;6:e16380.

36. Kiernan DF, Mieler WF. The use of intraocular corticosteroids. Expert Opinion on Pharmacotherapy. 2009;10:2511-25.

37. Ayalasomayajula SP, Ashton P, Kompella UB. Fluocinolone Inhibits VEGF Expression via Glucocorticoid Receptor in Human Retinal Pigment Epithelial (ARPE-19) Cells and TNF-α–Induced Angiogenesis in Chick Chorioallantoic Membrane (CAM). Journal of Ocular Pharmacology and Therapeutics. 2009;25:97-104.

38. Zhang X, Wang N, Schachat AP, Bao S, Gillies MC. Glucocorticoids: Structure, Signaling and Molecular Mechanisms in the Treatment of Diabetic Retinopathy and Diabetic Macular Edema. Current Molecular Medicine. 2014;14:376-84.

39. Zhang X, Bao S, Lai D, Rapkins RW, Gillies MC. Intravitreal Triamcinolone Acetonide Inhibits Breakdown of the Blood-Retinal Barrier Through Differential Regulation of VEGF-A and Its Receptors in Early Diabetic Rat Retinas. Diabetes. 2008;57:1026-33.

40. Salek SS, Leder HA, Butler NJ, Gan TJ, Dunn JP, Thorne JE. Periocular Triamcinolone Acetonide Injections for Control of Intraocular Inflammation Associated with Uveitis. Ocular Immunology and Inflammation. 2013;21:257-63.

41. Li W, He B, Dai W, Zhang Q, Liu Y. Evaluations of therapeutic efficacy of intravitreal injected polylactic-glycolic acid microspheres loaded with triamcinolone acetonide on a rabbit model of uveitis. Int Ophthalmol. 2014;34:465-76.

42. M. Becerra E, Morescalchi F, Gandolfo F, Danzi P, Nascimbeni G, Arcidiacono B, et al. Clinical Evidence of Intravitreal Triamcinolone Acetonide in the Management of Age-Related Macular Degeneration. Current Drug Targets. 2011;12:149-72.
43. Penfold PL, Wong JG, Gyory J, Billson FA. Effects of triamcinolone acetonide on microglial morphology and quantitative expression of MHC-II in exudative age-related macular degeneration. Clinical & Experimental Ophthalmology. 2001;29:188-92.
44. Wang Y, Wang VM, Chan CC. The role of anti-inflammatory agents in age-related macular degeneration (AMD) treatment. Eye. 2011;25:127-39.
45. Matsuda S, Gomi F, Oshima Y, Tohyama M, Tano Y. Vascular Endothelial Growth Factor Reduced and Connective Tissue Growth Factor Induced by Triamcinolone in ARPE19 Cells under Oxidative Stress. Investigative Ophthalmology & Visual Science. 2005;46:1062-8.
46. Elman MJ, Aiello LP, Beck RW, Bressler NM, Bressler SB, Edwards AR, et al. Randomized Trial Evaluating Ranibizumab Plus Prompt or Deferred Laser or Triamcinolone Plus Prompt Laser for Diabetic Macular Edema. Ophthalmology. 2010;117:1064-77.e35.
47. Gopal, Lekha, and Tarun Sharma. "Use of intravitreal injection of triamcinolone acetonide in the treatment of age-related macular degeneration." Indian journal of ophthalmology 55.6 (2007): 431.
48. Yeung CK, Chan KP, Chiang SWY, Pang CP, Lam DSC. The Toxic and Stress Responses of Cultured Human Retinal Pigment Epithelium (ARPE19) and Human Glial Cells (SVG) in the Presence of Triamcinolone. Investigative Ophthalmology & Visual Science. 2003;44:5293-300.

49. Durairaj C, Kadam RS, Chandler JW, Hutcherson SL, Kompella UB. Nanosized Dendritic Polyguanidilyated Translocators for Enhanced Solubility, Permeability, and Delivery of Gatifloxacin. Investigative Ophthalmology & Visual Science. 2010;51:5804-16.
50. Holden CA, Tyagi P, Thakur A, Kadam R, Jadhav G, Kompella UB, et al. Polyamidoamine dendrimer hydrogel for enhanced delivery of antiglaucoma drugs. Nanomedicine: Nanotechnology, Biology and Medicine. 2012;8:776-83.
51. Chung H, Hwang JJ, Koh JY, Kim J-g, Yoon YH. Triamcinolone Acetonide-Mediated Oxidative Injury in Retinal Cell Culture: Comparison with Dexamethasone. Investigative Ophthalmology & Visual Science. 2007;48:5742-9.
52. Narayanan R, Mungcal JK, Kenney MC, Seigel GM, Kuppermann BD. Toxicity of Triamcinolone Acetonide on Retinal Neurosensory and Pigment Epithelial Cells. Investigative Ophthalmology & Visual Science. 2006;47:722-8
53. Chang Y-S, Lin C-F, Wu C-L, Kuo P-Y, Wu F-S, Shieh C-C, et al. Mechanisms Underlying Benzyl Alcohol Cytotoxicity (Triamcinolone Acetonide Preservative) in Human Retinal Pigment Epithelial Cells. Investigative Ophthalmology & Visual Science. 2011;52:4214-22.
54. Kleinman ME, Westhouse SJ, Ambati J, Pearson PA, Halperin LS. Triamcinolone crystal size. Ophthalmology. 2010;117:1654, e1-4.
55. Kambhampati SP, Kannan RM. Dendrimer Nanoparticles for Ocular Drug Delivery. Journal of Ocular Pharmacology and Therapeutics. 2013;29:151-65.
56. Chaplot SP, Rupenthal ID. Dendrimers for gene delivery – a potential approach for ocular therapy? Journal of Pharmacy and Pharmacology. 2014;66:542-56.

57. Sk UH, Kambhampati SP, Mishra MK, Lesniak WG, Zhang F, Kannan RM. Enhancing the Efficacy of Ara-C through Conjugation with PAMAM Dendrimer and Linear PEG: A Comparative Study. Biomacromolecules. 2013;14:801-10.
58. Mishra MK, Beaty CA, Lesniak WG, Kambhampati SP, Zhang F, Wilson MA, et al. Dendrimer brain uptake and targeted therapy for brain injury in a large animal model of hypothermic circulatory arrest. ACS nano. 2014;8:2134-47.
59. Vandamme TF, Brobeck L. Poly(amidoamine) dendrimers as ophthalmic vehicles for ocular delivery of pilocarpine nitrate and tropicamide. Journal of Controlled Release. 2005;102:23-38.
60. Iezzi R, Guru BR, Glybina IV, Mishra MK, Kennedy A, Kannan RM. Dendrimer-based targeted intravitreal therapy for sustained attenuation of neuroinflammation in retinal degeneration. Biomaterials. 2012;33:979-88.
61. Lesniak WG, Mishra MK, Jyoti A, Balakrishnan B, Zhang F, Nance E, et al. Biodistribution of Fluorescently Labeled PAMAM Dendrimers in Neonatal Rabbits: Effect of Neuroinflammation. Molecular Pharmaceutics. 2013;10:4560-71.
62. Kannan S, Dai H, Navath RS, Balakrishnan B, Jyoti A, Janisse J, et al. Dendrimer-Based Postnatal Therapy for Neuroinflammation and Cerebral Palsy in a Rabbit Model. Science Translational Medicine. 2012;4:130ra46.
63. Mastorakos P, Kambhampati SP, Mishra MK, Wu T, Song E, Hanes J, et al. Hydroxyl PAMAM dendrimer-based gene vectors for transgene delivery to human retinal pigment epithelial cells. Nanoscale. 2014.
64. Mansoor S, Kuppermann B, Kenney MC. Intraocular Sustained-Release Delivery Systems for Triamcinolone Acetonide. Pharm Res. 2009;26:770-84.

65. Hong J, Kim B-K, Lim H, Lee S, Lee SJ. Identification and characterization of triamcinolone acetonide, a microglial-activation inhibitor. Immunopharmacology and Immunotoxicology. 2012;34:912-8.

66. Macky TA, Oelkers C, Rix U, Heredia ML, Künzel E, Wimberly M, et al. Synthesis, Pharmacokinetics, Efficacy, and Rat Retinal Toxicity of a Novel Mitomycin C-Triamcinolone Acetonide Conjugate. Journal of Medicinal Chemistry. 2002;45:1122-7.

67. Zhang X, Bao S, Lai D, Rapkins RW, Gillies MC. Intravitreal Triamcinolone Acetonide Inhibits Breakdown of the Blood-Retinal Barrier Through Differential Regulation of VEGF-A and Its Receptors in Early Diabetic Rat Retinas. Diabetes. 2008;57:1026-33.

68. Valamanesh F, Berdugo M, Sennlaub F, Savoldelli M, Goumeaux C, Houssier M, et al. Effects of triamcinolone acetonide on vessels of the posterior segment of the eye. Molecular vision. 2009;15:2634-48.

69. Penfold PL, Wen L, Madigan MC, King NJC, Provis JM. Modulation of Permeability and Adhesion Molecule Expression by Human Choroidal Endothelial Cells. Investigative Ophthalmology & Visual Science. 2002;43:3125-30.

70. Krieglstein CF, Granger DN. Adhesion molecules and their role in vascular disease. American Journal of Hypertension. 2001;14:S44-S54.

71. Penfold PL, Wen L, Madigan MC, Gillies MC, King NJC, Provis JM. Triamcinolone acetonide modulates permeability and intercellular adhesion molecule-1 (ICAM-1) expression of the ECV304 cell line: implications for macular degeneration. Clinical & Experimental Immunology. 2000;121:458-65.

72. Wang Y-S, Friedrichs U, Eichler W, Hoffmann S, Wiedemann P. Inhibitory effects of triamcinolone acetonide on bFGF-induced migration and tube formation in choroidal microvascular endothelial cells. Graefe's Arch Clin Exp Ophthalmol. 2002;240:42-8.

73. Pereira, A. D., Santos, M. C. M., Costa, V. M., Pianetti, G. A., & Da Silva, G. R. (2012). Development and validation of a high performance liquid chromatographic method for determination of triamcinolone acetonide from polyurethane intraocular implants. Int J Pharm Pharm Sci, 4(4), 132-136.

74. Bosnjakovic A, Mishra MK, Ren W, Kurtoglu YE, Shi T, Fan D, et al. Poly(amidoamine) dendrimer-erythromycin conjugates for drug delivery to macrophages involved in periprosthetic inflammation. Nanomedicine: Nanotechnology, Biology and Medicine. 2011;7:284-94.

75. Gruneich JA, Price A, Zhu J, Diamond SL. Cationic corticosteroid for nonviral gene delivery. Gene Ther. 2004;11:668-74.

76. Ma K, Hu M-X, Qi Y, Zou J-H, Qiu L-Y, Jin Y, et al. PAMAM–Triamcinolone acetonide conjugate as a nucleus-targeting gene carrier for enhanced transfer activity. Biomaterials. 2009;30:6109-18.

77. Szurman P, Kaczmarek R, Spitzer MS, Jaissle GB, Decker P, Grisanti S, et al. Differential toxic effect of dissolved triamcinolone and its crystalline deposits on cultured human retinal pigment epithelium (ARPE19) cells. Experimental Eye Research. 2006;83:584-92.

78. Henn A, Lund S, Hedtjam M, Porzgen P, Leist M. The suitability of BV2 cells as alternative model system for primary microglia cultures or animal experiments of brain inflammation. Eur J Cell Biol. 2009;88:72-.

79. Wang B, Navath RS, Romero R, Kannan S, Kannan R. Anti-inflammatory and anti-oxidant activity of anionic dendrimer–N-acetyl cysteine conjugates in activated microglial cells. International Journal of Pharmaceutics. 2009;377:159-68.

80. Glybina IV, Kennedy A, Ashton P, Abrams GW, Iezzi R. Photoreceptor Neuroprotection in RCS Rats via Low-Dose Intravitreal Sustained-Delivery of Fluocinolone Acetonide. Investigative Ophthalmology & Visual Science. 2009;50:4847-57.

81. Paulo CS, Pires das Neves R, Ferreira LS. Nanoparticles for intracellular-targeted drug delivery. Nanotechnology. 2011;22:494002.

82. Carrillo-de Sauvage MA, Maatouk L, Arnoux I, Pasco M, Sanz Diez A, Delahaye M, et al. Potent and multiple regulatory actions of microglial glucocorticoid receptors during CNS inflammation. Cell Death Differ. 2013;20:1546-57.

83. Zhang K, Zhang L, Weinreb RN. Ophthalmic drug discovery: novel targets and mechanisms for retinal diseases and glaucoma. Nat Rev Drug Discov. 2012;11:541-59.

84. Ma W, Zhao L, Fontainhas AM, Fariss RN, Wong WT. Microglia in the mouse retina alter the structure and function of retinal pigmented epithelial cells: a potential cellular interaction relevant to AMD. PloS one. 2009;4:e7945.

85. Ambati J, Atkinson JP, Gelfand BD. Immunology of age-related macular degeneration. Nature reviews Immunology. 2013;13:438-51.

86. McCarthy CA, Widdop RE, Deliyanti D, Wilkinson-Berka JL. Brain and retinal microglia in health and disease: an unrecognized target of the renin-angiotensin system. Clinical and experimental pharmacology & physiology. 2013;40:571-9.

87. Blaauwgeers HGT, Holtkamp GM, Rutten H, Witmer AN, Koolwijk P, Partanen TA, et al. Polarized Vascular Endothelial Growth Factor Secretion by Human Retinal Pigment

Epithelium and Localization of Vascular Endothelial Growth Factor Receptors on the Inner Choriocapillaris: Evidence for a Trophic Paracrine Relation. The American Journal of Pathology. 1999;155:421-8.

88. Felinski EA, Antonetti DA. Glucocorticoid Regulation of Endothelial Cell Tight Junction Gene Expression: Novel Treatments for Diabetic Retinopathy. Current Eye Research. 2005;30:949-57.
89. Ebrahem Q, Minamoto A, Hoppe G, Anand-Apte B, Sears JE. Triamcinolone Acetonide Inhibits IL-6– and VEGF-Induced Angiogenesis Downstream of the IL-6 and VEGF Receptors. Investigative Ophthalmology & Visual Science. 2006;47:4935-41.
90. Nauck M, Karakiulakis G, Perruchoud AP, Papakonstantinou E, Roth M. Corticosteroids inhibit the expression of the vascular endothelial growth factor gene in human vascular smooth muscle cells. European Journal of Pharmacology. 1998;341:309-15.
91. Benson WB. A randomized trial comparing the efficacy and safety of intravitreal triamcinolone with standard care to treat vision loss associated with macular edema secondary to branch retinal vein occlusion. Evidence-Based Ophthalmology. 2010;11:22-3 10.1097/IEB.0b013e3181c70dc3.
92. Liu MM, Tuo J, Chan CC. Gene therapy for ocular diseases. The British journal of ophthalmology. 2011;95:604-12.
93. Kambhampati SP, Kannan RM. Dendrimer nanoparticles for ocular drug delivery. Journal of ocular pharmacology and therapeutics : the official journal of the Association for Ocular Pharmacology and Therapeutics. 2013;29:151-65.

94. Berry V, Francis P, Kaushal S, Moore A, Bhattacharya S. Missense mutations in MIP underlie autosomal dominant 'polymorphic' and lamellar cataracts linked to 12q. Nature genetics. 2000;25:15-7.

95. Farrar GJ, Kenna PF, Humphries P. On the genetics of retinitis pigmentosa and on mutation-independent approaches to therapeutic intervention. The EMBO journal. 2002;21:857-64.

96. Ferreira PA. Insights into X-linked retinitis pigmentosa type 3, allied diseases and underlying pathomechanisms. Human molecular genetics. 2005;14:R259-67.

97. Molday RS. Photoreceptor membrane proteins, phototransduction, and retinal degenerative diseases. The Friedenwald Lecture. Investigative ophthalmology & visual science. 1998;39:2491-513.

98. Jacobson SG, Cideciyan AV, Ratnakaram R, Heon E, Schwartz SB, Roman AJ, et al. Gene therapy for leber congenital amaurosis caused by RPE65 mutations: safety and efficacy in 15 children and adults followed up to 3 years. Archives of ophthalmology. 2012;130:9-24.

99. Testa F, Maguire AM, Rossi S, Pierce EA, Melillo P, Marshall K, et al. Three-year follow-up after unilateral subretinal delivery of adeno-associated virus in patients with Leber congenital Amaurosis type 2. Ophthalmology. 2013;120:1283-91.

100. Chung DC, Lee V, Maguire AM. Recent advances in ocular gene therapy. Current opinion in ophthalmology. 2009;20:377-81.

101. Rolling F. Recombinant AAV-mediated gene transfer to the retina: gene therapy perspectives. Gene therapy. 2004;11:S26-32.

102. Chen Y, Moiseyev G, Takahashi Y, Ma JX. RPE65 gene delivery restores isomerohydrolase activity and prevents early cone loss in Rpe65-/- mice. Investigative ophthalmology & visual science. 2006;47:1177-84.

103. Aguirre GD, Baldwin V, Pearce-Kelling S, Narfstrom K, Ray K, Acland GM. Congenital stationary night blindness in the dog: common mutation in the RPE65 gene indicates founder effect. Molecular vision. 1998;4:23.

104. Thomas CE, Ehrhardt A, Kay MA. Progress and problems with the use of viral vectors for gene therapy. Nature reviews Genetics. 2003;4:346-58.

105. Olsen NJ, Stein CM. New drugs for rheumatoid arthritis. The New England journal of medicine. 2004;350:2167-79.

106. Xiao X, Li J, Samulski RJ. Efficient long-term gene transfer into muscle tissue of immunocompetent mice by adeno-associated virus vector. Journal of virology. 1996;70:8098-108.

107. Lentz TB, Gray SJ, Samulski RJ. Viral vectors for gene delivery to the central nervous system. Neurobiology of disease. 2012;48:179-88.

108. Chirmule N, Xiao W, Truneh A, Schnell MA, Hughes JV, Zoltick P, et al. Humoral immunity to adeno-associated virus type 2 vectors following administration to murine and nonhuman primate muscle. Journal of virology. 2000;74:2420-5.

109. Wu ZJ, Yang HY, Colosi P. Effect of Genome Size on AAV Vector Packaging. Molecular Therapy. 2010;18:80-6.

110. Bitner H, Mizrahi-Meissonnier L, Griefner G, Erdinest I, Sharon D, Banin E. A Homozygous Frameshift Mutation in BEST1 Causes the Classical Form of Best Disease in an Autosomal Recessive Mode. Investigative ophthalmology & visual science. 2011;52:5332-8.

111. Briggs CE, Rucinski D, Rosenfeld PJ, Hirose T, Berson EL, Dryja TP. Mutations in ABCR (ABCA4) in patients with Stargardt macular degeneration or cone-rod degeneration. Investigative ophthalmology & visual science. 2001;42:2229-36.

112. Mintzer MA, Simanek EE. Nonviral vectors for gene delivery. Chemical reviews. 2009;109:259-302.

113. Sunshine JC, Sunshine SB, Bhutto I, Handa JT, Green JJ. Poly(beta-amino ester)-nanoparticle mediated transfection of retinal pigment epithelial cells in vitro and in vivo. Plos One. 2012;7:e37543.

114. Farjo R, Skaggs J, Quiambao AB, Cooper MJ, Naash MI. Efficient Non-Viral Ocular Gene Transfer with Compacted DNA Nanoparticles. Plos One. 2006;1:e38.

115. de la Fuente M, Seijo B, Alonso MJ. Bioadhesive hyaluronan-chitosan nanoparticles can transport genes across the ocular mucosa and transfect ocular tissue. Gene therapy. 2008;15:668-76.

116. Akinc A, Thomas M, Klibanov AM, Langer R. Exploring polyethylenimine-mediated DNA transfection and the proton sponge hypothesis. The journal of gene medicine. 2005;7:657-63.

117. Suk JS, Kim AJ, Trehan K, Schneider CS, Cebotaru L, Woodward OM, et al. Lung Gene Therapy with Highly Compacted DNA Nanoparticles that Overcome the Mucus Barrier. Journal of controlled release : official journal of the Controlled Release Society. 2014;178:8-17.

118. Xu Q, Boylan NJ, Suk JS, Wang YY, Nance EA, Yang JC, et al. Nanoparticle diffusion in, and microrheology of, the bovine vitreous ex vivo. Journal of controlled release : official journal of the Controlled Release Society. 2013;167:76-84.

119. Pathak A, Patnaik S, Gupta KC. Recent trends in non-viral vector-mediated gene delivery. Biotechnology journal. 2009;4:1559-72.

120. Ke W, Shao K, Huang R, Han L, Liu Y, Li J, et al. Gene delivery targeted to the brain using an Angiopep-conjugated polyethyleneglycol-modified polyamidoamine dendrimer. Biomaterials. 2009;30:6976-85.

121. Reebye V, Saetrom P, Mintz PJ, Huang KW, Swiderski P, Peng L, et al. Novel RNA oligonucleotide improves liver function and inhibits liver carcinogenesis in vivo. Hepatology. 2014;59:216-27.

122. Patil ML, Zhang M, Minko T. Multifunctional triblock Nanocarrier (PAMAM-PEG-PLL) for the efficient intracellular siRNA delivery and gene silencing. ACS nano. 2011;5:1877-87.

123. Shah V, Taratula O, Garbuzenko OB, Patil ML, Savla R, Zhang M, et al. Genotoxicity of different nanocarriers: possible modifications for the delivery of nucleic acids. Current drug discovery technologies. 2013;10:8-15.

124. Kannan S, Dai H, Navath RS, Balakrishnan B, Jyoti A, Janisse J, et al. Dendrimer-based postnatal therapy for neuroinflammation and cerebral palsy in a rabbit model. Science translational medicine. 2012;4:130ra46.

125. Patil ML, Zhang M, Taratula O, Garbuzenko OB, He H, Minko T. Internally cationic polyamidoamine PAMAM-OH dendrimers for siRNA delivery: effect of the degree of quaternization and cancer targeting. Biomacromolecules. 2009;10:258-66.

126. Lee JH, Lim YB, Choi JS, Lee Y, Kim TI, Kim HJ, et al. Polyplexes assembled with internally quaternized PAMAM-OH dendrimer and plasmid DNA have a neutral surface and gene delivery potency. Bioconjugate chemistry. 2003;14:1214-21.

127. Becerra EM, Morescalchi F, Gandolfo F, Danzi P, Nascimbeni G, Arcidiacono B, et al. Clinical evidence of intravitreal triamcinolone acetonide in the management of age-related macular degeneration. Current drug targets. 2011;12:149-72.

128. Elman MJ, Aiello LP, Beck RW, Bressler NM, Bressler SB, Edwards AR, et al. Randomized trial evaluating ranibizumab plus prompt or deferred laser or triamcinolone plus prompt laser for diabetic macular edema. Ophthalmology. 2010;117:1064-77 e35.

129. Jonas JB. Intravitreal triamcinolone acetonide: a change in a paradigm. Ophthalmic research. 2006;38:218-45.

130. Beck RW, Edwards AR, Aiello LP, Bressler NM, Ferris F, Glassman AR, et al. Three-year follow-up of a randomized trial comparing focal/grid photocoagulation and intravitreal triamcinolone for diabetic macular edema. Archives of ophthalmology. 2009;127:245-51.

131. Shahin V, Albermann L, Schillers H, Kastrup L, Schafer C, Ludwig Y, et al. Steroids dilate nuclear pores imaged with atomic force microscopy. Journal of cellular physiology. 2005;202:591-601.

132. Ma K, Hu M, Xie M, Shen H, Qiu L, Fan W, et al. Investigation of polyethylenimine-grafted-triamcinolone acetonide as nucleus-targeting gene delivery systems. The journal of gene medicine. 2010;12:669-80.

133. Ma K, Hu MX, Qi Y, Zou JH, Qiu LY, Jin Y, et al. PAMAM-triamcinolone acetonide conjugate as a nucleus-targeting gene carrier for enhanced transfer activity. Biomaterials. 2009;30:6109-18.

134. Mishra MK, Beaty CA, Lesniak WG, Kambhampati SP, Zhang F, Wilson MA, et al. Dendrimer brain uptake and targeted therapy for brain injury in a large animal model of hypothermic circulatory arrest. ACS nano. 2014;8:2134-47.

135. del Pozo-Rodriguez A, Delgado D, Solinis MA, Gascon AR, Pedraz JL. Solid lipid nanoparticles for retinal gene therapy: transfection and intracellular trafficking in RPE cells. International journal of pharmaceutics. 2008;360:177-83.

136. Abul-Hassan K, Walmsley R, Boulton M. Optimization of non-viral gene transfer to human primary retinal pigment epithelial cells. Current eye research. 2000;20:361-6.

137. Urtti A, Polansky J, Lui GM, Szoka FC. Gene delivery and expression in human retinal pigment epithelial cells: effects of synthetic carriers, serum, extracellular matrix and viral promoters. Journal of drug targeting. 2000;7:413-21.

138. Lakowicz JR. Principles of frequency-domain fluorescence spectroscopy and applications to cell membranes. Sub-cellular biochemistry. 1988;13:89-126.

139. Iezzi R, Guru BR, Glybina IV, Mishra MK, Kennedy A, Kannan RM. Dendrimer-based targeted intravitreal therapy for sustained attenuation of neuroinflammation in retinal degeneration. Biomaterials. 2012;33:979-88.

140. Lesniak WG, Mishra MK, Jyoti A, Balakrishnan B, Zhang F, Nance E, et al. Biodistribution of fluorescently labeled PAMAM dendrimers in neonatal rabbits: effect of neuroinflammation. Molecular pharmaceutics. 2013;10:4560-71.

141. Yurek DM, Fletcher AM, Smith GM, Seroogy KB, Ziady AG, Molter J, et al. Long-term transgene expression in the central nervous system using DNA nanoparticles. Molecular therapy : the journal of the American Society of Gene Therapy. 2009;17:641-50.

142. Konstan MW, Davis PB, Wagener JS, Hilliard KA, Stern RC, Milgram LJ, et al. Compacted DNA nanoparticles administered to the nasal mucosa of cystic fibrosis subjects are safe and demonstrate partial to complete cystic fibrosis transmembrane regulator reconstitution. Human gene therapy. 2004;15:1255-69.

143. Mishra S, Webster P, Davis ME. PEGylation significantly affects cellular uptake and intracellular trafficking of non-viral gene delivery particles. European journal of cell biology. 2004;83:97-111.

144. Thiagarajan G, Greish K, Ghandehari H. Charge affects the oral toxicity of poly(amidoamine) dendrimers. European journal of pharmaceutics and biopharmaceutics : official journal of Arbeitsgemeinschaft fur Pharmazeutische Verfahrenstechnik eV. 2013;84:330-4.

145. Kukowska-Latallo JF, Raczka E, Quintana A, Chen C, Rymaszewski M, Baker JR, Jr. Intravascular and endobronchial DNA delivery to murine lung tissue using a novel, nonviral vector. Human gene therapy. 2000;11:1385-95.

146. Paulo CSO, das Neves RP, Ferreira LS. Nanoparticles for intracellular-targeted drug delivery. Nanotechnology. 2011;22:49.

147. Amoozgar Z, Yeo Y. Recent advances in stealth coating of nanoparticle drug delivery systems. Wiley interdisciplinary reviews Nanomedicine and nanobiotechnology. 2012;4:219-33.

148. Hatakeyama H, Akita H, Harashima H. A multifunctional envelope type nano device (MEND) for gene delivery to tumours based on the EPR effect: a strategy for overcoming the PEG dilemma. Advanced drug delivery reviews. 2011;63:152-60.

149. Pamujula S, Hazari S, Bolden G, Graves RA, Chinta DD, Dash S, et al. Cellular delivery of PEGylated PLGA nanoparticles. The Journal of pharmacy and pharmacology. 2012;64:61-7.

150. Hu Y, Xie J, Tong YW, Wang CH. Effect of PEG conformation and particle size on the cellular uptake efficiency of nanoparticles with the HepG2 cells. Journal of controlled release : official journal of the Controlled Release Society. 2007;118:7-17.

151. Sonawane ND, Szoka FC, Jr., Verkman AS. Chloride accumulation and swelling in endosomes enhances DNA transfer by polyamine-DNA polyplexes. The Journal of biological chemistry. 2003;278:44826-31.

152. Zhang C, Lam TT, Tso MOM. Heterogeneous populations of microglia/macrophages in the retina and their activation after retinal ischemia and reperfusion injury. Experimental Eye Research. 2005;81:700-9.

153. Li S-Y, Yang D, Yeung C-M, Yu W-Y, Chang RC-C, So K-F, et al. Lycium barbarum polysaccharides reduce neuronal damage, blood-retinal barrier disruption and oxidative stress in retinal ischemia/reperfusion injury. PloS one. 2011;6:e16380

154. Lesniak WG, Mishra MK, Jyoti A, Balakrishnan B, Zhang F, Nance E, et al. Biodistribution of Fluorescently Labeled PAMAM Dendrimers in Neonatal Rabbits: Effect of Neuroinflammation. Molecular Pharmaceutics. 2013;10:4560-71.

155. Sk UH, Kambhampati SP, Mishra MK, Lesniak WG, Zhang F, Kannan RM. Enhancing the efficacy of Ara-C through conjugation with PAMAM dendrimer and linear PEG: a comparative study. Biomacromolecules. 2013;14:801-10.

156. Saghizadeh M, Kramerov AA, Yaghoobzadeh Y, Hu J, Ljubimova JY, Black KL, et al. Adenovirus-driven overexpression of proteinases in organ-cultured normal human corneas leads to diabetic-like changes. Brain research bulletin. 2010;81:262- 72.

157. Zheng L, Gong B, Hatala DA, Kern TS. Retinal ischemia and reperfusion causes capillary degeneration: similarities to diabetes. Invest Ophthalmol Vis Sci. 2007;48:361-7.

158. Lutty GA, Merges C, Threlkeld AB, Crone S, McLeod DS. Heterogeneity in localization of isoforms of TGF-b in human retina, vitreous, and choroid. Invest Ophthalmol Vis Sci. 1993;34:477-87.

159. Riches AC, Sharp JG, Thomas DB, Smith SV. Blood volume determination in the mouse. The Journal of Physiology. 1973;228:279-84.

160. Bhutto, Imran, and Gerard Lutty. "Understanding age-related macular degeneration (AMD): relationships between the photoreceptor/retinal pigment epithelium/Bruch's membrane/choriocapillaris complex." Molecular aspects of medicine 33.4 (2012): 295-317.

161. 55.Campochiaro, Peter A. "Retinal and choroidal neovascularization." Journal of cellular physiology 184.3 (2000): 301-310.

162. 56.Langmann, Thomas. "Microglia activation in retinal degeneration." Journal of leukocyte biology 81.6 (2007): 1345-1351.

163. Schuetz, Erik, and Solon Thanos. "Microglia-targeted pharmacotherapy in retinal neurodegenerative diseases." Current drug targets 5.7 (2004): 619-627.

164. Tsutsumi, Chikako, et al. "The critical role of ocular-infiltrating macrophages in the development of choroidal neovascularization." Journal of leukocyte biology 74.1 (2003): 25-32.

165. Fung AE, Rosenfeld PJ, Reichel E. The International Intravitreal Bevacizumab Safety Survey: using the internet to assess drug safety worldwide. Br J Ophthalmol 2006;90:1344-9.

166. Lee, Sun Young, et al. "N-acetylcysteine promotes long-term survival of cones in a model of retinitis pigmentosa." Journal of cellular physiology 226.7 (2011): 1843-1849.

167. Becerra EM, Morescalchi F, Gandolfo F, Danzi P, Nascimbeni G, Arcidiacono B, et al. Clinical Evidence of Intravitreal Triamcinolone Acetonide in the Management of Age-Related Macular Degeneration. Curr Drug Targets. 2011; 12(2):149-72. PMID: 20887246

168. Kiernan DF, Mieler WF. The use of intraocular corticosteroids. Expert Opin Pharmacother. 2009; 10(15):2511-25. PMID: 19761356

169. Diabetic Retinopathy Clinical Research Network, Elman MJ, Aiello LP, Beck RW, Bressler NM, Bressler SB, Edwards AR, Ferris FL 3rd, Friedman SM, Glassman AR, Miller KM, Scott IU, Stockdale CR, Sun JK. Randomized trial evaluating ranibizumab plus prompt or deferred laser or triamcinolone plus prompt laser for diabetic macular edema. Ophthalmology. 2010; 117(6):1064-1077.e35. PMID: 20427088

170. Diabetic Retinopathy Clinical Research Network (DRCR.net), Beck RW, Edwards AR, Aiello LP, Bressler NM, Ferris F, Glassman AR, Hartnett E, Ip MS, Kim JE, Kollman C. Three-year follow-up of a randomized trial comparing focal/grid photocoagulation and intravitreal triamcinolone for diabetic macular edema. Arch Ophthalmol. 2009; 127(3):245-51. PMID: 19273785

171. Jonas JB. Intravitreal triamcinolone acetonide: a change in a paradigm. Ophthalmic Res. 2006; 38(4):218-45. PMID:16763379

172. Wang YS, Friedrichs U, Eichler W, Hoffmann S, Wiedemann P. Inhibitory effects of triamcinolone acetonide on bFGF-induced migration and tube formation in choroidal microvascular endothelial cells. Graef Arch Clin Exp. 2002; 240:42-8. PMID: 11954780

173. Jonas JB, Degenring RF, Kreissig I, Akkoyun I, Kamppeter BA. Intraocular pressure elevation after intravitreal triamcinolone acetonide injection. Ophthalmology. 2005; 112(4):593-8. PMID: 15808249

174. Sakurai E, Anand A, Ambati BK, van Rooijen N, Ambati J. Macrophage depletion inhibits experimental choroidal neovascularization. Invest Ophth Vis Sci. 2003; 44:3578-85. PMID: 12882810

175. Orr AG, Orr AL, Li XJ, Gross RE, Traynelis SF. Adenosine A(2A) receptor mediates microglial process retraction. Nat Neurosci. 2009;12(7):872-8. PMID: 19525944.

176. Ambati J, Atkinson JP, Gelfand BD. Immunology of age-related macular degeneration. Nat Rev Immunol. 2013; 13(6):438-51. PMID: 23702979.

177. Kannan S, Dai H, Navath RS, Balakrishnan B, Jyoti A, Janisse J, Romero R, Kannan RM. Dendrimer-based postnatal therapy for neuroinflammation and cerebral palsy in a rabbit model. Sci Transl Med. 2012; 4(130):130ra46. PMID: 22517883

178. Liu Y, Yang X, Utheim TP, Guo C, Xiao M, Liu Y, Yin Z, Ma J. Correlation of cytokine levels and microglial cell infiltration during retinal degeneration in RCS rats. PLoS One. 2013; 8(12):e82061. PMID: 24349184.

ABSTRACT

DENDRIMER BASED NANOTHERAPEUTICS FOR OCULAR DRUG DELIVERY

by

SIVA PRAMODH KAMBHAMPATI

May 2015

Advisor(s): Dr. Kannan M. Rangaramanujam and Dr. Howard Matthew.

Major: Biomedical Engineering

Degree: Doctor of Philosophy

PAMAM dendrimers are a class of well-defined, hyperbranched polymeric nanocarriers that are being investigated for ocular drug and gene delivery. Their favorable properties such as small size, multivalency and water solubility can provide significant opportunities for many biologically unstable drugs and allows potentially favorable ocular biodistribution. This work exploits hydroxyl terminated dendrimers (G4-OH) as drug/gene delivery vehicles that can target retinal microglia and pigment epithelium *via* systemic delivery with improved efficacy at much lower concentrations without any side effects.

Two different drugs Triamcinolone acetonide (TA) and N-Acetyl Cysteine (NAC) conjugated to G4-OH dendrimers showed tailorable sustained release in physiological relevant solutions and were evaluated *in-vitro* and *in-vivo*. Dendrimer-TA conjugates enhanced the solubility of TA and were 100 fold more effective at lower concentrations than free TA in its anti-inflammatory activity in activated microglia and in suppressing VEGF production in hypoxic RPE cells. Dendrimers targeted activated microglia/macrophages and RPE and retained for a period of 21 days in I/R mice model. The relative retention of intravitreal and intravenous dendrimers was comparable, if a 30-fold intravenous dose is used; suggesting intravenous route targeting retinal diseases are possible with dendrimers. D-NAC when injected intravenously

attenuated retinal and choroidal inflammation, significantly reduced (~73%) CNV growth at early stage of AMD in rat model of CNV. A combination therapy of D-NAC + D-TA significantly suppressed microglial activation and promoted CNV regression in late stages of AMD without causing side-effects.

G4-OH was modified with linker having minimal amine groups and incorporation of TA as a nuclear localization enhancer resulted in compact gene vectors with favorable safety profile and achieved high levels of transgene expression in hard to transfect human retinal pigment epithelial cells (hRPE). Prepared dendrimer-gene complexes were non-toxic and achieved significant cell uptake and safe delivery of gene in to the nucleus. Further, polyethylene glycol (PEG) surface coating enhanced colloidal stability in physiological relevant solutions without affecting its transfection efficacy.

AUTOBIOGRAPHICAL STATEMENT

SIVA PRAMODH KAMBHAMPATI

BIRTH: November 27, 1986, Chennai, Tamil Nadu, India.

EDUCATION: Ph.D. in Biomedical Engineering, Expected December 2014, Wayne State University, Detroit, MI

MS in Biomedical Engineering, December 2011, Wayne State University, Detroit, MI

B-Tech in Bioengineering, May 2008, SASTRA University, Tamil Nadu, India

SELECTED PUBLICATIONS:

1. **Kambhampati, SP.**, Bhutto, I.A., Mishra, M.K., Lutty, G.A., Dendrimer based intravenous therapy for choroidal and retinal neovascularization and inflammation. (Manuscript in preparation).
2. **Kambhampati, S.P.**, Mishra, M.K., Mastorakos, P., Kannan, R.M. (2014) Intracellular delivery of dendrimer triamcinolone acetonide conjugates into microglial and human retinal pigment epithelial cells (submitted to EJPB).
3. *Clunies-Ross, A.,***Kambhampati, S.P**., Bhutto, I.A., Mishra, M.K., et al. (2014) Transport and microglial uptake of dendrimers in normal and ischemia reperfusion mouse retina. (Submitted to IOVS).
4. ***Kambhampati, S.P.**, *Mastorakos, P., Mishra MK, Wu T, Song E, Hanes J, et al. Hydroxyl PAMAM dendrimer-based gene vectors for transgene delivery to human retinal pigment epithelial cells. Nanoscale. 2014.
5. **Kambhampati, SP.,** Kannan RM. Dendrimer Nanoparticles for Ocular Drug Delivery. Journal of Ocular Pharmacology and Therapeutics. 2013; 29(2): 151-165.
6. *Sk UH, ***Kambhampati, SP.,** *Mishra MK, Lesniak WG, Zhang F, Kannan RM. Enhancing the Efficacy of Ara-C through Conjugation with PAMAM Dendrimer and Linear PEG: A Comparative Study. Biomacromolecules. 2013; 14:801-10.
7. Xu Q, **Kambhampati, S.P.,** Kannan RM. Nanotechnology approaches for ocular drug delivery. Middle East African Journal of Ophthalmology. 2013; 20:26.
8. Mishra, M. K., Beaty, C. A., Lesniak, W. G., **Kambhampati, S. P.,** Zhang, F., et al. (2014). Dendrimer Brain Uptake and Targeted Therapy for Brain Injury in a Large Animal Model of Hypothermic Circulatory Arrest. ACS nano, 8(3), 2134-2147.

*** indicates equal first authors**